AD-A134 521 ANNUAL REPORT OF LAWRENCE LIVERMORE NATIONAL LABORATORY 1/2
TO THE FEDERAL AV.. (U) LAWRENCE LIVERMORE NATIONAL LAB
CA F M LUTHER DEC 80 UCRL-50042-80 FAA/EE-83-8
UNCLASSIFIED DOT-FA79WAI-034 F/G 4/1 NL

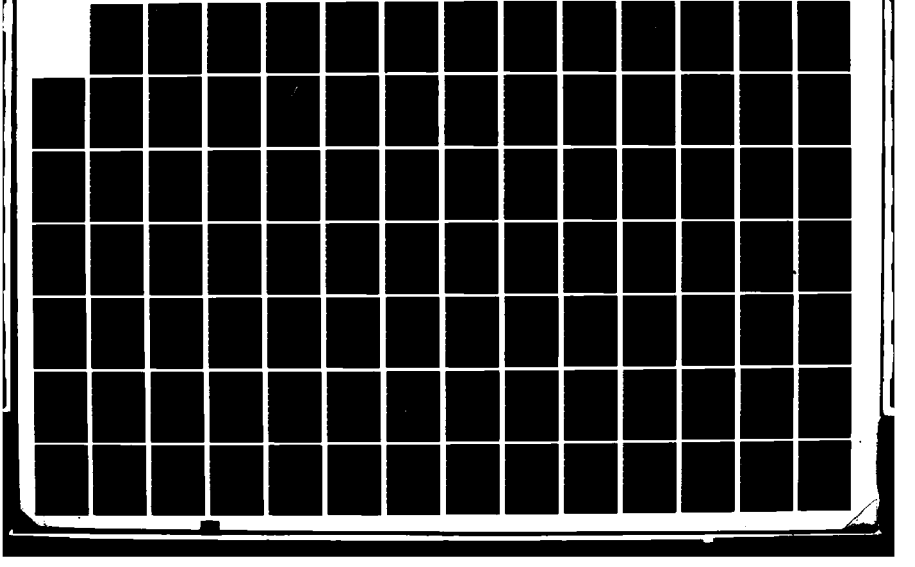

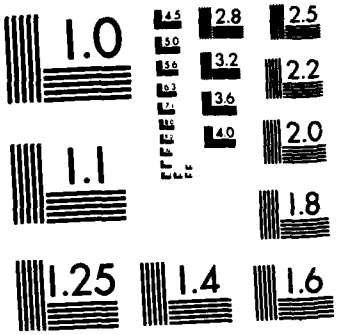

FAA-EE-83-8

U.S. Department of Transportation
Federal Aviation Administration

Annual Report of Lawrence Livermore National Laboratory to the FAA on the High Altitude Pollution Program—1980

Office of Environment
and Energy
Washington, D.C. 20591

Frederick M. Luther
Principal Investigator

Technical Report Documentation Page

1. Report No.	2. Government Accession No.	3. Recipient's Catalog No.
FAA-EE-83-8	AD-A134521	

4. Title and Subtitle	5. Report Date
Annual Report of Lawrence Livermore National Laboratory to the Federal Aviation Administration on the High Altitude Pollution Program - 1980	December 1980
	6. Performing Organization Code
	8. Performing Organization Report No.
7. Author(s)	
Frederick M. Luther, Principal Investigator	UCRL-50042-80
9. Performing Organization Name and Address	10. Work Unit No. (TRAIS)
Lawrence Livermore National Laboratory University of California Livermore, California 94550	11. Contract or Grant No. DOT-FA79WA1-034
	13. Type of Report and Period Covered
12. Sponsoring Agency Name and Address	Annual Report October 1, 1979 - December 31, 1980
U.S. Department of Transportation Federal Aviation Administration Office of Environment and Energy, Air Quality Division Washington, D.C. 20591	14. Sponsoring Agency Code

15. Supplementary Notes

16. Abstract

This annual report documents the progress made on research in support of the High Altitude Pollution Program (HAPP) between October 1, 1979 and December 31, 1980. The primary research emphases at LLNL are numerical modeling of the atmospheric response to stratospheric perturbations and processing and analysis of satellite infrared radiance data to determine global distributions of stratospheric ozone. The modeling effort at LLNL covers three major research areas: photochemical kinetics, coupled kinetics and transport, and radiative transfer. Tasks completed during the past year include: comparison of model simulations of stratospheric composition with observational data, assessments of potential changes resulting from aircraft engine emissions and other perturbations, ozone trend analyses, and assessments of coupled perturbations.

The satellite data processing task has three major areas of effort: (1) radiative transfer and ozone retrieval methodology, (2) data processing, archiving, and distribution, and (3) data analysis, interpretation, and quality assurance. Progress in each of these areas is reviewed. Preliminary data from January and February 1979 were processed for comparison with other data. The retrieval methodology has been finalized, and regular data processing will begin in early 1981.

17. Key Words	18. Distribution Statement
Ozone Perturbations, Ozone Trend, NO_x Injections, Stratospheric Model, Satellite Monitoring, Ozone Data Basing.	Document is available to the public through the National Technical Information Service, Springfield, VA 22161

19. Security Classif. (of this report)	20. Security Classif. (of this page)	21. No. of Pages	22. Price
Unclassified	Unclassified	97	

Form DOT F 1700.7 (8-72) Reproduction of completed page authorized

PREFACE

Since July 1, 1975, Lawrence Livermore National Laboratory (LLNL) has been participating in the High Altitude Pollution Program sponsored by the U. S. Department of Transportation's Federal Aviation Administration. This report describes the major accomplishments and significant findings during the period from October 1, 1979 to December 31, 1980, for work performed at LLNL under Reimbursable Agreement DOT-FA79WAI-034. Two major research areas are covered by this agreement: (1) numerical modeling of the atmospheric response to stratospheric perturbations, and (2) the processing, archiving, and analysis of satellite ozone data. Each of these research areas has been divided into a number of subtasks, and the successful accomplishment of these subtasks has required contributions and cooperation from many participants. The work reported here should be considered the collective effort of all those listed below.

On April 12, 1980, our colleague and friend, Dr. William Duewer, drowned while on one of his frequent family outings to Point Reyes National Seashore to collect clams, mussels, and shells — a hobby reflecting his earlier interest in marine biology. Since joining LLNL in 1972, Bill made many significant contributions to advancing understanding of stratospheric chemistry. In other areas of research, Bill played a leading role in the development, verification and application of a regional air quality model capable of simulating the evolution of photochemical air pollution.

Bill's love of chemistry, his trained, almost intuitive, understanding of chemical kinetics, and his intense desire to determine the reason for everything contributed to his important research accomplishments. It is tragic that he died just when his efforts were becoming so widely recognized. He will be long remembered by his many friends.

Scientific Administration
Joseph B. Knox, Division Leader
Frederick M. Luther, Principal Investigator

Numerical Modeling
Julius S. Chang
William H. Duewer
Joyce E. Penner
Raymond L. Tarp
Donald J. Wuebbles

Satellite Ozone Data Analysis
James D. Ellis
Stanley L. Grotch
Ambrosio R. Licuanan
James E. Lovill
H. Alex Magee
Linda L. Ott
Thomas J. Sullivan
Sandra S. Taylor
Roger L. Weichel
Patrick P. Weidhaas

A-1

CONTENTS

Annual Report of Lawrence Livermore National Laboratory to the FAA on the High Altitude Pollution Program—1980

ABSTRACT

This annual report documents the progress made on research in support of the High Altitude Pollution Program (HAPP) between October 1, 1979 and December 31, 1980. The primary research emphases at LLNL are numerical modeling of the atmospheric response to stratospheric perturbations and processing and analysis of satellite infrared radiance data to determine global distributions of stratospheric ozone. The modeling effort at LLNL covers three major research areas: photochemical kinetics, coupled kinetics and transport, and radiative transfer. Tasks completed during the past year include: comparison of model simulations of stratospheric composition with observational data, assessments of potential changes resulting from aircraft engine emissions and other perturbations, ozone trend analyses, and assessments of coupled perturbations.

The satellite data processing task has three major areas of effort: (1) radiative transfer and ozone retrieval methodology, (2) data processing, archiving, and distribution, and (3) data analysis, interpretation, and quality assurance. Progress in each of these areas is reviewed. Preliminary data from January and February 1979 were processed for comparison with other data. The retrieval methodology has been finalized, and regular data processing will begin in early 1981.

1. INTRODUCTION

This annual report documents the progress made on research in support of the High Altitude Pollution Program (HAPP) between October 1, 1979 and December 31, 1980. Work performed during previous years at Lawrence Livermore National Laboratory (LLNL) is described in our earlier annual reports (Luther et al., 1976, 1977, 1978, 1979a).

The research effort at LLNL is divided between two major areas of investigation: (1) numerical modeling of the atmospheric response to stratospheric perturbations, and (2) the processing, archiving, and analysis of satellite ozone data. Due to the complexity of the system of governing physical and chemical processes, theoretical models of atmospheric trace species distributions are essential tools in perturbation assessment studies related to stratospheric ozone. Models with coupled atmospheric transport and photochemical kinetics are used to assess the potential effects of aircraft engine emissions and other proposed perturbations. Potential perturbations currently under study include NO_x and HO_x from aircraft engine emissions, chlorofluorocarbons (CFC), increases in CH_3CCl_3 and N_2O, and a doubling of CO_2. The effect of coupling between perturbations is also investigated. Because significant new measurements of key chemical reaction rates became available late in fiscal year 1980, the reporting period was extended to include assessments made with updated model chemistry.

In August 1976, LLNL's participation in HAPP was extended to include a feasibility study to determine whether good quality total ozone data could be derived from infrared radiance measurements taken by a multichannel filter radiometer (MFR) sensor carried aboard a series of satellites operated by the U. S. Air Force. These satellites are a part of the Defense Meteorological Satellite Program Block 5D series. The first four satellites in this series carried MFR sensors from which total ozone data can be derived. The first satellite began transmitting MFR measurements in March 1977, and MFR data were received from these satellites until February 1980. These MFR data will be used to determine the temporal and spatial variability of ozone over this period of time.

The feasibility study was completed in May 1978 with the successful processing of 20 days of data taken during 1977. The quality of the derived total ozone data was demonstrated by comparison with corresponding ozone data obtained at selected stations in the world surface network of Dobson spectrophotometer observatories. A description of the methodology used and global maps of the total ozone data for the 20 days are contained in the report by Lovill et al. (1978).

Since completion of the feasibility study, LLNL's effort has been directed toward archiving and processing the MFR data. Before routine data processing could begin, an automated data-basing system had to be developed in order to handle the large volume of data. We have also been evaluating various aspects of the ozone retrieval methodology and making refinements.

The satellite data processing task has three major areas of effort: (1) radiative transfer and ozone retrieval methodology, (2) data processing, archiving, and distribution, and (3) data analysis, interpretation, and quality assurance. Work on these tasks is supported in part by the National Aeronautics and Space Administration (NASA).

2. ATMOSPHERIC MODELING

2.1 Model Simulations Compared with Observations

An important aspect of validating numerical model representations of the physical and chemical processes believed to be occurring in the stratosphere is the comparison of computed values with data from atmospheric measurements. In this section, we compare the results from the current LLNL one-dimensional model with available measurements. The chemistry used in these calculations is that recommended by the NASA Panel on Laboratory Measurements in December 1980 (JPL Publication 81-3, 1981).

The difficulty in developing a diffusion coefficient (K_z) for one-dimensional models that is capable of calculating distributions of all species with long chemical lifetimes (which compare well with observations) was discussed in NASA 1049 (1979), and this problem still exists. Current K_z's designed to fit CH_4 measurements do not compare well with N_2O and CFC data, and vice versa. Because of this, two different K_z's (see Fig. 1) were used in the LLNL model for the comparison with observations. The first is the K_z that has been the standard for the LLNL model since it was developed for the National Academy of Sciences report in 1976 (Chang, 1976). The results using this K_z will be labeled with the

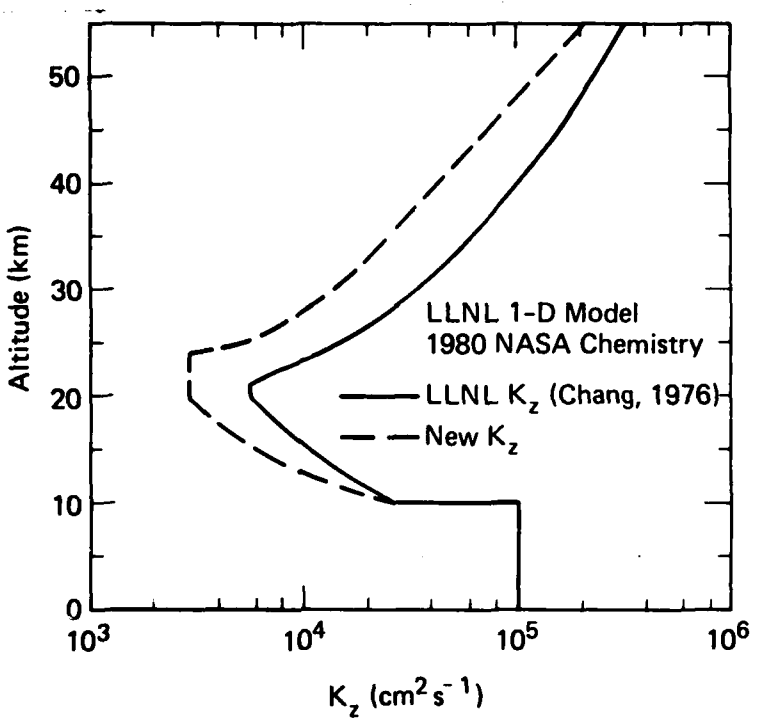

FIGURE 1. Vertical transport coefficients used in LLNL model calculations. The new K_z profile is used for test purposes.

designation LLNL K_z. The second K_z represents a test profile used in the LLNL model to better fit available N_2O and CFC data. A rigorous approach was not used in developing this K_z. It is used here primarily for comparison purposes, and should not be construed as representing the best possible representation.

In the discussion that follows, emphasis is placed on those species comparisons with observations most affected by model changes since NASA 1049 (1979). This discussion is divided into two parts: (1) the long-lived species and (2) the free radicals and other species having relatively short chemical lifetimes. Calculations were made with two different reaction rates for OH + HNO_4. The slower rate (8.0×10^{-13}) is based on the recommendation of the NASA Panel on Laboratory Measurements (1980), and the faster rate (3.0×10^{-12}) is the average of two recent rate measurements: $(4.0 \pm 1.0) \times 10^{-12}$ by Trevor et al. (1980) and $(2.0 \pm 1.0) \times 10^{-12}$ by Littlejohn and Johnston (1980). The slower rate was used in the calculations unless otherwise noted.

2.1.1 Long-Lived Species

Comparisons of one-dimensional model results with observations of species having long chemical lifetimes are shown in Figs. 2 to 11. The distributions of these species are individually affected by transport processes as well as by atmospheric photochemistry. As seen in Fig. 2, the test K_z produces a much better comparison with N_2O data of Goldan et al. (1979) than we get using the LLNL K_z. Similar results are found for CF_2Cl_2 (Figs. 4 and 5), $CFCl_3$ (Figs. 6 and 7) and CH_3Cl (Fig. 8). However, the comparison with CH_4 (Fig. 3) is better with the LLNL K_z, particularly in the upper stratosphere. It is clear that there is a need for more data to corroborate the few measurements at these altitudes. The

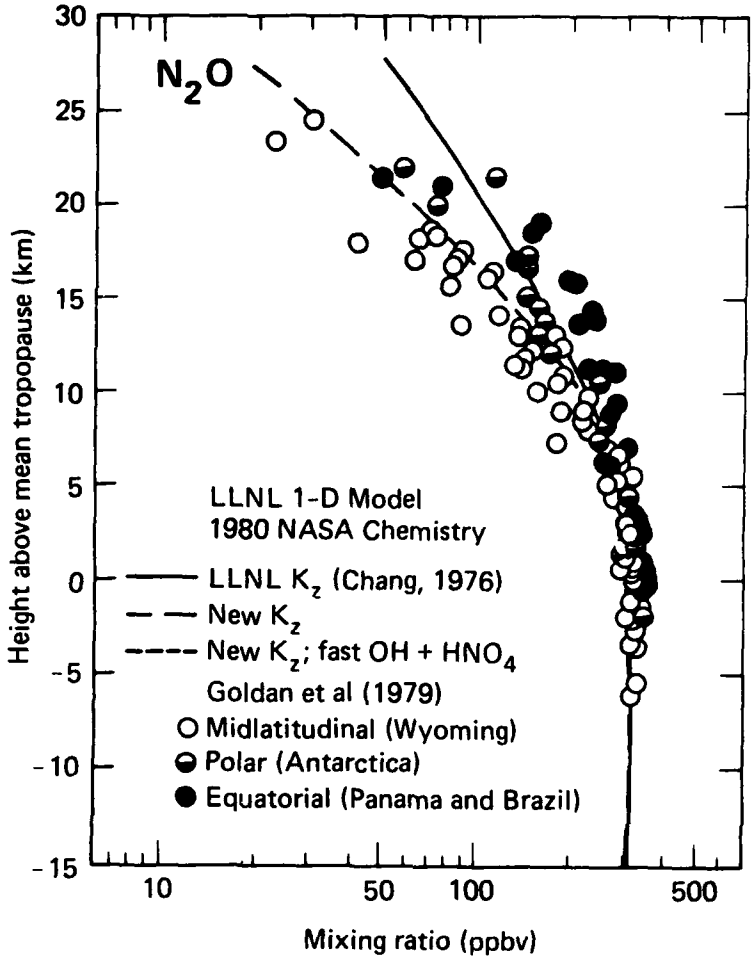

FIGURE 2. Comparison of computed and observed N_2O mixing ratio profiles.

CH_4 measurements by Heidt and Ehhalt (see Ehhalt and Tonnissen, 1980) have not been converted upward based on recent published corrections to their data (Heidt and Ehhalt, 1980).

While the comparison with observations of $CF_2C\ell_2$ with the test K_z is quite good, the distribution of $CFC\ell_3$, while closer to that observed with the test K_z still does not fall off as rapidly with altitude as indicated by the observed data. A better comparison is found with the Schmidt et al. (1980) data at 43°N than with the data of Goldan et al. (1979), which has more of a global coverage, extending from equatorial to polar latitudes. Current two-dimensional models also compare better with the $CF_2C\ell_2$ data than with $CFC\ell_3$ data.

The H_2 concentrations (Fig. 9) fall off rapidly above 20 km with the new K_z. In fact, much more rapidly than the measurements of Ehhalt (1978) and Fabian et al. (1979) indicate. However, H_2 is produced photochemically as well as being destroyed photochemically. Uncertainties in our understanding of stratospheric chemistry may influence the H_2 distribution derived, and may make H_2 unsuitable for evaluating the usefulness of a particular K_z representation at this time. Examining the model results with measured CO data (Fig. 10) gives no clear indication of which K_z profile produces the better results.

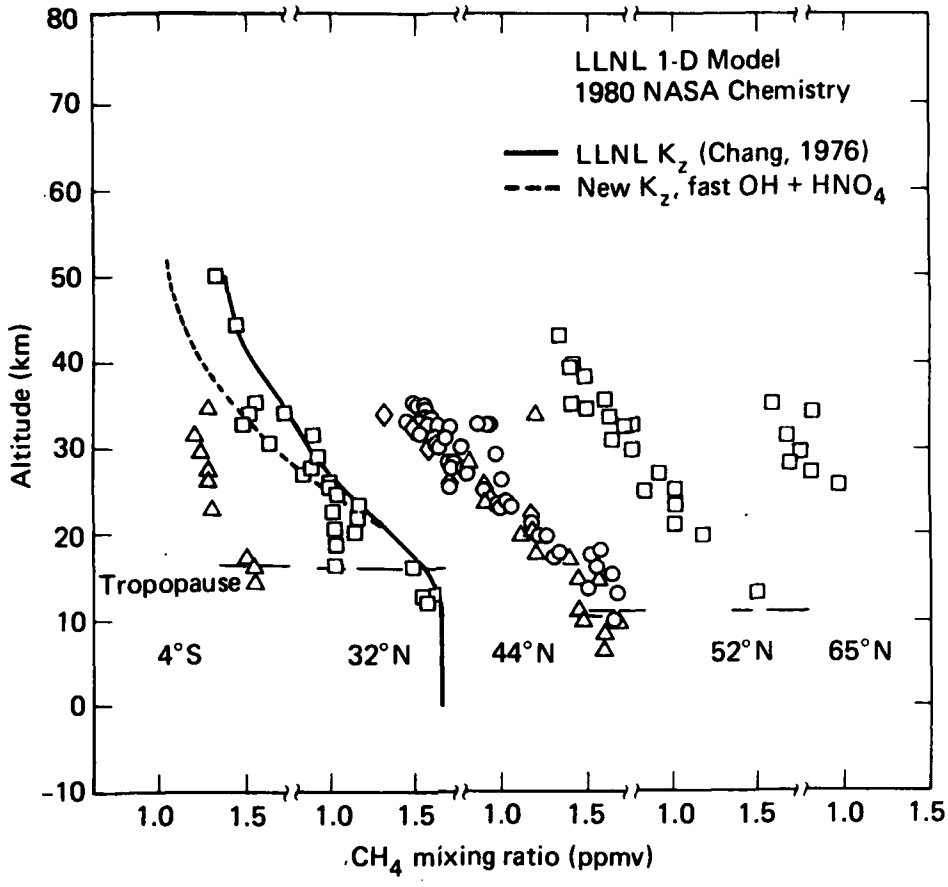

FIGURE 3. Comparison of computed and observed CH_4 mixing ratio profiles.

Model calculated ozone concentrations using the LLNL and new test K_Z profiles are shown in Fig. 11. Both K_Z's give a reasonable comparison with available ozone data.

In summary, because only a few upper atmospheric measurements of CH_4 have been made and because of possible uncertainties in both CH_4 and H_2 chemistry, it would seem that a slower transport representation such as the test K_Z produces better comparison overall than the LLNL K_Z. However, the absorption cross sections for photolysis of N_2O, $CF_2C\ell_2$ and $CFC\ell_3$ lie primarily in the region of the O_2 Schumann-Runge bands. Because of potential errors both in the measurements of the fine structure of the Schumann-Runge bands and in the model representation of O_2 absorption in these bands, the photolysis rates of these three species may be sufficiently uncertain in the stratosphere to make the best choice of K_Z difficult. Although other tracers (e.g., ^{14}C) have been suggested for developing transport coefficients for the one-dimensional models, measurements of these tracers are sufficiently poor to make these comparisons inconclusive. At present, therefore, the development of a single K_Z to best represent global averaged distributions of long-lived trace species remains subjective.

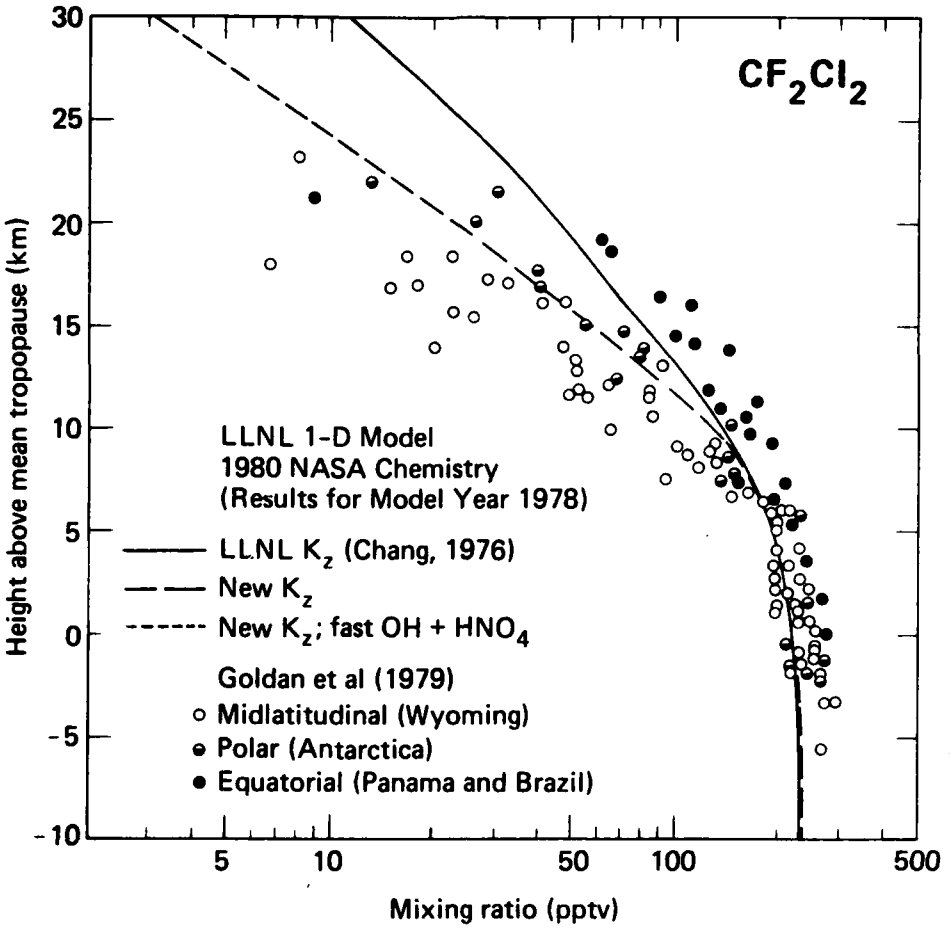

FIGURE 4. Comparison of computed $CF_2C\ell_2$ mixing ratio profiles with observations made at various latitudes.

2.1.2 Free Radicals and Other Short-Lived Species

Comparison of one-dimensional model results with measurements of free radicals is much improved over NASA 1049 (1979). Changes in model chemistry, particularly in reducing lower stratospheric HO_x concentrations, have, for example, resulted in improved comparisons with the $C\ell O$ observations of Anderson et al. (1980) and with the measured ratio of HNO_3 to NO_2 derived from the data of Evans et al. (1976), Harries et al. (1976), and Harries (1978).

2.1.2.1 HO_x species. Comparisons with the few available measurements of OH and HO_2 in the upper stratosphere (Figs. 12 and 13) still remain excellent. However, in the lower stratosphere where the new chemistry has greatly reduced concentrations of OH and HO_2, there are no measurements.

2.1.2.2 NO_x species. Figures 14 to 18 show comparison of model results with measurements of NO, NO_2, HNO_3 and HNO_4. While NO and NO_2 concentrations are still high compared to some of the published data, the overall comparison is much better than found in 1979 (e.g., see discussion in NASA 1049 or Luther et al., 1979). Calculated HNO_3 concentrations still appear to be too high when compared to observations above 25 km. The HNO_3/NO_2 ratio (Fig. 17) is much closer to that observed by Evans et al. (1976) near sunset and that observed by

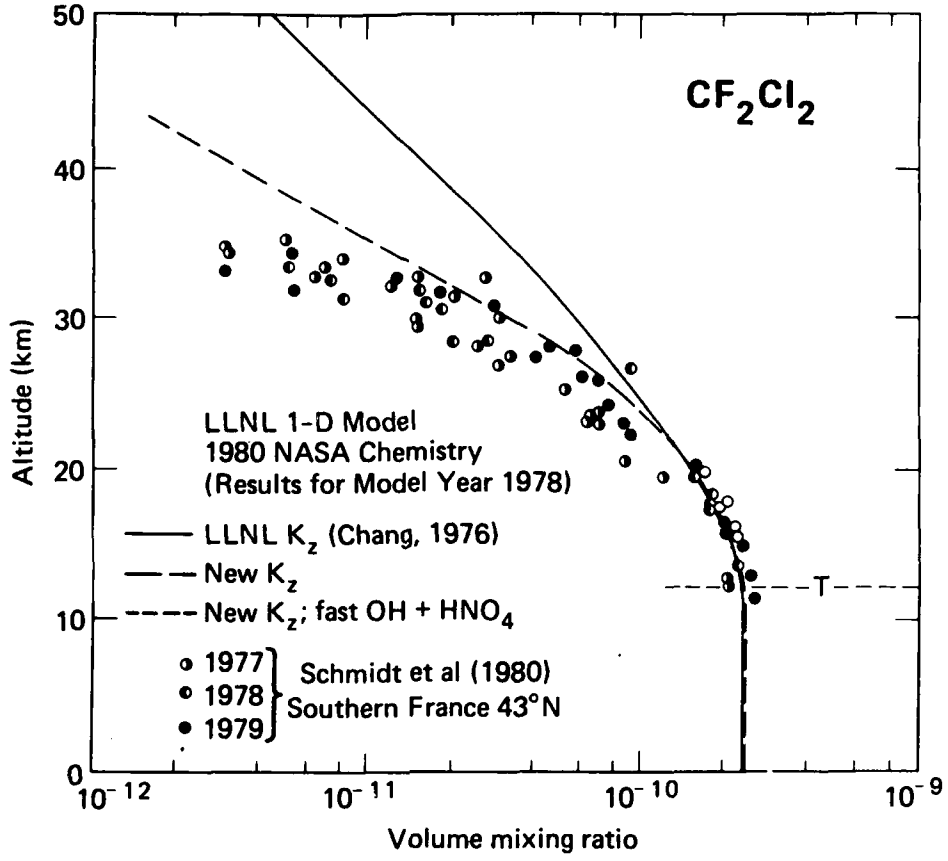

FIGURE 5. Comparison of computed $CF_2C\ell_2$ mixing ratio profiles with observations made in 1977, 1978 and 1979 at the same latitude.

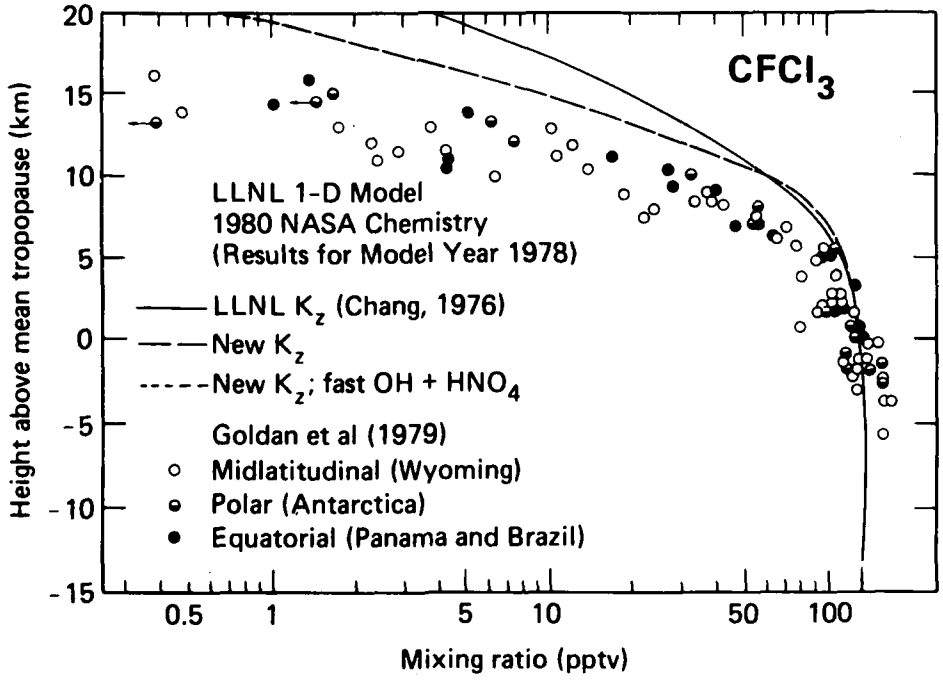

FIGURE 6. Comparison of computed $CFC\ell_3$ mixing ratio profiles with observations made at various latitudes.

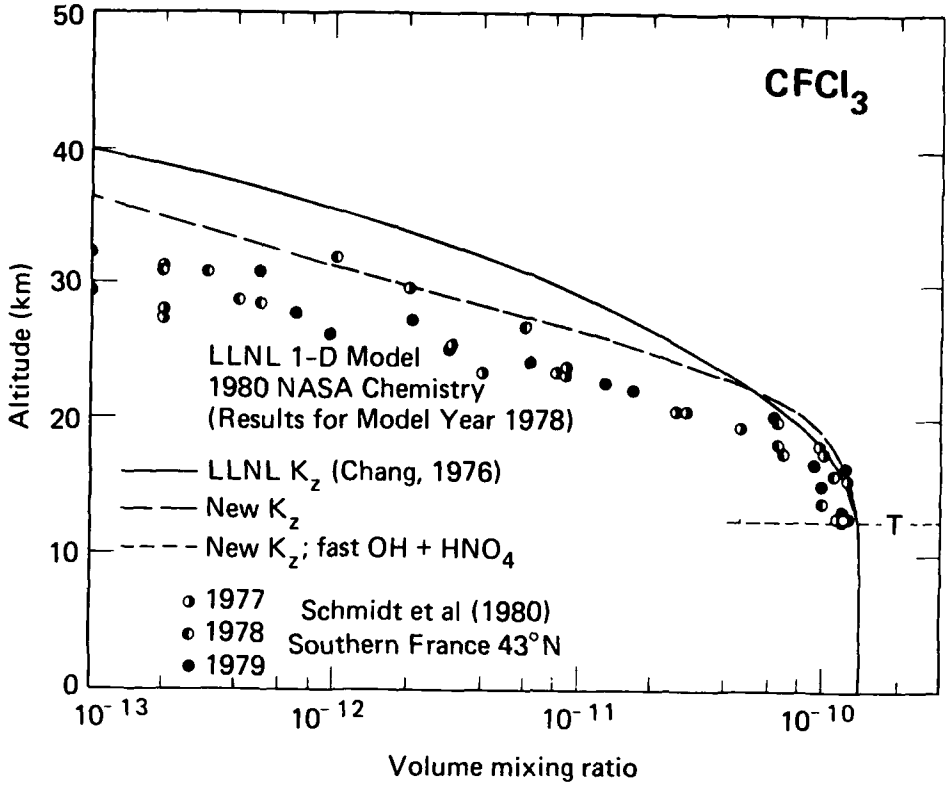

FIGURE 7. Comparison of computed $CFC\ell_3$ mixing ratio profiles with observations made in 1977, 1978 and 1979 at the same latitude.

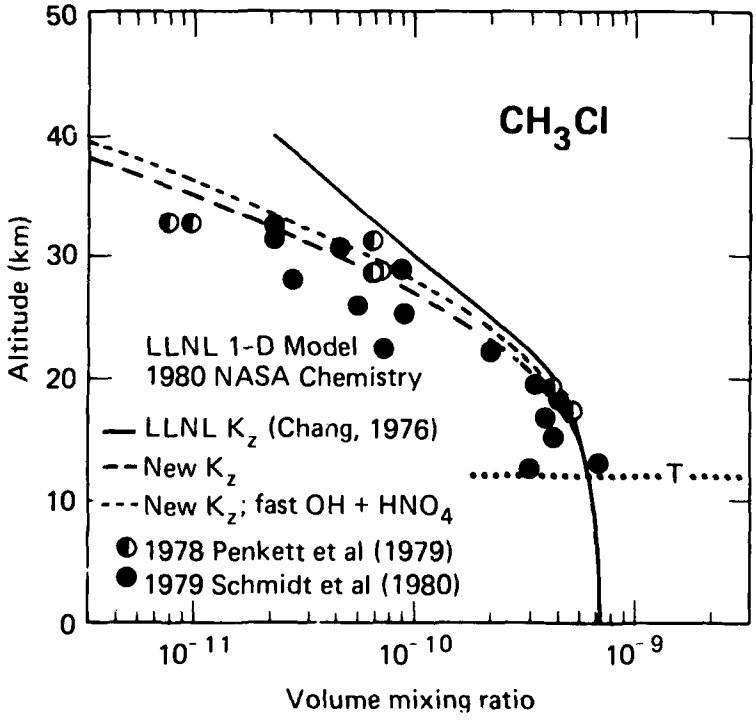

FIGURE 8. Comparison of computed and observed $CH_3C\ell$ mixing ratio profiles.

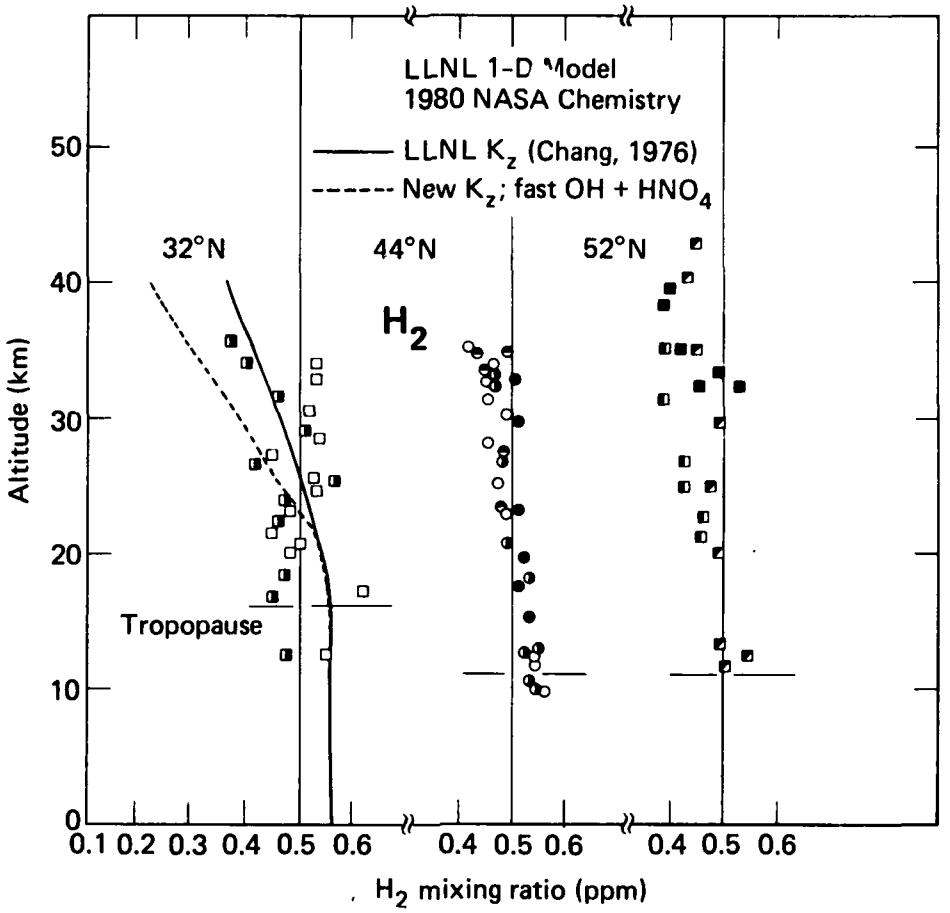

FIGURE 9. Comparison of computed and observed H_2 mixing ratio profiles.

Harries (1978) at noon. However, because HNO_3 has a much longer chemical lifetime than NO_2, it is strongly influenced by atmospheric transport processes. Therefore, because the measurements of NO_2 and HNO_3 may be from different air masses, any agreement between existing measurements and theory for the ratio HNO_3/NO_2 may be fortuitous. Using the cross-sections for HNO_4 photolysis measured by Molina and Molina (1980), we compute peak HNO_4 concentrations that are higher than the upper limit suggested by Murcray (1979). However, use of a faster rate for OH + HNO_4 of 3.0×10^{-12} decreases the peak HNO_4 mixing ratio from 1.5 to 1.0 ppb for the chemistry used, but the peak concentration is still above the suggested upper limit.

2.1.2.3 $\underline{Cl O_x}$ species. Figures 19 and 20 show comparisons of model results with measurements of ClO and HCl. A much better comparison of the calculated ClO distribution with measurements is found with the new results than was previously (i.e., NASA 1049 or Luther et al., 1979). The improved comparison results primarily from the reduced hydroxyl radical in the lower stratosphere (destroying less CH_3Cl and CH_3CCl_3 and changing the partition between Cl + ClO and HCl in this region). While the data still suggest a sharper slope in the lower stratosphere than calculated, the calculated slope is nonetheless much closer to that measured than was the case with previous results. A possible discrepancy may exist in the upper stratosphere where the model results suggest a sharper decrease with altitude than is indicated by the data. More data above 40 km are needed to verify the concentration profile in this region.

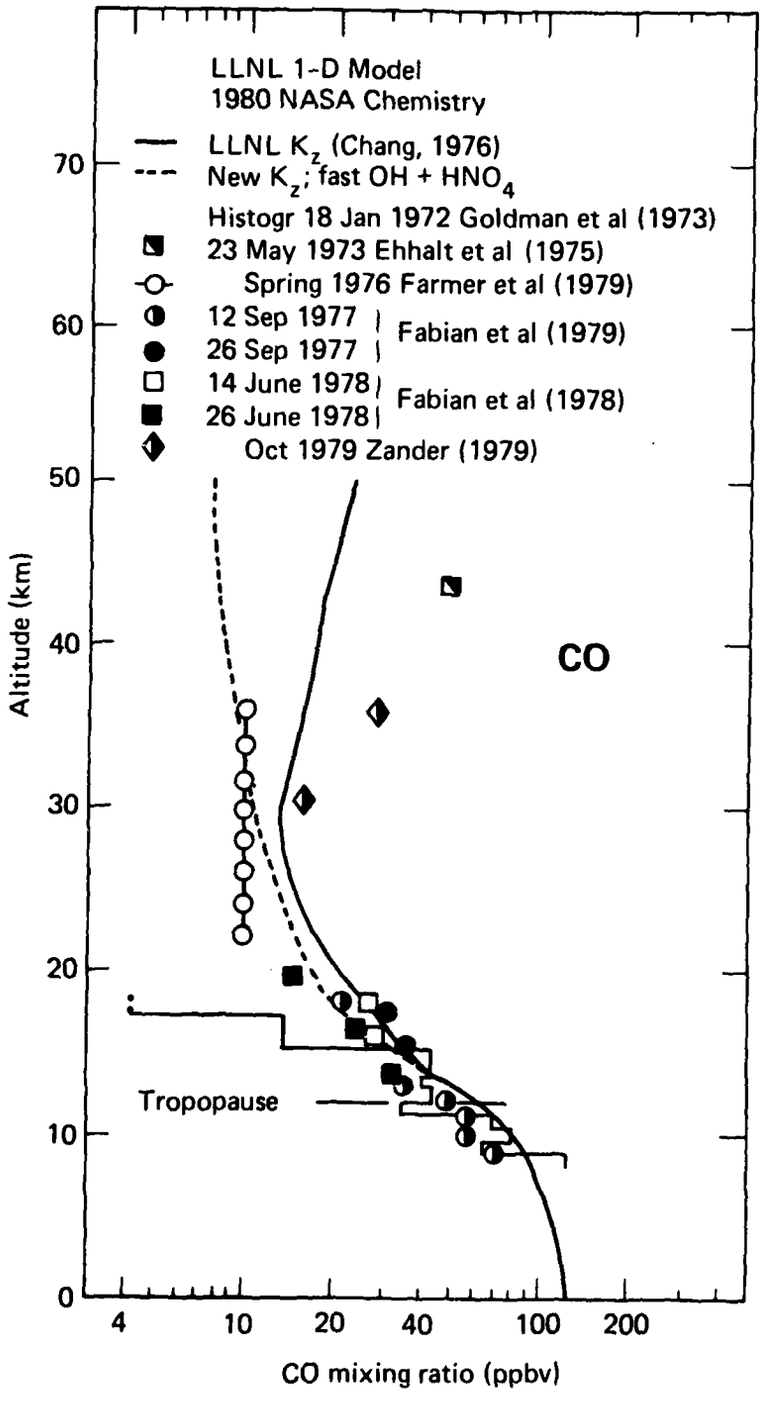

FIGURE 10. Comparison of computed and observed CO mixing ratio profiles.

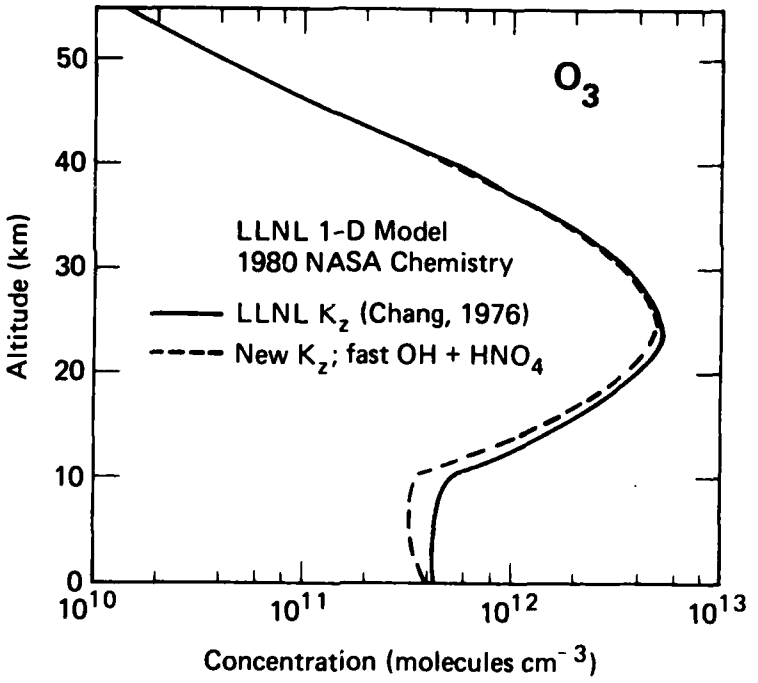

FIGURE 11. Computed concentration profiles of O_3.

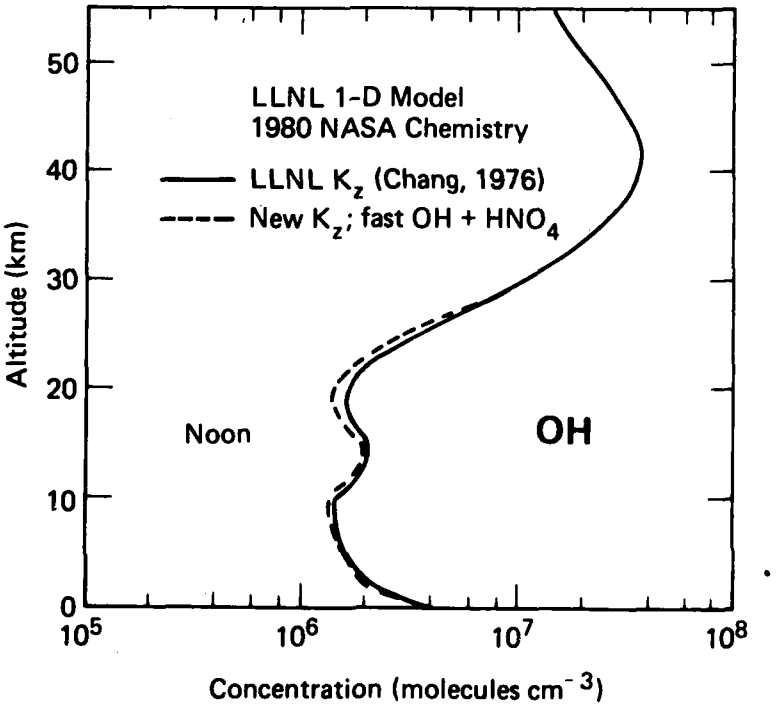

FIGURE 12. Computed concentration profiles of OH.

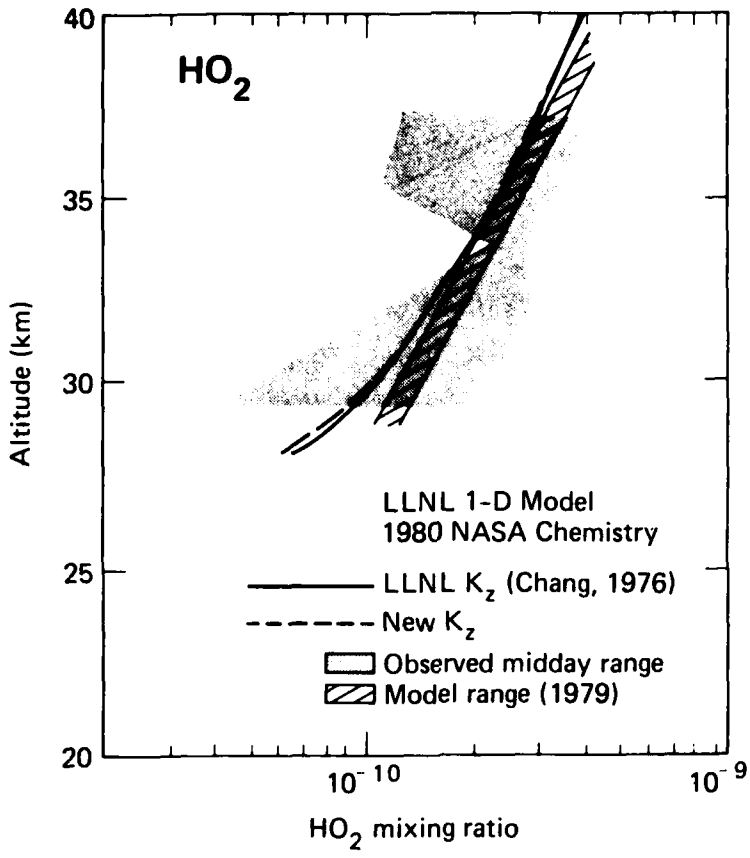

FIGURE 13. Comparison of computed and observed HO_2 mixing ratio profiles. The model range refers to that reported in NASA 1049 (1979).

A good comparison with the measurements of $C\ell ONO_2$ (Fig. 21) by Murcray et al. (1979) still exists if the fast rate of $C\ell ONO_2$ formation is used. Peak concentrations are approximately a factor of three less if the slower rate is used.

2.2 Potential Changes in Ozone Caused by Aircraft Emissions

The LLNL one-dimensional transport-kinetics model has been used to assess the potential effects of NO_x and H_2O emissions from aircraft on the troposphere and stratosphere. Calculations were made using projected fleet sizes for subsonic and supersonic aircraft as well as for a range of emission rates at particular injection altitudes. The details of how emission profiles for the various scenarios were developed are contained in a previous report (Luther et al., 1979) and will only be briefly discussed in this report.

In all of the perturbation calculations to be discussed, the "ambient" or "unperturbed" atmospheric conditions refer to the model-calculated initial state rather than to atmospheric measurements. The change in ozone calculated for the perturbation is relative to this "ambient" state.

As mentioned previously in Section 2.1, two different transport coefficients (K_z) are examined in this report. We use the K_z which has been the standard

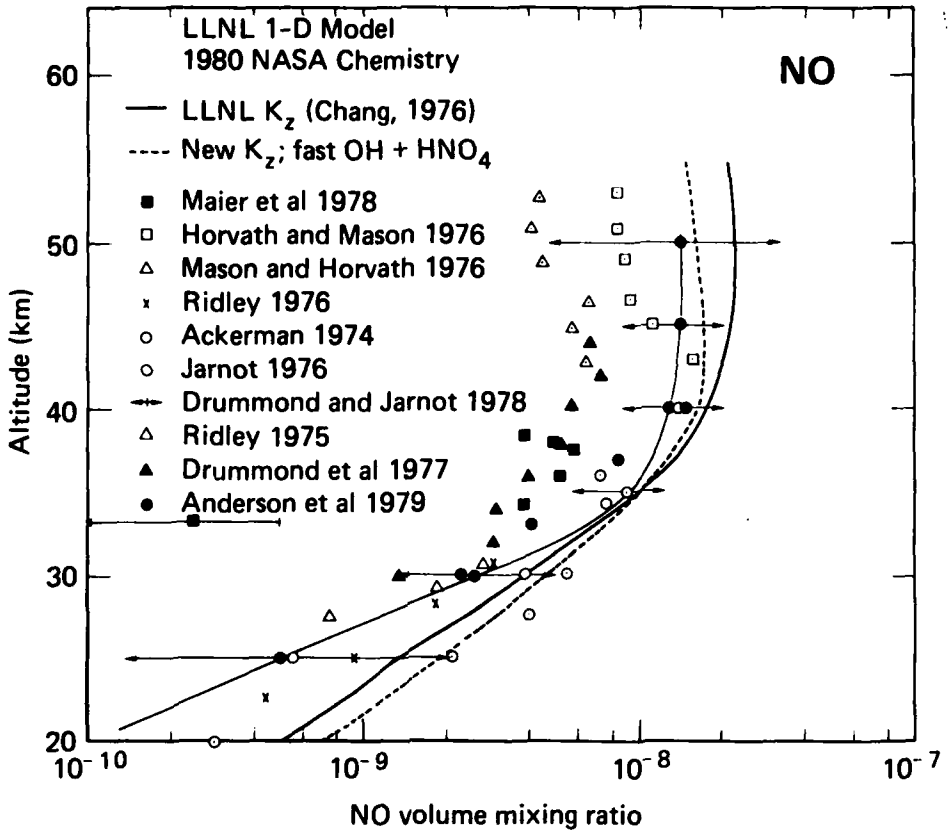

FIGURE 14. Comparison of computed and observed NO mixing ratio profiles.

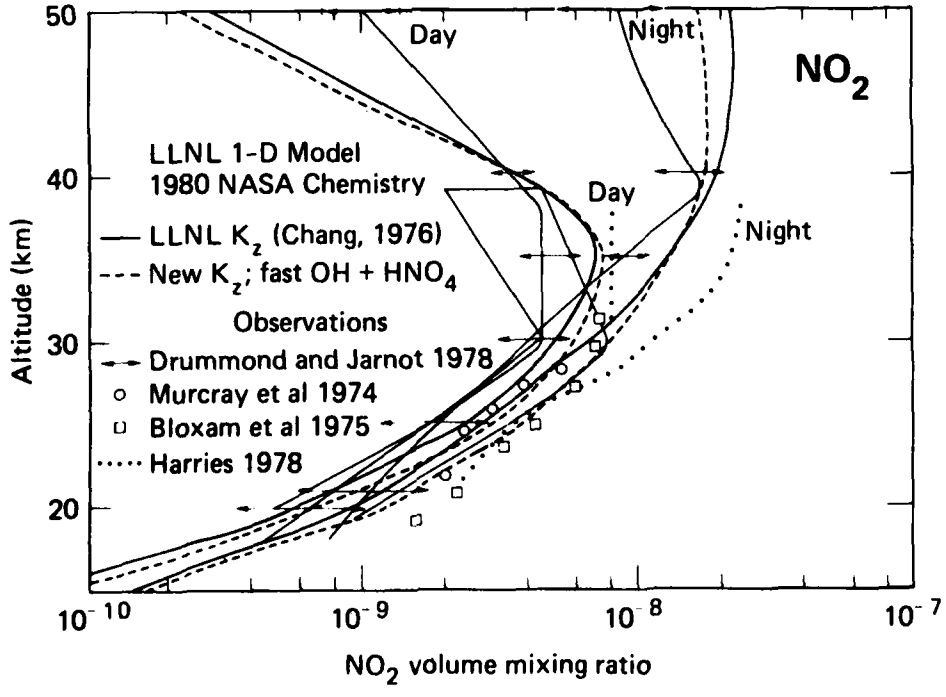

FIGURE 15. Comparison of computed and observed NO_2 mixing ratio profiles.

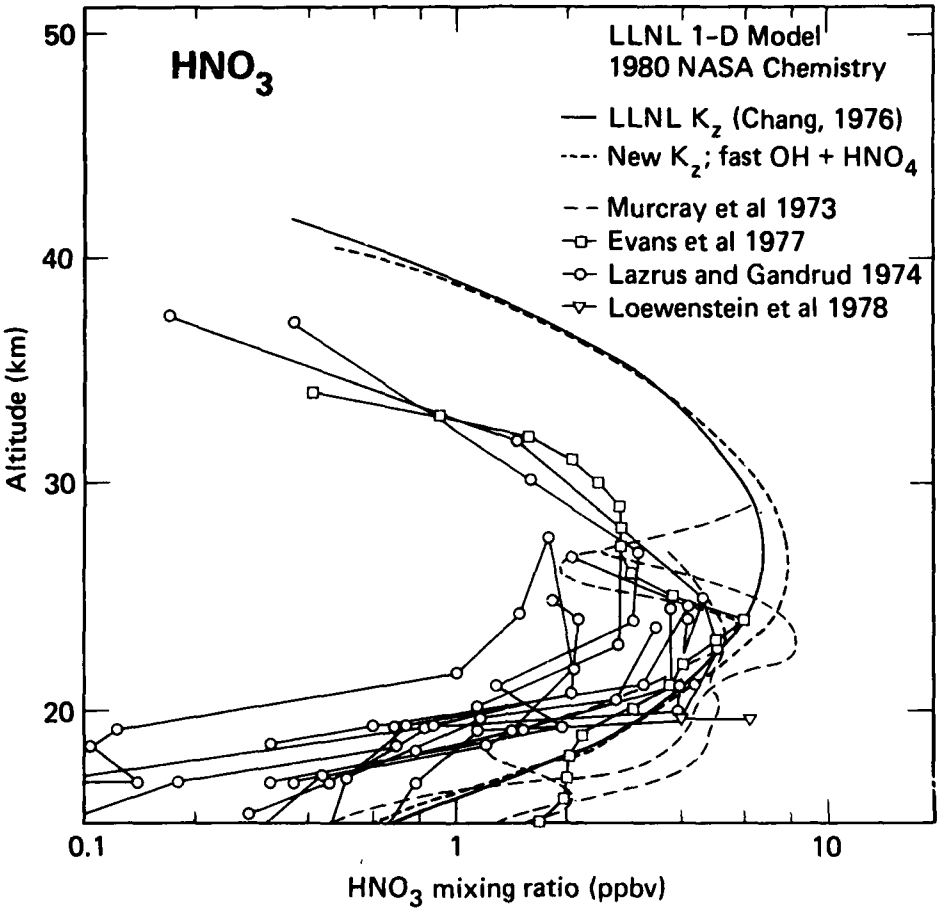

FIGURE 16. Comparison of computed and observed HNO_3 mixing ratio profiles.

(Chang, 1976) at LLNL in recent years and a new "test" K_Z, which is designed to produce a better fit with available N_2O and CFC data. The LLNL standard K_Z still fits available CH_4 data better than the new K_Z. Many of the potential atmospheric perturbations examined were calculated with both K_Z's.

2.2.1 Subsonic and Supersonic Aircraft Fleets

Modifications to model chemistry since the previous evaluation in Luther et al. (1979) greatly affects the change in total ozone expected from subsonic and supersonic aircraft emissions. Table 1 shows the effect on total ozone at steady state from NO_X injections of 1000 and 2000 molecules $cm^{-3}s^{-1}$ distributed over a 1-km-thick layer, centered at the injection altitude for a number of different altitudes of injection. These injection altitudes correspond to typical flight altitudes of various existing or proposed subsonic and supersonic (SST) aircraft. These rates of injection are standard values used for comparison purposes and are not intended to correspond to a particular fleet size.

The results in Table 1 can be contrasted to the results in Luther et al. (1979), in which the 17 and 20 km injections of 1000 molecules $cm^{-3}s^{-1}$ of NO_X resulted in a change in total ozone of +1.34% and +1.31%, respectively, for the LLNL K_Z. The current results show a change in total ozone of +0.01% and -2.0%,

TABLE 1. The change in total ozone resulting from NO_x injections distributed over a 1-km-thick layer centered at the injection altitude.

Injection altitude (km)	NO_x injection[a] rate ($cm^{-3}s^{-1}$)	Change in total ozone (%)	
		LLNL K_z (Chang, 1976)	"Test" K_z
9	2000	+0.5	+0.7
11	2000	+0.8	+1.1
13	2000	+0.9	+1.4
17	1000	+0.01	-0.2
	2000	-0.7	-2.1
20	1000	-2.0	-4.2
	2000	-5.3	-11.1

[a] Rate of emission over a 1-km-thick layer centered at the injection altitude; base model has current level of CFCs.

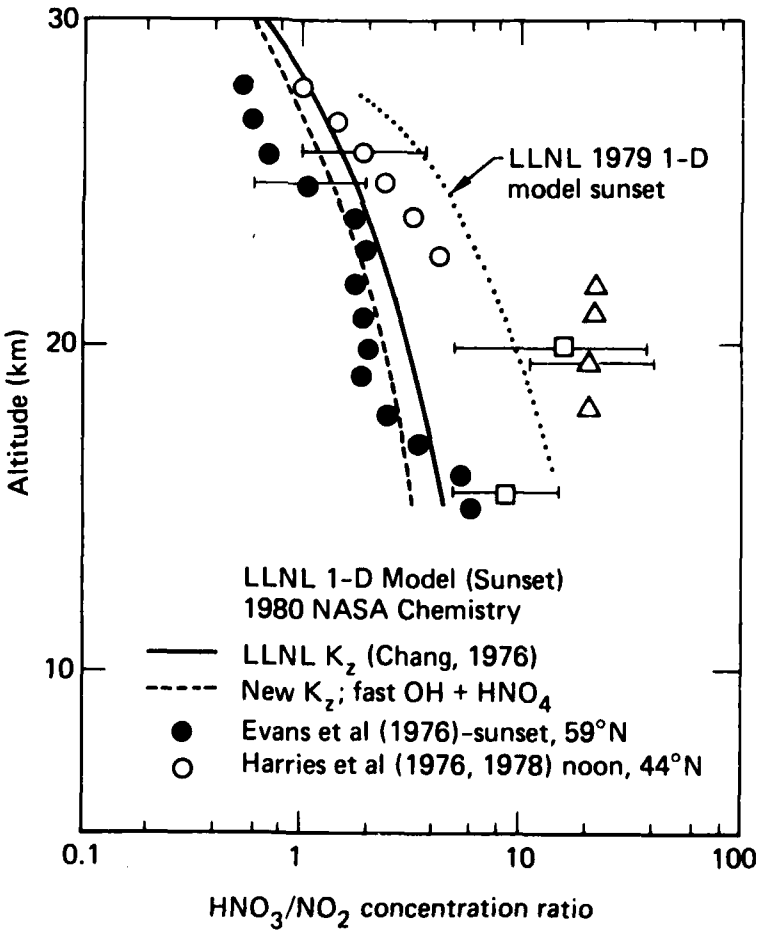

FIGURE 17. Comparison of computed and observed HNO_3/NO_2 concentration ratios.

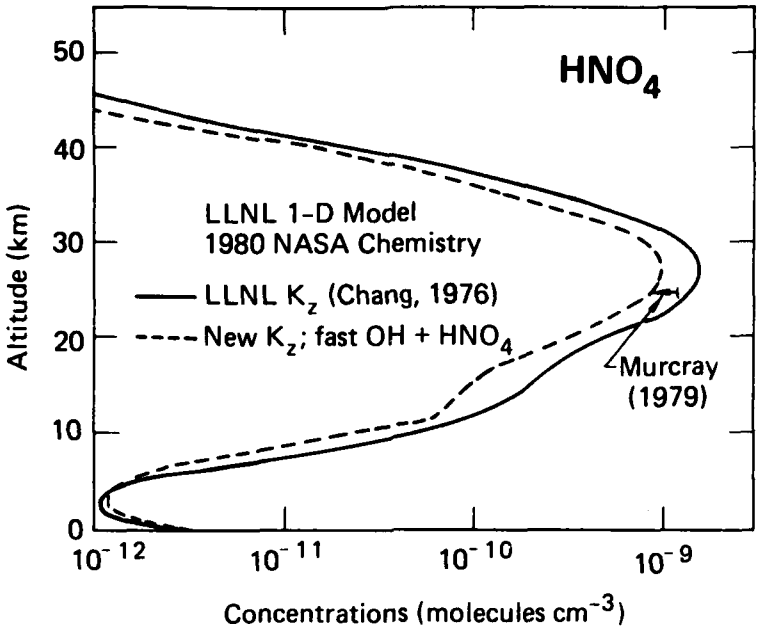

FIGURE 18. Computed HNO_4 concentration profiles compared with the upper limit of Murcray (1979).

respectively, for these two cases. In general, the calculated NO_x-induced perturbations to total ozone are much less positive than in 1979, and for some altitudes and injection rates, the perturbations to total ozone have changed sign. As has been seen previously, the altitude of injection has a significant effect on the computed change in total ozone because of the increase in residence time with altitude, and because of the variation with altitude of the dominant chemical reactions and cycles. Emissions from subsonic aircraft are still expected to result in a net production of total ozone.

Figures 22-24 show the local changes in ozone calculated corresponding to several of the NO_x perturbations listed in Table 1. The increases of local ozone in the lower stratosphere and decreases in upper stratospheric ozone still persist, but with different relative magnitudes than before. However, the importance of the HO_x catalytic cycles in the lower stratosphere has been reduced by the recent chemistry modifications, particularly due to the rate changes for OH + HNO_3, OH + H_2O_2 and OH + HNO_4, which result in reduced HO_x levels in this region. Because of these reduced HO_x levels, the positive changes in ozone previously found in the lower stratosphere due to NO_x injections are greatly reduced. Also, the relative importance of the NO_x catalytic cycle in the upper atmosphere has increased.

Figures 25 and 26 show the change in total ozone column computed as a function of NO_x injection rate for 17- and 20-km injection altitudes. For injection rates less than 1000 molecules $cm^{-3}s^{-1}$, the 17-km injection results in a net increase in total ozone. Progressively larger decreases in total ozone were found for injection rates greater than 1000 molecules $cm^{-3}s^{-1}$. The 20-km injection produces a net reduction in ozone for all injection rates. While the change in ozone is nonlinear for both the 17 and 20 km injections at injection rates less than 1000 molecules $cm^{-3}s^{-1}$, both are nearly linear at higher injection rates.

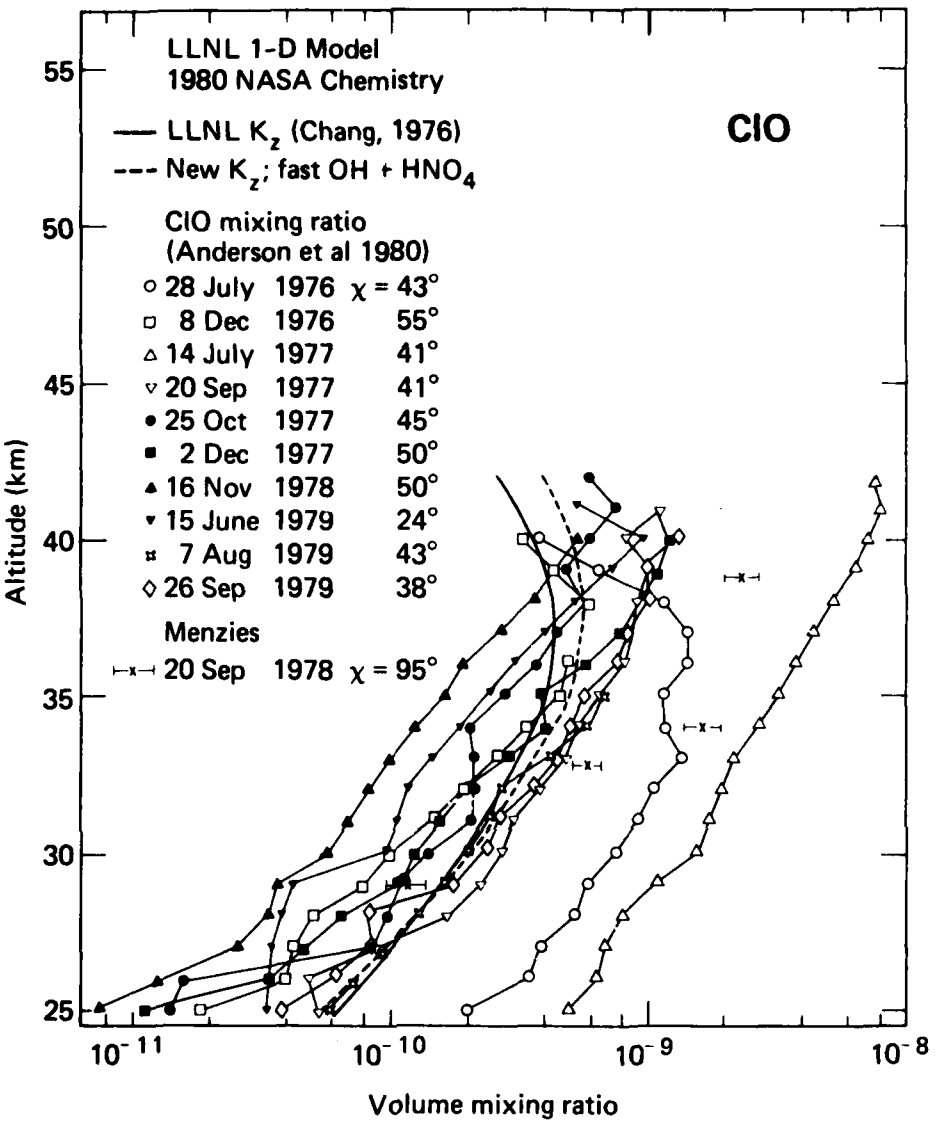

FIGURE 19. Comparison of computed and measured ClO mixing ratio profiles.

Table 2 shows the NO_x emission rates as a function of injection altitude that were used to estimate the potential impact of 1990 aircraft fleet emissions. As with the similar calculations in Luther et al. (1979), these emission rates are based on the Oliver et al. (1977) high 1990 fleet estimate.

The effect of NO_x emissions by subsonic and supersonic fleets projected for 1990 are given in Table 3 and Fig. 27. In 1979, we calculated a net increase in ozone for the 1990 fleet of 2.0% using the LLNL K_z. The change in total ozone now found is 1.3% with both the LLNL K_z and new test K_z.

Assessments of potential changes in ozone due to future large fleets of supersonic aircraft have focused on injection altitudes of 17 and 20 km. In addition to the NO_x injections discussed earlier, we have also reexamined the effect on total ozone of including both the NO_x and H_2O injections that would be expected from supersonic aircraft. We have assumed an emission index of 18 g/kg

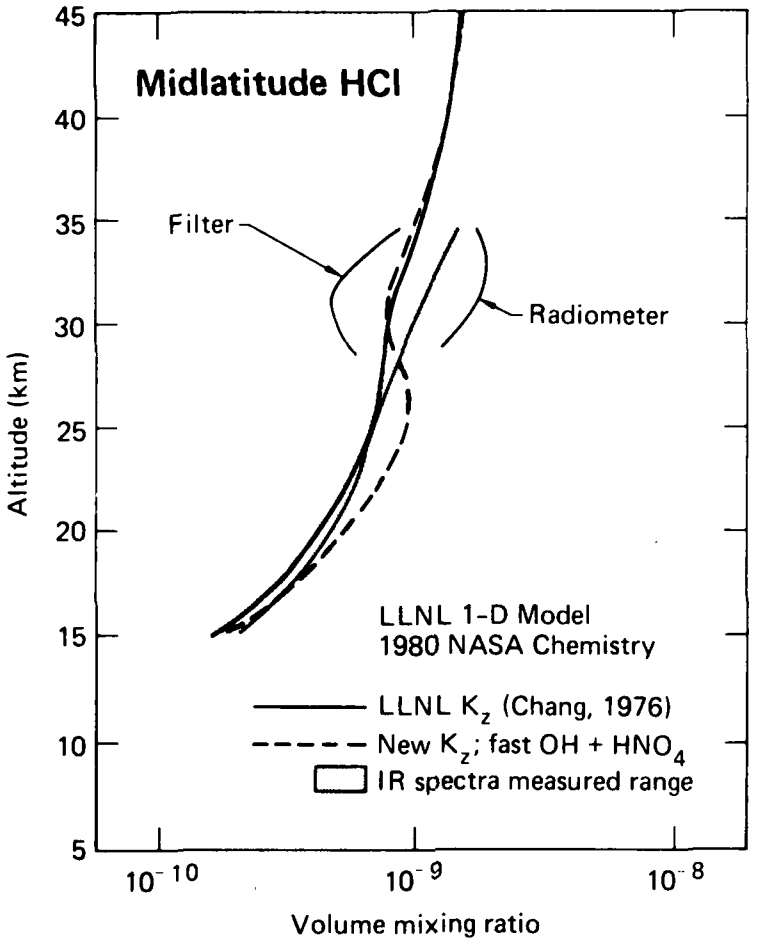

FIGURE 20. Comparison of computed and observed HCℓ mixing ratio profiles.

fuel for NO_x and 1250 g/kg fuel for H_2O. These are based on current engine technology. We have also assessed the impact of future advances that may result in approximately one-third as much NO_x being emitted. The effect of the combined NO_x and H_2O injections on total ozone is shown in Table 4. The effect of including H_2O injections is opposite to that found in Luther et al. (1979). Because of the reduced relative importance in the ambient atmosphere of the HO_x catalytic cycle and increased importance of the NO_x catalytic cycle, the added water vapor now slightly increases total ozone compared to NO_x perturbation only. For the 17-km injection, the added water vapor has only a very small effect (approximately 0.1% change with the new test K_z). For the 20-km injection, the added water vapor results in a smaller decrease in total ozone (relative to NO_x injection only) by 0.2% for the LLNL K_z and 0.6% for the new test K_z.

Two different estimates for the expected NO_x and H_2O emissions from a fleet of 500 Boeing-type supersonic transports are given in the CIAP Report of Findings (Grobecker et al., 1974). The early estimate, based on Johnston (1971), assumes 7.5 h/d cruising at 20 km with a fuel flow of 60,000 kg/h and emissions of 1360 kg/h of NO_x. The NO_x and H_2O emissions as a function of altitude corresponding to this fleet are shown in Table 5 (labeled Case 1). A ratio of 141 molecules of water/NO_x molecule is assumed in this case. The other estimate (labeled Case 2 in Table 5) assumes 4.5 h/d at cruising altitude with a fuel flow of 52,000 kg/h and 560 kg/h of NO_x. A ratio of 296 molecules of H_2O per NO_x

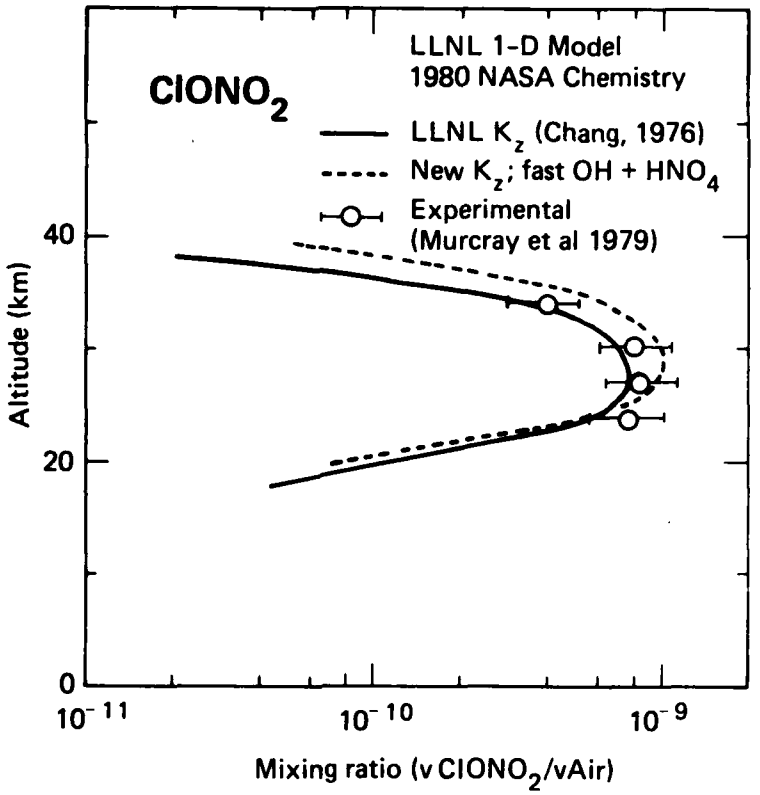

FIGURE 21. Comparison of computed and observed $C\ell ONO_2$ mixing ratio profiles.

TABLE 2. Projected 1990 aircraft emissions of NO_x (Oliver et al., 1977) (high estimate) used in this study.

Injection altitude (km)	NO_x injection rate total fleet (molecules $cm^{-3}s^{-1}$)
6	90
7	179
8	265
9	665
10	1167
11	1161
12	520
13	75
14	18[a]
15	18
16	33
17	43
18	29
19	8

[a]Emissions from the projected 1990 SST fleet are included at 14 km and above.

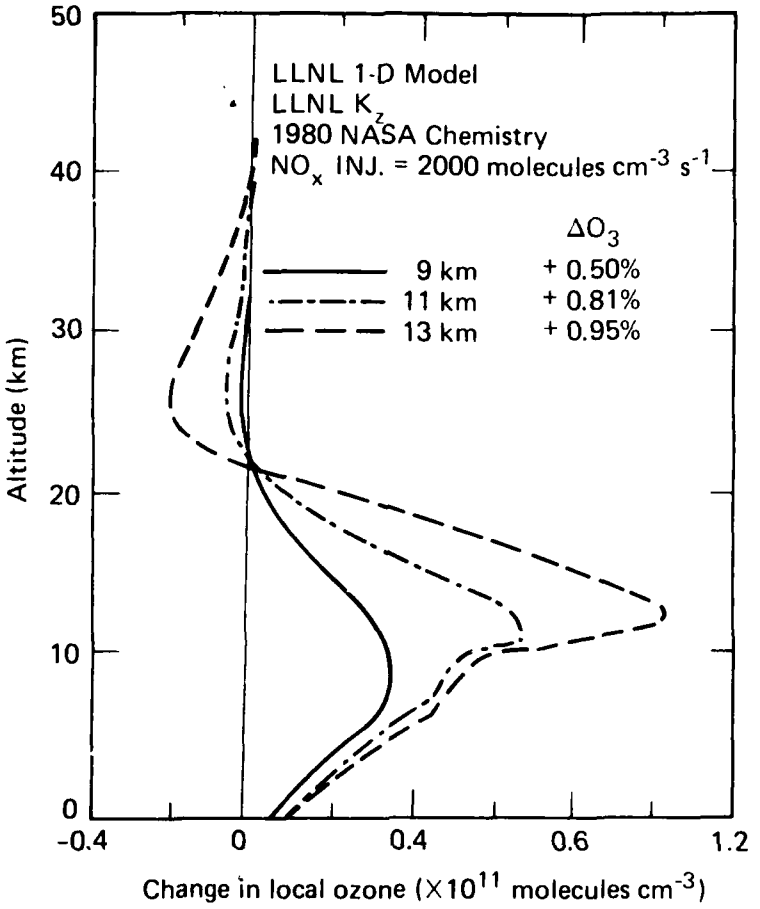

FIGURE 22. The change in local ozone concentration due to NO_x injections of 2000 molecules $cm^{-3}s^{-1}$ over a 1-km thick layer centered at 9, 11, or 13 km.

TABLE 3. Change in total ozone at steady state computed for projected 1990 aircraft fleet emissions of NO_x.

Model	ΔO_3(%)
LLNL K_z NASA chemistry	+1.27
New test K_z NASA chemistry with fast OH + HNO_4 ($k = 3.0 \times 10^{-12}$)	+1.36

molecule is assumed in Case 2. The calculated change in total ozone for these two cases is also shown in Table 5. A change in total ozone of -5.5% was computed for Case 1 and -0.8% for Case 2.

2.2.2 Comparison with Past Results

Table 6 and Fig. 28 provide a summary of previous LLNL assessments of the effects of supersonic transport operations based on an injection of 2000 molecules (NO) $cm^{-3}s^{-1}$ distributed over a 1-km-thick layer centered at 17 or 20 km. The results in Table 6 are based on published calculations made with the LLNL

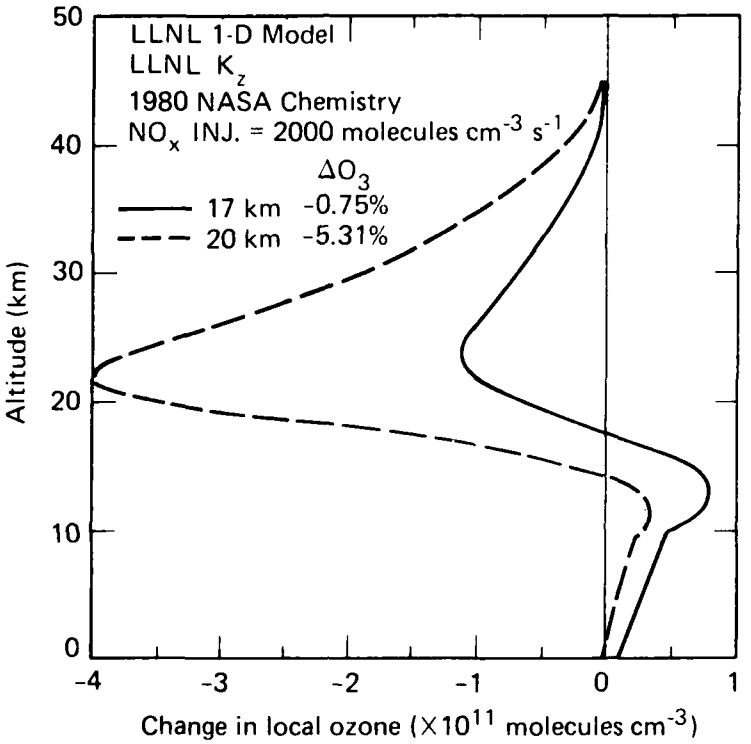

FIGURE 23. The change in local ozone concentration due to NO_x injections of 2000 molecules $cm^{-3}s^{-1}$ over a 1-km thick layer centered at 17 or 20 km.

TABLE 4. The change in total ozone due to NO_x and H_2O emissions distributed over a 1-km-thick layer centered at the injection altitude.

Injection altitude (km)	Injection rate (molecules $cm^{-3}s^{-1}$)		Change in total ozone (%)	
	NO_x	H_2O	LLNL K_z	New test K_z
17	1000	0	+0.01	-0.2
	1000	177000	+0.04	-0.1
	333	177000	+0.08	+0.2
20	1000	0	-2.0	-4.2
	1000	177000	-1.8	-3.6
	333	177000	-0.5	-0.7

one-dimensional model since mid-1974. These results demonstrate the combined effects of the evolution of our understanding of stratospheric chemistry and evolution of the treatment of physical phenomena in the one-dimensional model.

Figure 28 shows the local change in ozone calculated for 17 km injections for four calculations dating from early 1975 to the present (October 1980). Only negative changes in local ozone were found in the early 1975 results. By late 1975, the positive region in the lower atmosphere had appeared due to increased

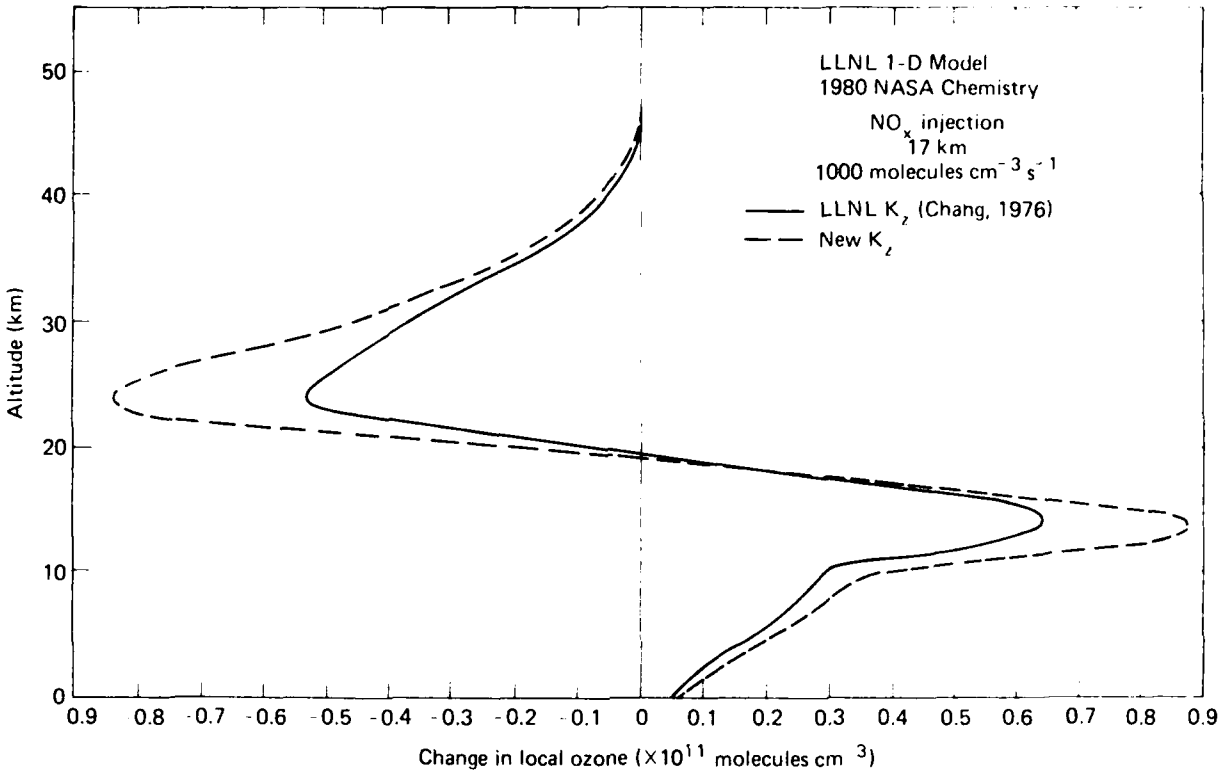

FIGURE 24. The change in the local ozone concentration due to an NO_X injection of 1000 molecules $cm^{-3}s^{-1}$ at 17 km computed using different K_Z profiles.

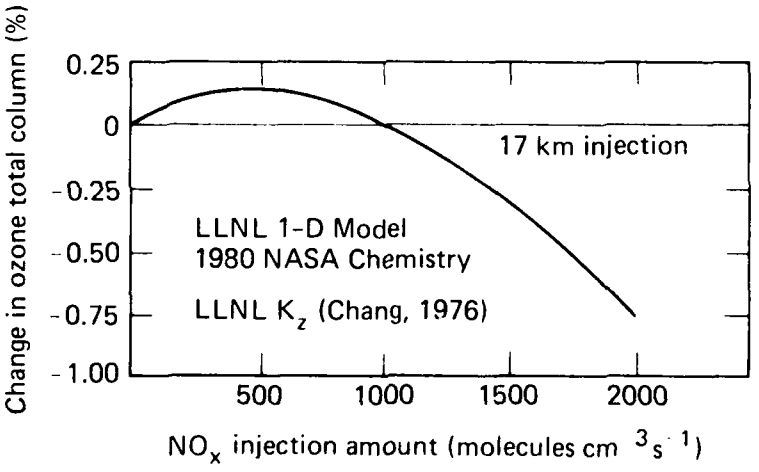

FIGURE 25. The change in total ozone at steady state versus the NO_X injection rate at 17 km altitude.

importance of HO_X. However, an increase in total ozone was not calculated until the reaction HO_2 + NO was found to be quite fast in mid-1977.

The historical record shows that model predictions have changed significantly over the last six years. Although we have greatly improved our understanding of the chemical and physical processes that determine the ozone distribution in the troposphere and stratosphere, there is little that suggests similar changes in model sensitivity might not occur in the future.

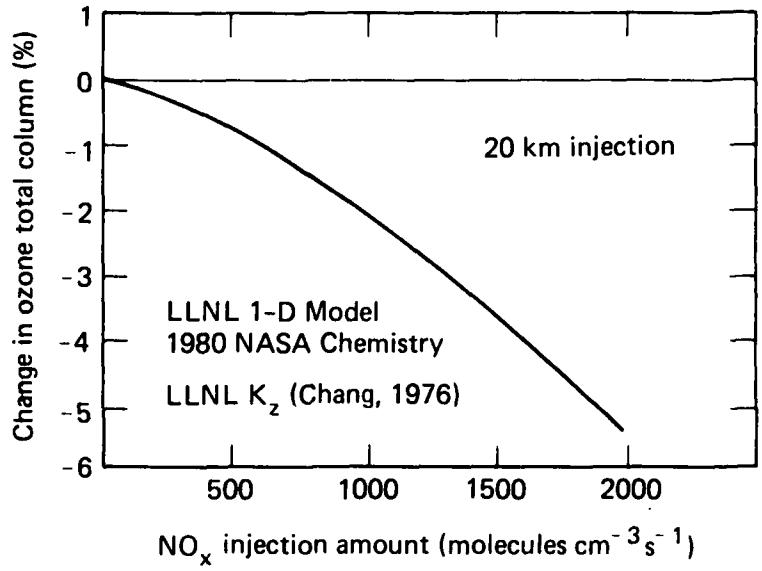

FIGURE 26. The change in total ozone at steady state versus the NO_x injection rate at 20 km altitude.

TABLE 5. Effect of estimate from CIAP Report of Findings (Grobecker et al., 1974) for emissions from a fleet of 500 Boeing-type SSTs on total ozone.

	Case 1	Case 2
Fuel flow, kg/h - SST	60,000	52,000
Cruise h/d - SST	7.5	4.5
Fuel flow, kg/yr	7.67E10	4.27E10
Emission index NO_x (as NO_2), g/kg	22.7	10.8
NO_x emission (as NO_2), kg/yr	1.75E9	4.60E8
H_2O emission, kg/yr	9.59E10	5.34E10
Molecules NO_x cm^{-3} s^{-1} (1 km) (hemisphere)	2826[a]	749[a]
Change in total ozone	-5.5%	-0.8%

[a] Assumed altitude distribution of emission (based on Oliver et al., 1977)

Altitude bands (km)	Percent in each band
15.5-16.5	4.75
16.5-17.5	13.35
17.5-18.5	20.25
18.5-19.5	23.30
19.5-20.5	20.25
20.5-21.5	13.35
21.5-22.5	4.75

TABLE 6. Historical evolution of LLNL one-dimensional model calculations of the change in total ozone expected from NO_x emissions at 17 and 20 km injection altitudes (emission rate = 2000 molecules $cm^{-3}s^{-1}$).

	ΔO_3 (%)		
	17 km	20 km	Comments
Mid-1974	-4.8	-10.2	Based on CIAP Monographs (also Chang and Johnston, 1974)
Early 1975	-5.3	-11.2	Based on MacCracken et al. (1975); minor chemical changes
Mid-1975	-4.3	-9.8	Based on Duewer et al. (1977); used Chang (1974) K_z; NBS 866 (1975) chemistry, fast $OH+HO_2$
Mid- to late 1975	-1.8	-5.2	Same as above with slow $OH+HO_2$
Late 1975	-1.1	-3.5	Same as above with $NO_3+h\nu \rightarrow NO_2+O$
Mid-1976	-0.7	-2.9	"Old" Chang (1974) K_z; no $C\ell O_x$
	-1.2	-4.2	"New" Chang (1976) K_z; no $C\ell O_x$
Mid- to late 1976	-0.7	-3.3	Same with 1 ppb $C\ell O_x$
Mid-1977	-1.3	-4.8	Based on Luther et al. (1977); NASA 1010 chemistry (1977); slow HO_2+NO
Mid- to late 1977	+2.0	+0.5	Fast HO_2+NO
Mid-1978	+3.2	+3.6	Based on Luther et al. (1978); NBS 513 (1978) chemistry except modified $HO_2 + O_3$, $HO_2 + NO$; 1.2 ppb $C\ell O_x$
Early 1979	+2.6	+2.2	Based on Luther et al. (1979); JPL 79-27 (1979) chemistry
Mid-1979	+2.0	+1.1	NASA 1049 (1979) chemistry
Early 1980	+1.7	+0.6	Same with minor chemistry changes
October 1980	-0.3	-4.5	With new $OH+HNO_3$ (Wine et al., 1981)
December 1980	-0.7	-5.3	With new NASA chemistry
	-2.1	-11.1	NASA chemistry with new text K_z

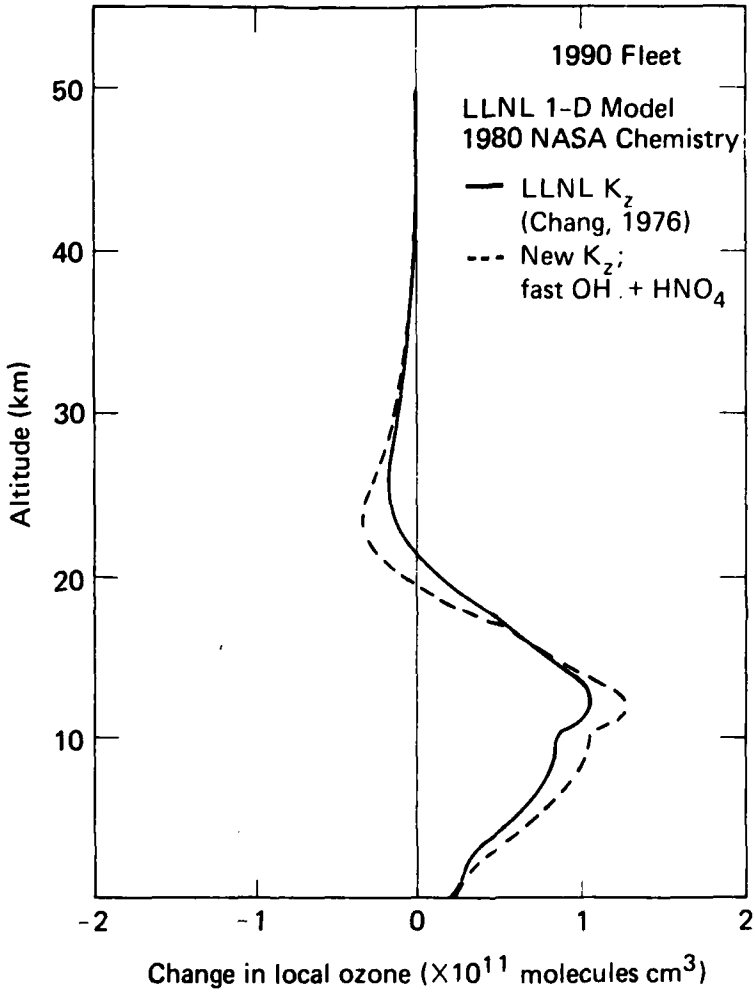

FIGURE 27. The change in local ozone concentration due to subsonic and supersonic aircraft computed for 1990 fleet estimates.

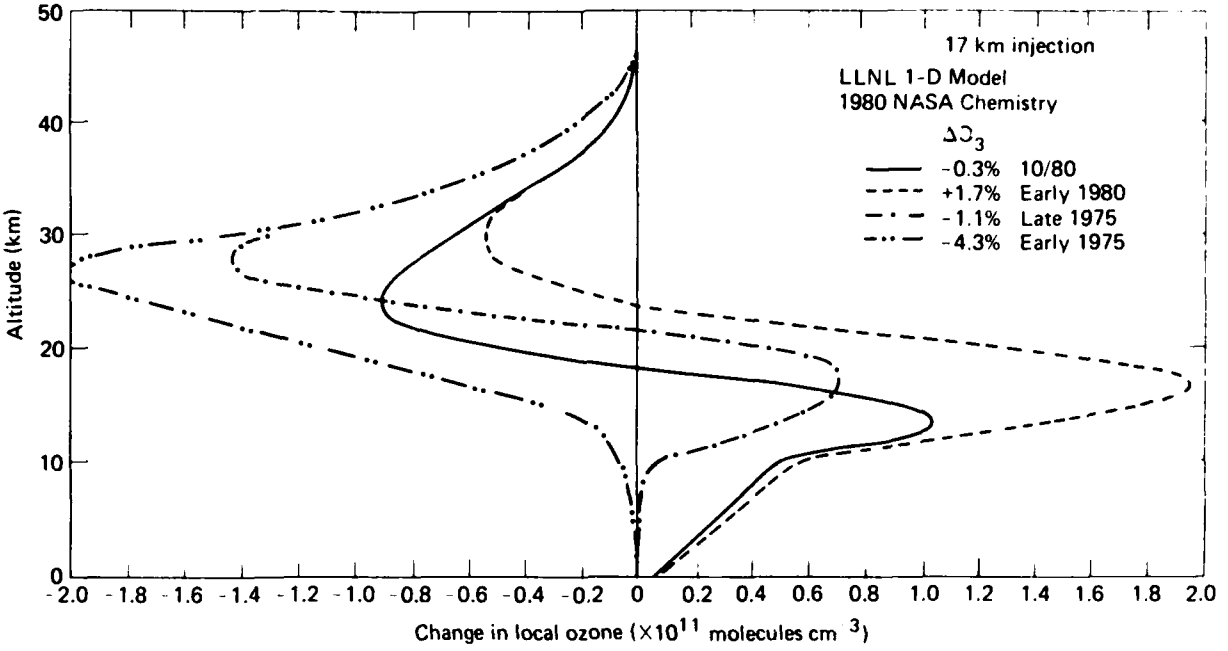

FIGURE 28. Historical variations in the change in local ozone concentration computed using the LLNL model for NO_x injections of 2000 molecules $cm^{-3}s^{-1}$ at 17 km.

2.3 Potential Changes in Ozone Resulting from Other Perturbations

2.3.1 Chlorofluorocarbons

Table 7 compares recent calculations of the expected steady-state change in total ozone from constant emissions of $CFCl_3$ (F-11) and CF_2Cl_2 (F-12) at 1976 levels and constant emissions of CH_3CCl_3 at 1979 levels with similar calculations made in 1979 (Luther et al., 1979). The effect on total ozone expected for January 1980 based on global emissions of these compounds since 1950 is also shown in Table 7. The change in total ozone at steady state was -13.7% using NASA 1049 (1979) chemistry with the exception that OH + H_2O_2 was updated based on Keyser (1980). With currently recommended chemistry (W. DeMore, private communication, 1980), we calculate a change in total ozone of -9.1%. As discussed previously (Section 2.2), the recent chemistry modifications have reduced HO_x concentrations in the lower stratosphere. The resulting reduction in the importance of the HOCℓ chemistry (see Wuebbles and Chang, 1980) and in the importance of the reaction OH + HCℓ → Cℓ + H_2O in the lower stratosphere strongly contribute to the calculated reduced change in total ozone. With the new test K_z, the change in ozone calculated at steady state is -14.2%. This increased sensitivity is expected due to the increased stratospheric residence times found with the new test K_z. A faster rate constant for OH + HNO_4 → H_2O + NO_2 + O_2 (changed from 8.0×10^{-13} to 3.0×10^{-12}) would give a total ozone change of -9.6% rather than -14.2%.

TABLE 7. Effect on total ozone from constant release rates of $CFC\ell_3$ and $CF_2C\ell_2$ at 1976 levels and constant release rate of $CH_3CC\ell_3$ at 1979 levels.

	January 1980			At steady state		
	$\frac{\Delta O_3}{(\%)}$	$\Delta C\ell_x$[a] (ppb)	$\frac{\Delta O_3}{\Delta C\ell_x}$	$\frac{\Delta O_3}{(\%)}$	$\Delta C\ell_x$[a] (ppb)	$\frac{\Delta O_3}{\Delta C\ell_x}$
LLNL K_z NASA 1049 (1979) chemistry with fast $OH+H_2O_2$ (Keyser, 1980)	-1.92	0.84	2.28	-13.9	6.09	2.28
LLNL K_z 1980 NASA chemistry	-0.94	0.89	1.06	-9.1	6.55	1.39
New "Test" K_z 1980 NASA chemistry	-0.59	0.58	1.02	-14.2	10.5	1.35
New "Test" K_z 1980 NASA chemistry with fast $OH+HNO_4$ ($k = 3.0\times10^{-12}$)	-0.33	0.58	0.57	-9.6	10.7	0.90

[a] $\Delta C\ell_x$ = Changes in total inorganic chlorine in upper stratosphere.

The change in total ozone expected for January 1980 is also greatly reduced relative to the results found in 1979, from a calculated change of -1.9% previously to -0.9% with the current model. Using the new K_z reduces the January 1980 expected change to -0.6% because of the slower chlorofluorocarbon flux into the stratosphere. These calculated changes are those expected from chlorofluorocarbon emissions only. Therefore, because of natural variability and additional anthropogenic influences (e.g., CO_2 increase and subsonic aircraft), the actual expected trend in total ozone may be quite different from that derived here (see Section 2.3.3).

Previously, the ratio of the change in total ozone divided by the change in total inorganic chlorine was constant with time. As seen in Table 7, this is no longer the case.

As seen in Fig. 29, the large change in local ozone found previously below 30 km (Luther et al., 1979; Wuebbles and Chang, 1980) has been greatly reduced in the current model with the 1980 NASA chemistry recommendations. The effectiveness of the $HOC\ell$ and $C\ell ONO_2$ catalytic cycles for odd-oxygen destruction at these altitudes (see Wuebbles and Chang, 1980) has been greatly reduced. The large reduction in lower stratospheric HO_x resulting from these chemistry changes and the change in NO_3 photolysis quantum yields are largely responsible for the reduced effectiveness of these catalytic mechanisms.

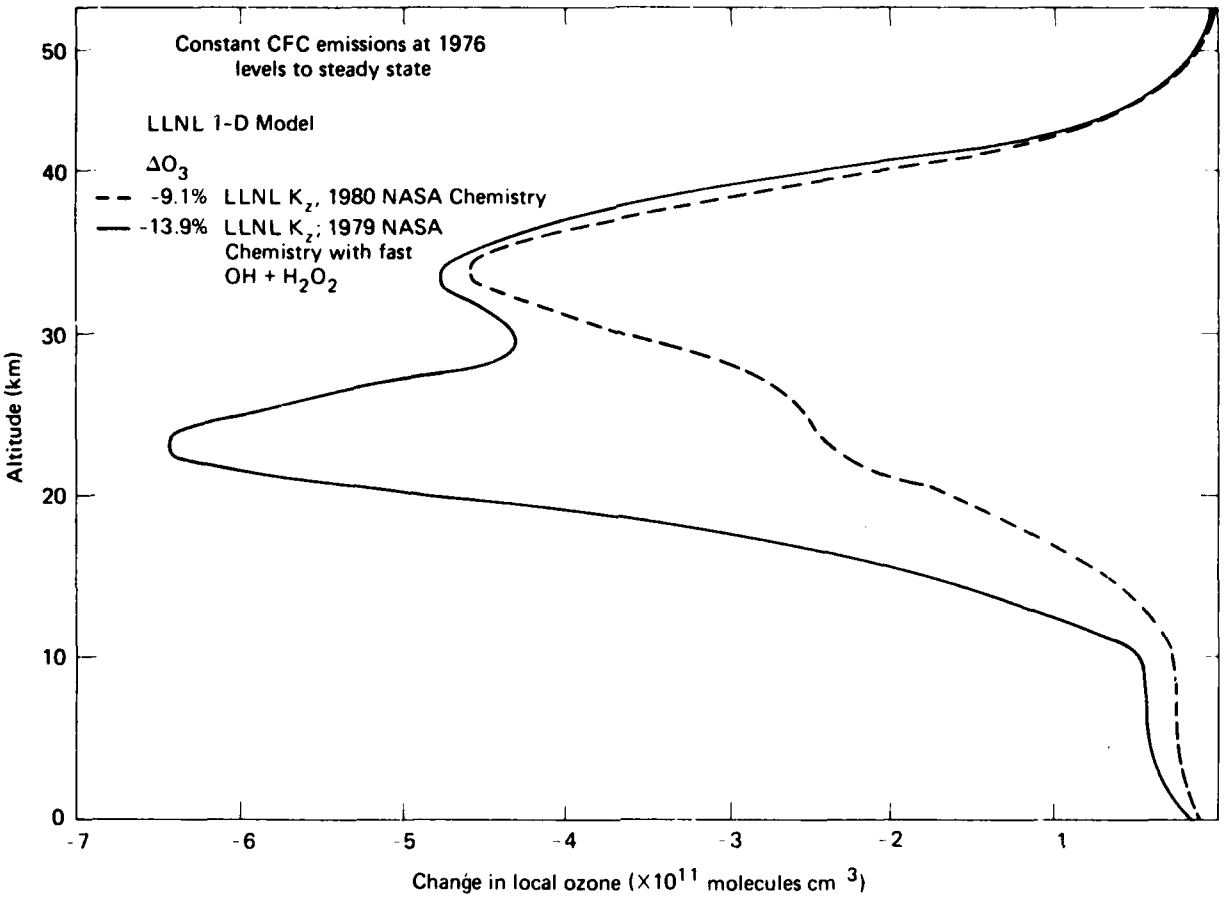

FIGURE 29. The computed change in local ozone concentration at steady state due to CFC emissions at 1976 levels.

Table 8 shows the historical evolution of the change in total ozone at steady state from constant emissions of F-11 and F-12 computed using the LLNL one-dimensional model. As with the SST calculations in Section 2.2, the changes to model chemistry and model representation of physical processes since 1975 have significantly affected the expected change in total ozone from CFC emissions. Because uncertainties still remain in our understanding of the processes determining stratospheric ozone, significant variations seem likely to continue.

2.3.2 Increase in N_2O

Doubling the N_2O lower boundary mixing ratio in the model results in a decrease in total ozone of -11.5% with the 1980 chemistry and the LLNL K_Z (Table 9). An ozone decrease of -2.8% was calculated by Luther et al. (1979). Also shown in Table 9 is the nonlinear response of doubling N_2O and including constant emission rates of $CFC\ell_3$, $CF_2C\ell_2$ and $CH_3CC\ell_3$. Including doubled N_2O and CFC release results in an ozone decrease of -11.5% as compared to the change in ozone of -11.5% for doubled N_2O by itself and -9.1% for CFC release by itself.

Figure 30 shows the change in local ozone for these perturbations. Interferences between the additional NO_x produced by the doubled N_2O and the additional $C\ell O_x$ produced by the CFCs occur at all altitudes, but they are

TABLE 8. Historical evolution of LLNL one-dimensional model calculations of the expected effect on total ozone from constant emissions of F-11 and F-12.

	ΔO_3(%)	Comments
Emissions at 1973 levels		
Mid-1975	-14.0	Chang et al. (1976) as discussed in NRC (1976); no $C\ell ONO_2$
Early 1976	-7.5	Includes $C\ell ONO_2$ chemistry
Emissions at 1975 levels		
Mid-1977	-7.3	Luther et al. (1978)
	-14.2	NASA 1010 (1977) chemistry; fast HO_2 + NO
Mid-1978	-15.9	Luther et al. (1978)
Emissions at 1976 levels		
Early 1979	-18.6	NRC (1979) (actually used 1977 emission levels)
Mid-1979	-19.3	Luther et al. (1979); NASA 1049 (1979) chemistry with slow $C\ell ONO_2$ formation
	-14.2	Same with fast $C\ell ONO_2$ formation
Early 1980	-13.9	Wuebbles and Duewer (1980); same as above with Bass et al. (1980) CH_2O absorption cross sections
	-14.3	Molina and Molina (1980) HNO_4 absorption cross section
	-13.9	Keyser (1980) rate for OH + H_2O_2
Mid-1980	-9.5	Wine et al. (1980); includes new rate for OH + HNO_3
Late 1980	-9.1	1980 NASA chemistry recommendation

TABLE 9. Effect on total ozone of doubling tropospheric N_2O concentration.

	Change in total ozone (%)		
Model	2 x N_2O	CFC release	2 x N_2O + CFC
LLNL K_z 1980 NASA chemistry	-11.5	-9.1	-11.5

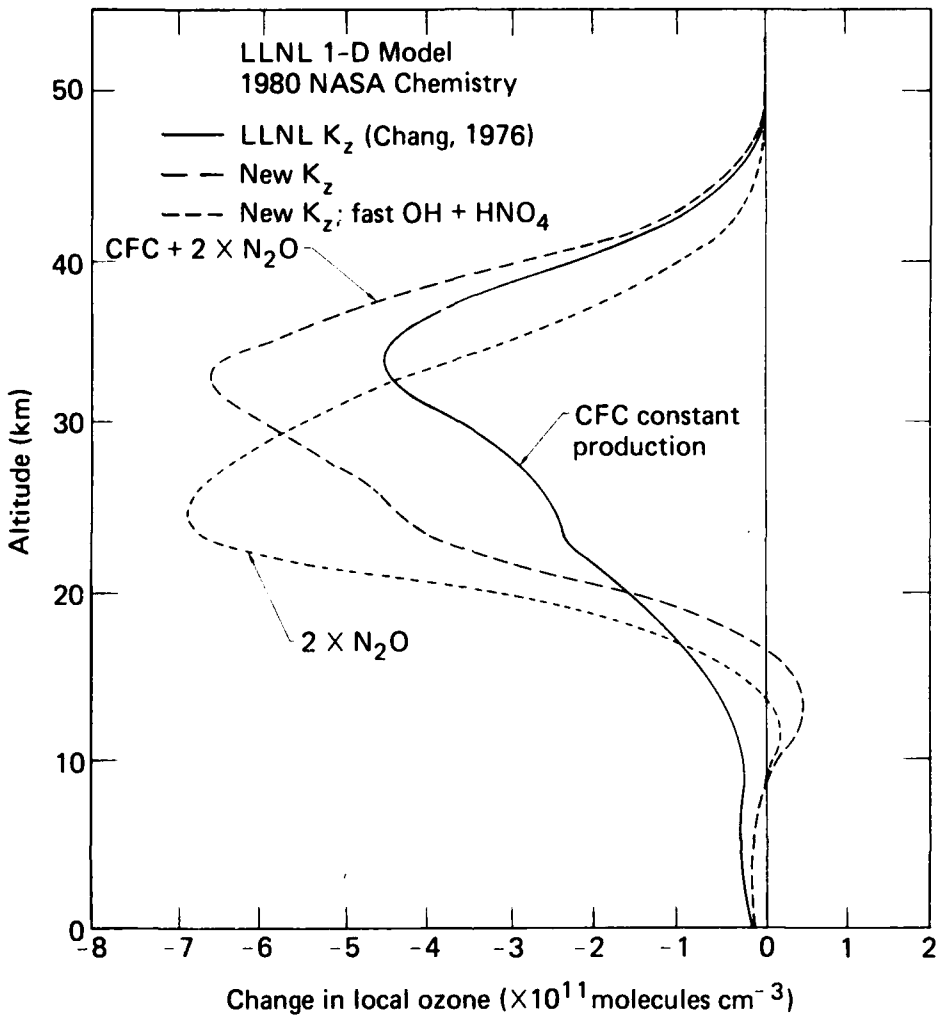

FIGURE 30. The change in local ozone concentration computed for doubling of tropospheric N_2O concentration and for a coupled perturbation combining CFC releases with doubled N_2O.

particularly important below 30 km where $C\ell O + NO \rightarrow C\ell + NO_2$ and $C\ell O + NO_2 \rightarrow C\ell ONO_2$ are most important in interfering with the catalytic cycle mechanisms.

2.3.3 Doubling of CO_2

Atmospheric CO_2 has been increasing due to the use of fossil fuels. Instead of depleting O_3, the expected effect of CO_2 is to increase total ozone. The tendency for CO_2 to increase ozone will complicate efforts to detect changes in ozone caused by increases in CFC's. Since the calculated changes in ozone concentration caused by CO_2 or CFC perturbations are largest at high altitudes, one might expect to detect changes in high altitude O_3 sooner than changes in total ozone. We have compared the calculated change in O_3 at high altitude to statistical detection limits for change as developed from Umkehr data from Arosa, Switzerland, and we discuss the significance of these results for trend detection. The mechanisms for such effects were studied, and significant changes in the NO_x-catalyzed ozone loss rates were found (Penner, 1980).

Table 10 shows the calculated percent change in total ozone at steady state for three perturbations. In all three calculations the percentage change is referenced to an ambient atmosphere that contained 320 ppmv CO_2 and 1.2 ppbv Cl_x, which was derived from CH_3Cl and CCl_4. As shown in Table 10, doubling the CO_2 concentration increases total ozone by 5.8%. At the upper levels sensed by the Umkehr technique, the increase is larger: 13.3% and 20.3% for Levels 7 and 8, respectively. The CFC perturbation describes the change in ozone that results from constant production and release of CF_2Cl_2 and $CFCl_3$ at 1976 rates with constant CO_2. In this case the effect is to decrease total ozone by -13.9%. The calculated effect at higher levels is larger in this case also, namely, -24.4% and -31.6% for Umkehr Levels 7 and 8, respectively.

Table 10 also shows the decrease in ozone calculated for the combined effect of doubled CO_2 and constant CFC production. The coupled effect on ozone is larger than would be predicted if one evaluated the effects separately and then added them. This nonlinear effect results primarily because the odd oxygen loss rate from Cl_x-catalyzed mechanisms are a much larger percentage of the total ozone loss rate in the CFC-perturbed atmosphere than in the ambient atmosphere. Since the Cl_x-catalyzed loss rates are not very sensitive to temperature changes (see discussion below), the effect of increased CO_2 is lessened.

Figure 31 shows a time history for changes in total O_3 relative to 1980, for three different scenarios. The dotted line shows the calculated change in O_3 when CF_2Cl_2 and $CFCl_3$ are released at 1976 production rates, but CO_2 remains constant. The dash-dot line describes a time history for the same CFC perturbation coupled with a linear increase in CO_2 such that its atmospheric concentration doubles in 100 years. For the solid line the CFC perturbation was coupled with a faster CO_2 increase that reflects its growth rate in recent years, namely, an increase in CO_2 emission rate of 4%/yr (CO_2 reaches 600 ppm in $\sim$ 2035).

Figure 31 shows that increases in CO_2 will probably have a significant effect on near-term (0-50 years) changes in stratospheric ozone and, therefore, will complicate efforts to detect the influence of increased CFC's on stratospheric ozone.

Figures 32a and b show the predicted change in O_3 for the same three scenarios as described above for Umkehr Levels 7 and 8, respectively. As in the steady state results described above, the initial predicted change is larger at upper levels. However, for the fast CO_2 growth rate (solid line), the decreasing trend in O_3 is actually reversed in the year 2010, and O_3 at these levels begins to recover. The arrows shown in these figures refer to statistical detection limits for changes in O_3, as determined from a statistical fit of the Umkehr data from Arosa (Penner et al., 1981). The method used to derive these limits is similar to that described for total O_3 by Hill et al. (1977). These limits may be interpreted to say that for Umkehr Level 7, any change in O_3 would need to be larger than 3.5%, 4.2%, or 6% after 10, 20, or 50 years of additional observation, respectively, in order to be perceived as an abnormal change that is statistically significant. An abnormal change or trend is one that is not present in the base period data used for statistical fitting. As shown in Fig. 32b, the corresponding statistical detection limits for Umkehr Level 8 are 10.4%, 13.4%, and 20% for 10, 20, and 50 additional years of observation, respectively. The figure shows that with the data available to date, it is easier to detect a change in O_3 in Umkehr Level 7 than at higher levels, even though the predicted percent change in O_3 is larger above Level 7. This is because the data in Umkehr Level 7 are considerably less noisy than those at upper levels, and therefore are easier to model statistically.

TABLE 10. Nonlinear effects of coupled perturbations.

Percent change in O_3 at steady state			
Perturbation	Total O_3	Umkehr Level 7 (∿33-38 km)	Umkehr Level 8 (∿38-43 km)
2 x CO_2	5.8	13.3	20.3
CFC	-13.9	-24.4	-31.6
2 x CO_2 + CFC	-10.8	-14.8	-19.8

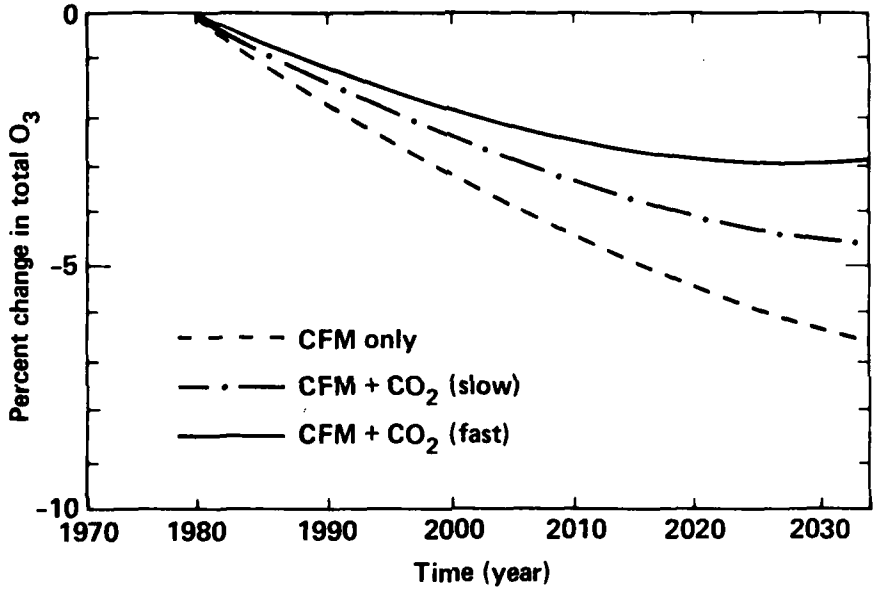

FIGURE 31. The percent change in total ozone relative to 1980 is shown as a function of time for three different scenarios. For the dashed line, CF_2Cl_2 and $CFCl_3$ were assumed to be released at 1976 production rates and CO_2 was held constant. For the dash-dot line the same CFC perturbation was assumed and CO_2 was increased linearly, such that its concentration would double in 100 years. For the solid line the same CFC increase was coupled to the growth rate for CO_2, namely an increase in CO_2 emission rates of 4%/yr.

The statistical detection limit for total ozone developed by Hill et al. (1977) was 1.6% for 10 additional years of observation (see NASA 1049, 1979). This detection limit is small because the data from 9 Dobson stations could be used for the base period statistical model. Comparison of the predicted trend for total O_3 (Fig. 31) and this 9 station detection limit shows that trends in total O_3 caused by CO_2 and CFC increases are easier to detect with the information that is currently available from the Dobson network than trends at upper levels as obtained by the Umkehr method. Efforts to detect trends in upper-level O_3 should be pursued, however, since effects of transport-caused changes and other changes that would be perceived as abnormal, but would not necessarily have been caused by CO_2 and

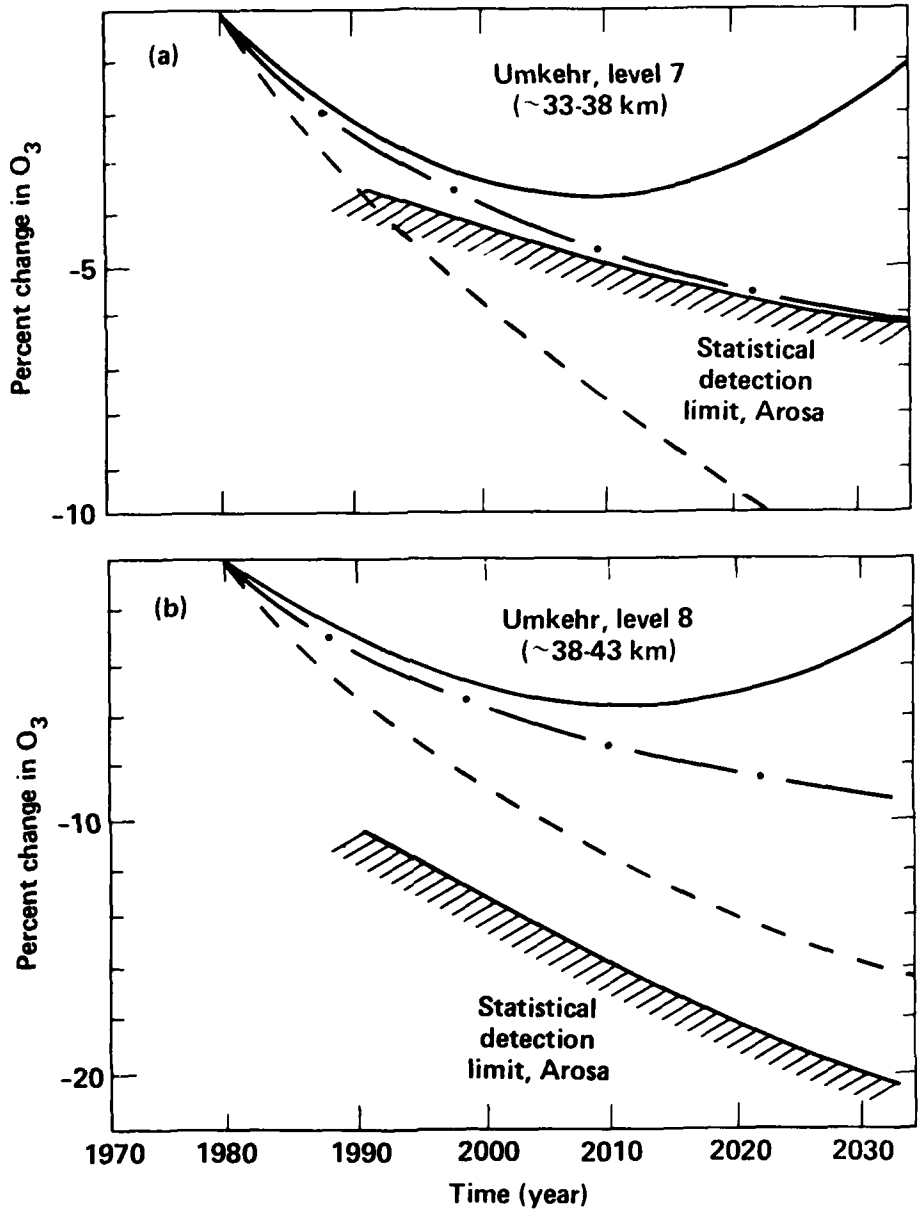

FIGURE 32. The percent change in O_3 in the 7th and 8th layers sensed by the Umkehr technique is shown as a function of time. The three scenarios are the same as for Fig. 31. The arrows refer to statistical detection limits for 10, 20, and 50 more years of observation, as calculated for the Umkehr data from Arosa (see text).

CFC changes, are different for upper-level O_3 (see NASA 1049, 1979). Also, detected changes in upper-level O_3 would provide additional validation for any perceived trend in total O_3.

Because CO_2-caused effects on O_3 will be significant in the near term, it is important to understand the changes induced by CO_2. Increases in CO_2 cause

temperature decreases in the stratosphere due to increased infrared emission rates. The temperature decrease is large at upper levels (∿10°K near 40 km), so that temperature-sensitive reaction rates are significantly altered in the perturbed atmosphere. The feedback effect from the oxygen reactions,

$$O + O_2 + M \rightarrow O_3 + M\,, \quad k = 1.05 \times 10^{-34} \exp(510/T) \tag{1}$$

and

$$O + O_3 \rightarrow O_2 + O_2\,, \quad k = 1.5 \times 10^{-11} \exp(-2218/T) \tag{2}$$

has been analyzed in detail before (for example see Blake and Lindzen, 1973). We have found that the temperature sensitivity of the reaction

$$N + O_2 \rightarrow NO + O\,, \quad k = 4.4 \times 10^{-12} \exp(-3220/T) \tag{3}$$

is of equal importance for the predicted O_3 increase. As a result of the large activation energy for this reaction, when the temperature is decreased, the N atom concentration is increased. This increases the rate for the reaction

$$N + NO \rightarrow N_2 + O \quad . \tag{4}$$

As discussed by Duewer et al. (1977), reaction (4) is an important NO_x sink in the stratosphere, so the net effect of the decreased temperature is to decrease total stratospheric NO_x. As a result of this reduction, the NO_x-catalyzed ozone loss rate is decreased, and O_3 is increased.

Table 11 summarizes the effects of temperature changes on O_3 loss rates from the four chemical families, O_x, NO_x, Cl_x, and HO_x. The O_3 loss rates at 12 mb (∿30 km) and 3 mb (∿40 km) are shown as a percentage of the odd oxygen production rate from O_2 photolysis in the ambient atmosphere. For the O_x family the loss rate refers to two times the rate for

TABLE 11. Summary of effects of temperature changes on O_3 loss rates from different chemical families.

		O_x loss rates (percent of O_2 photolysis)	
Family		12 mb (∿ 30 km)	3 mb (∿ 40 km)
O_x	ambient	12.6	19.4
	2 x CO_2	10.3	16.3
NO_x	ambient	60.4	47.8
	2 x CO_2	50.6	14.0
Cl_x	ambient	7.8	12.0
	2 x CO_2	7.5	13.3
HO_x	ambient	9.8	15.1
	2 x CO_2	9.2	14.1

$$O + O_3 \rightarrow 2O_2 \quad . \tag{5}$$

Similarly, the other loss rates refer to the odd oxygen loss from the following reactions:

$$NO_2 + O \rightarrow NO + O_2 \quad , \tag{6}$$

$$NO_3 + h\nu \rightarrow NO + O_2 \quad , \tag{7}$$

$$C\ell O + O \rightarrow C\ell + O_2 \quad , \tag{8}$$

$$HO_2 + C\ell O \rightarrow HOC\ell + O_2 \quad , \tag{9}$$

$$HO_2 + O \rightarrow OH + O_2 \quad , \tag{10}$$

and

$$OH + O \rightarrow H + O_2 \quad . \tag{11}$$

We have assigned odd oxygen loss through reactions (6) and (7) to the NO_x family, loss through reactions (8) and (9) to the $C\ell_x$ family, and loss through reactions (10) and (11) to the HO_x family, although these reactions sometimes represent the rate limiting step for cycles which include reactions involving other families (Wuebbles and Chang, 1980). As shown in Table 11, the decrease in the NO_x-catalyzed O_3 loss rate is as large or larger than the decrease in the pure oxygen loss rate when CO_2 is doubled. Temperature effects on the HO_x- and $C\ell_x$-catalyzed ozone loss rates are small.

We conclude that: (1) the O_3 decrease at steady state from the coupled CFC and CO_2 perturbation is larger than the decrease calculated by summing the separate effects of these perturbations; (2) the expected increase in CO_2 can significantly affect predicted O_3 trends in the next 50 years; (3) O_3 changes in Umkehr Level 7 are more detectable, in a statistical sense, than those at higher levels; and (4) the temperature effect of CO_2 on the NO_x-catalyzed O_3 destruction rate is as large or larger than the effect of temperature on the pure oxygen loss rate.

2.4 Sensitivity Studies

There are several reactions in the chemical system used in the model that are known to have particularly large uncertainties. In Table 12, we examine four reactions that have a potential for causing a major change in the predicted effects of supersonic aircraft or chlorofluorocarbon emissions.

New evidence indicates that the reaction $OH + HNO_4$ may be as fast as 2×10^{-12} to 4×10^{-12} (Trevor et al., 1980; Littlejohn and Johnston, 1980) rather than the rate 8.0×10^{-13} used in our standard model. This reaction, if as fast as the new measurements indicate, further reduces HO_x concentrations in the lower stratosphere. As seen in Table 12, changing to the faster rate results in significantly larger decreases in total ozone from NO_x emissions and smaller decreases for CFC emission.

TABLE 12. Results of sensitivity calculations for various model parameters (results are shown as the percentage change in total ozone).

Model content	Change in total ozone (%)		
	17 km NO_x injection[a]	20 km NO_x injection[a]	CFC production[b]
LLNL K_z 1980 NASA chemistry	+0.007	-1.98	-9.1 (-0.94% at 1980)
New "test" K_z 1980 NASA chemistry with fast OH + HNO_4 ($k = 3.0 \times 10^{-12}$)	-0.22	-4.30	-14.2 (-0.59% at 1980)
New "test" K_z 1980 NASA chemistry with slow $C\ell ONO_2$ formation	+0.01	-3.85	-16.2 (-1.03% at 1980)
New "test" K_z 1980 chemistry with fast OH + HO_2 ($k = 1.0 \times 10^{-10}$)	-0.78	-5.00	-11.3 (-0.39% at 1980)
New "test" K_z 1980 NASA chemistry with slow OH + HNO_3 ($k = 8.5 \times 10^{-14}$)	+1.66	+0.53	-20.4 (-1.35% at 1980)

[a] Rate of emission is 1000 molecules (NO) $cm^{-3}s^{-1}$ over a 1-km-thick layer, base model has current levels of CFCs.

[b] Constant release rates of $CFC\ell_3$ and $CF_2C\ell_2$ at 1976 levels; constant release rate of $CH_3CC\ell_3$ at 1979 levels.

The rate of formation of $C\ell ONO_2$ is still highly uncertain. Two rates are given in the 1980 NASA chemistry, and no firm recommendation is stated. The standard model uses the faster of these two rates. If the slower rate is used, the calculated effects of an SST fleet becomes less negative than in the base case, while the computed effects of CFCs become more negative. Recent measurements (Molina, private communication, 1980) indicate that the rate of $C\ell ONO_2$ formation is less than the disappearance rate of $C\ell O + NO_2$. If isomers of $C\ell ONO_2$ are indeed being produced, the final impact of this reaction will depend on the form and stability of these isomers.

The sensitivity to the uncertainty in the reaction $OH + HO_2 \rightarrow H_2O + O_2$ is not as large as it was a year ago (Luther et al., 1979; Duewer and Wuebbles, 1980) due to changes in other reactions that have reduced HO_x concentrations in the lower stratosphere of the model. Nonetheless, using a rate of 1.0×10^{-10} rather than 4.0×10^{-11} will reduce the effect of CFC release on ozone from -14.2% to -11.3%.

Also shown in Table 12 is the impact of using the slow rate for OH + HNO_3 rather than the recent measurement by Wine et al. (1980). The sign of the NO_x perturbation changes (becoming positive as found previously [Luther et al., 1979]) and the CFC effect on total ozone changes from -14.2% to -20.4%.

2.5 Calculations with Temperature Feedback and Hydrostatic Adjustment

The concentration of ozone in the stratosphere is determined by a complex coupling of chemistry, dynamics and temperature. Most models of the stratosphere that consider perturbations to the chemistry ignore possible changes due to coupling and feedbacks from dynamics and temperature. These models provide a reasonable first-order picture of how the atmosphere might respond to changes in chemistry. A more detailed and accurate picture, however, is obtained with the use of a model capable of also calculating the temperature structure of the atmosphere.

There are three major mechanisms that couple changes in temperature and changes in atmospheric composition. The first mechanism is radiative coupling between temperature and species concentrations. Perturbations to the atmospheric composition affect the temperature profile via the solar and longwave radiation balance. The species O_3, O_2 and NO_2 are the most effective absorbers of solar radiation in the stratosphere, and O_3, O_2 and H_2O are the most effective absorbers and emitters of longwave radiation in the ambient stratosphere. Large increases in the concentrations of trace species such as $CFCl_3$, CF_2Cl_2 and N_2O also can significantly affect stratospheric and tropospheric temperatures by their longwave effect (Wang et al., 1976).

The temperature profile in the upper stratosphere is controlled strongly by the amount of solar absorption by O_3. Consequently, a decrease in O_3 in the upper stratosphere results in a decrease in the local temperature in that region. In the lower stratosphere the temperature change may have either the same or the opposite sign as the change in ozone depending upon the magnitude of the change to other species and on the structure of the ambient temperature profile (Luther et al., 1977).

The second mechanism is the coupling between temperature and chemical reaction rate coefficients. Changes in temperature may affect species concentrations directly by changing rate coefficients that affect rates of production and destruction of that species or indirectly by changing the concentration of other species upon which production and destruction rates depend.

The third mechanism is the coupling between changes in air density and changes in rates of reaction. Under conditions of hydrostatic equilibrium and the ideal gas law, changes in the temperature profile change the air density at a given altitude or pressure level as the atmosphere expands or contracts. Species concentrations at a given level are affected both by changes in density at the level and by changes in rates of reaction due to changes in species concentrations and changes in M (third-body concentration).

We used the LLNL fully coupled one-dimensional transport-kinetics model with radiative equilibrium submodel in this theoretical study. The solar flux, reaction rate coefficients, and absorption coefficients are those recommended in NASA 1049 (1979) (see also Luther et al., 1979). Note that the model chemistry used here differs from the updated chemistry used in the previous sections.

The vertical distributions of N_2 and O_2 are adjusted to satisfy hydrostatic equilibrium at each time step, and the concentrations of the other species are adjusted using interpolation based on the adjustment to N_2 and O_2. The column abundances of O_2 and O_3 at the top boundary are calculated consistent with the calculated temperature and density at that level.

The temperature is computed using the radiative transfer model assuming radiative equilibrium in the stratosphere. The temperature profile is computed above 13 km and is specified below this altitude according to the U. S. Standard Atmosphere (1976). Changes in surface and tropospheric temperatures up to 13 km may be imposed. A full description of model results for the ambient atmosphere and comparisons with observations for the chemical model used in this study are included in Luther et al. (1979).

For some of the perturbations that we consider, we assume that the change in surface temperature is negligible. Small temperature changes in the troposphere (<0.5 K) are expected for perturbations to N_2O, $CF_2C\ell_2$ and $CFC\ell_3$, and the stratospheric temperature changes due to the infrared properties of these species are also expected to be small (V. Ramanathan, NCAR, private communication, 1979). Based on the work of Manabe and Wetherald (1967), it can be estimated that an increase in the stratospheric water vapor mixing ratio of 2 ppmv will cause an increase in surface temperature of ≤ 0.2 K. Increasing the surface temperature (and tropospheric temperatures) in our model by 0.5 K causes an increase in total ozone of 0.1%. Neglecting changes in surface temperature of this magnitude has no significant effect on the results. When significant changes in surface temperature are expected, they are imposed in the model.

Imposing a change in tropospheric temperatures has little effect on the stratosphere at a given pressure level because the major effect of hydrostatic adjustment is just to raise or lower the stratosphere as the troposphere expands or contracts. There are slight temperature changes at pressure levels in the lower stratosphere because the upward longwave flux from the troposphere into the stratosphere is changed. When the resulting changes in species concentrations are plotted in a constant altitude frame of reference, the changes in species concentrations may appear significant even though the change in total column is small. This effect is illustrated in Fig. 33, which shows the percent change in O_3 as a function of altitude resulting from an imposed 2.0-K increase in tropospheric temperature. Ozone concentrations decreased slightly below 25 km and increased by as much as 6.5% at 40 km. The apparent changes are caused by a lifting of the ozone profile in the stratosphere due to expansion of the troposphere. Since most studies in the past have presented results in terms of altitude coordinates, we too shall illustrate changes in this frame of reference. However, it is important expecially for high-altitude changes that the results be plotted in pressure coordinates because remote sensing techniques provide ozone concentrations as functions of pressure. In the following discussion we illustrate changes in both frames of reference in order to determine the differences and to show when it is important to distinguish between pressure and altitude coordinates.

We considered four types of perturbations. Each one is interesting as a possible atmospheric change and illustrates a different sort of change in the temperature structure so that the effects from including or not including temperature feedback and hydrostatic adjustment are quite different.

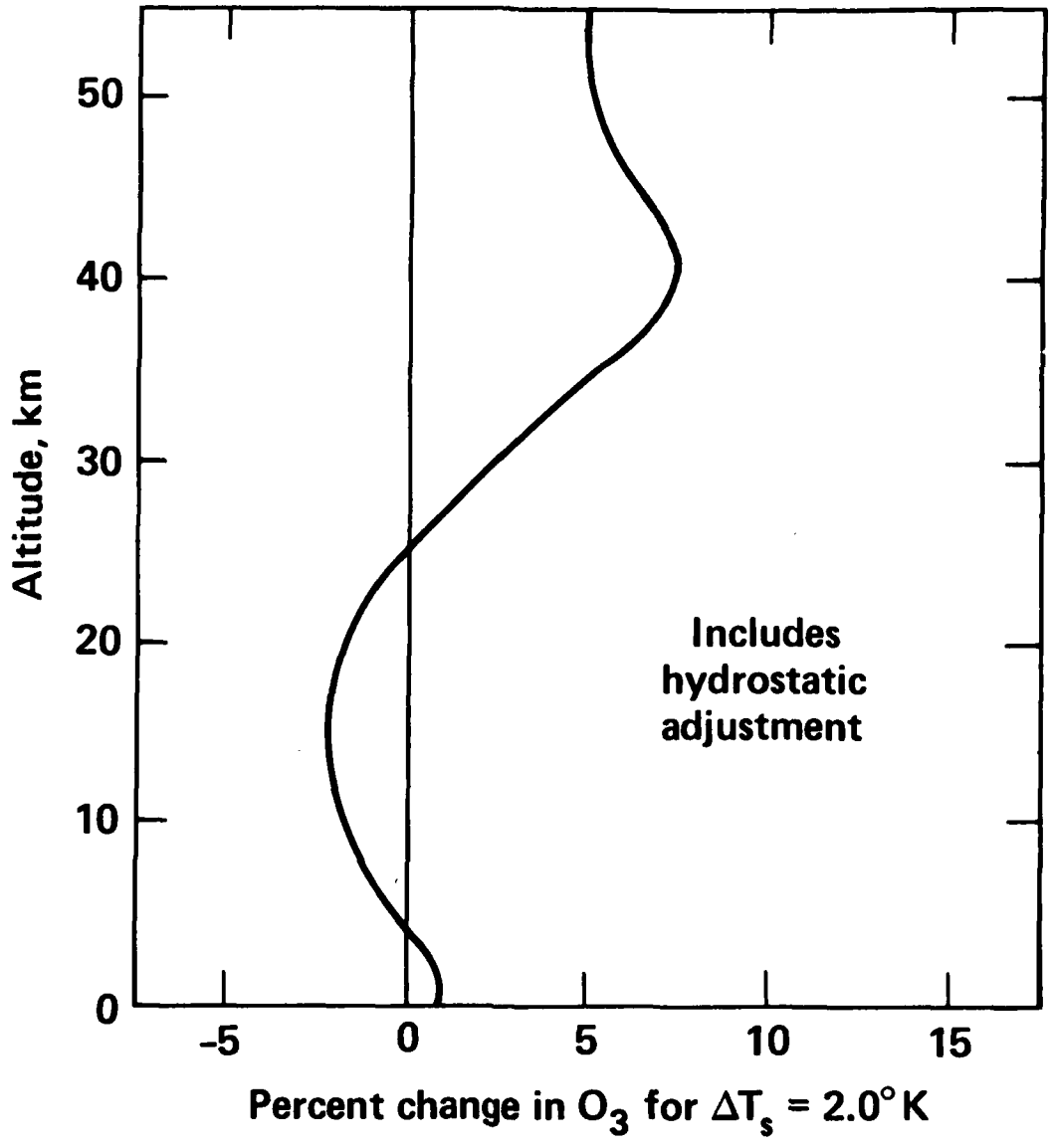

FIGURE 33. Percent change in O_3 for a tropospheric temperature increase of 2.0 K.

2.5.1 Doubling of N_2O

Increases in atmospheric N_2O cause an increase in stratospheric NO_x. The effect on O_3 of increases in NO_x depends on altitude. At altitudes below $\sim$24 km in our model, O_3 is increased when the N_2O concentration at the ground is doubled, primarily because of increased production by a chain of reactions, similar to those that produce O_3 in urban smog (see NASA 1049, 1979).

At altitudes above 24 km, catalytic destruction of ozone by the NO_x destruction cycle is more efficient, and the net effect is that O_3 (i.e., odd-oxygen) is destroyed. The effect on the temperature structure in a temperature-coupled model, therefore, is also different in the two altitude regions. The temperature is increased in the lower stratosphere and decreased in the upper stratosphere.

The separate effects of including temperature feedback and hydrostatic adjustment in the perturbation calculation for a doubling of the concentration of N_2O at the ground from 320 to 640 ppb are illustrated in Fig. 34. Figure 34a shows the percent change in O_3 as a function of altitude for three cases: no temperature feedback, temperature feedback without hydrostatic adjustment and a fully coupled calculation with temperature feedback and hydrostatic adjustment. Including temperature feedback alone acts to lessen the effects of the perturbation locally, as expected from the temperature dependence of reactions (1) and (2). As shown in Fig. 34b, the temperature perturbation is small, less than ±1.3 K, and of opposite sign at low and high altitudes. Thus, the effects of hydrostatic adjustment are also small and, in fact, cannot be distinguished in the figure from the case of no hydrostatic adjustment. Similar remarks apply for changes plotted with respect to pressure coordinates. Since the temperature change is small, there is only a small change in the air density. Consequently, the results appear nearly the same when plotted in constant pressure coordinates and are not shown separately for this perturbation.

2.5.2 Chlorofluorocarbons

Figures 35a, b, and c show the calculated percent change in O_3 concentration and the change in temperature when $CF_2C\ell_2$ and $CFC\ell_3$ have increased to 1.8 and 0.75 ppb, respectively, compared to an ambient atmosphere which contained 0.22 ppb $CF_2C\ell_2$ and 0.14 ppb $CFC\ell_3$ (approximately present day conditions). This represents the expected change at steady state for constant production and release of $CF_2C\ell_2$ and $CFC\ell_3$ at 1976 rates. Three cases are again considered: no temperature feedback, temperature feedback without hydrostatic adjustment, and the complete model calculation. The results in Fig. 35a for constant altitude coordinates are similar to those presented by Chandra et al. (1978) for this perturbation.

Comparison of Figs. 35a and c illustrates the differences caused by viewing changes in constant altitude coordinates and constant pressure coordinates. In constant altitude coordinates, the difference between the fully coupled calculation and the calculation that includes hydrostatic adjustment begins to be important at levels above 45 km, due to the cumulative effects of temperature changes below that level. In constant pressure coordinates, only local changes in temperature and therefore air density are able to perturb the chemistry, so that differences between including or not including hydrostatic adjustment are confined to pressure levels where large changes in temperature are calculated (cf. Fig. 35b). In addition, in regions where O_3 is photochemically controlled, reductions in temperature always have the effect of restoring the ozone concentration in pressure coordinates, whereas they can be associated with a decrease in ozone at high altitude if viewed in constant altitude coordinates.

2.5.3 Doubling of N_2O

The changes in ozone concentration and temperature caused by increasing CO_2 from 320 to 640 ppm are shown in Figs. 36a, b, and c. The calculated temperature change is large (nearly 10 K) near 40 km. Because the temperature change is large, the difference between the calculated change in ozone including temperature feedback alone is also large even when viewed in a constant pressure level frame of reference (Fig. 36c). For this perturbation, a significantly larger increase in local ozone concentration ($\sim$5% larger at pressure levels near 40 km) is predicted with the fully coupled model.

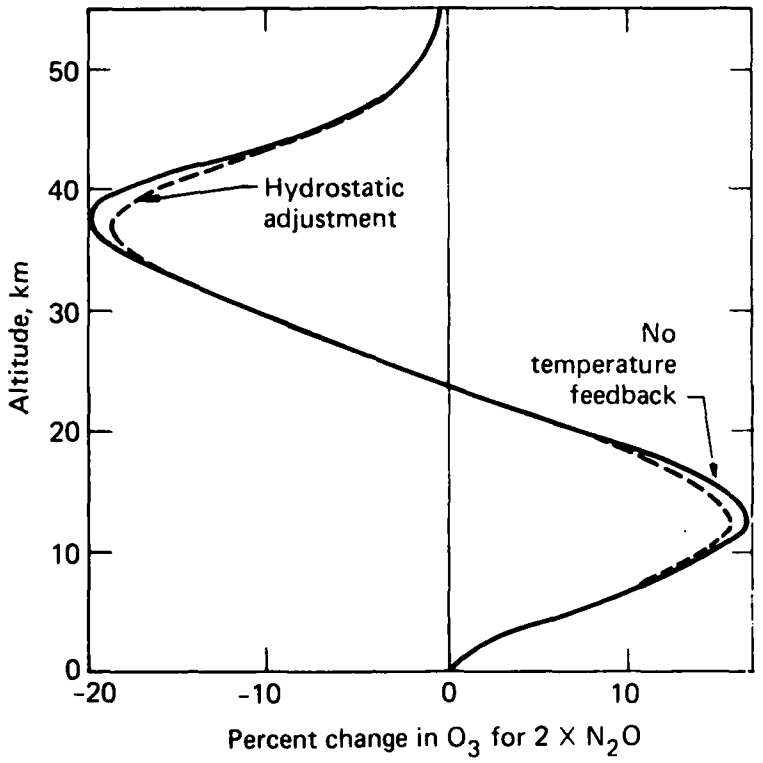

FIGURE 34a. Percent change in O_3 for a doubling of the surface N_2O concentration. The full line shows a calculation that did not include temperature feedback. The dashed line shows the results including temperature feedback only and including temperature feedback and hydrostatic adjustment (same line).

Figure 36a also shows the results of a calculation in which we increased the tropospheric temperature by 2.0 K, which is the approximate steady-state surface temperature increase expected for doubled CO_2 (Schneider, 1975). As noted above, tropospheric temperature changes cause changes in air density and concentrations in a constant altitude coordinate system due to hydrostatic adjustment. In this model when the tropospheric temperature is increased 2.0 K, the predicted ozone change at 40 km is increased from 10% to almost 16%. Differences caused by tropospheric temperature changes are negligible, however, if the change in O_3 is plotted as a function of pressure.

2.5.4 Doubling of Stratospheric H_2O

This perturbation is included to test the model sensitivity to changes in ambient H_2O levels. This perturbation is also relevant because changes in tropical tropopause temperatures (due perhaps to CO_2 increases) or changes in tropospheric-stratospheric exchange rates may lead to increases in stratospheric water vapor.

Figures 37a and b show the calculated change in O_3 and temperature caused by doubling stratospheric water vapor from 3.6 to 7.2 ppm at 14 km. In this case the calculated temperature change results from both increased H_2O and decreased O_3. The decrease in O_3 is mainly the result of increased HO_x, which is produced from the reaction of $O(^1D)$ with H_2O. As was the case for the preceeding

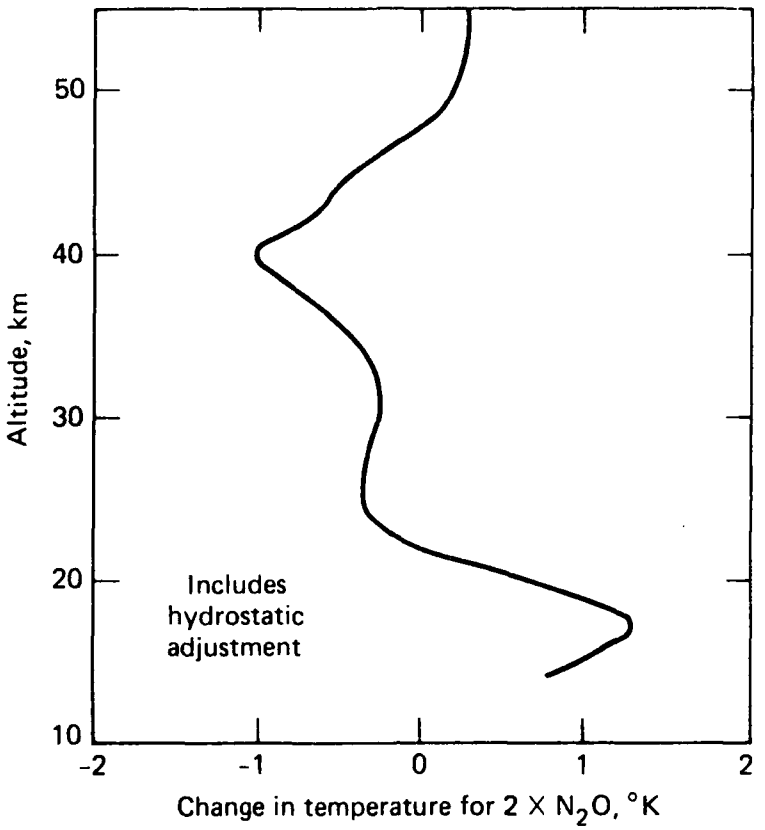

FIGURE 34b. Change in temperature for a doubling of the surface N_2O concentration.

calculations, when temperature feedback is included, the perturbation is reduced. When hydrostatic adjustment is also included, differences are large throughout the region when viewed in constant altitude coordinates (Fig. 37a), but are confined to pressure levels where temperature changes are significant in constant pressure coordinates (cf. Fig. 37b and c).

The results presented here have focused on calculated changes in local ozone concentration as a function of altitude. The altitude structure of predicted changes is important because it may be easier to detect anthropogenic changes to the ozone layer at high altitude (NASA 1049, 1979), where local changes are largest on a percentage basis.

Table 13 summarizes our results for the percent change in O_3 at 2 mb ($\sim$40 km) for all perturbations considered. The percent changes in total O_3 are shown in Table 14. In most cases the differences in the predicted change in total O_3 for the three cases (no temperature feedback, temperature feedback without hydrostatic adjustment, and temperature feedback with hydrostatic adjustment) are small — less than 1% in absolute amount.

To summarize, simulations using the LLNL one-dimensional stratosphere model show significant differences in predicted local ozone changes depending on whether or not temperature feedback and hydrostatic adjustment are included. We find that the calculated effects at high altitude are sensitive to tropospheric temperature changes, but that differences are minimized when results are plotted in

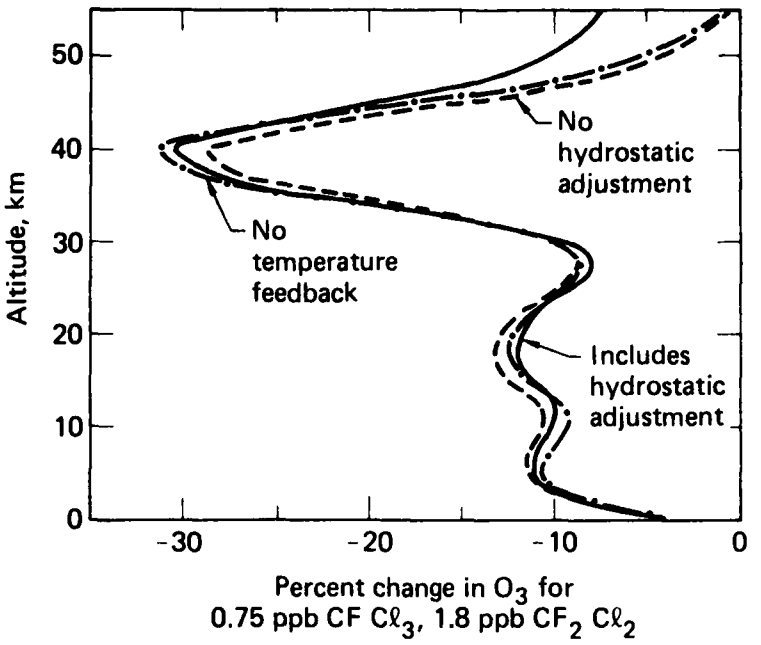

FIGURE 35a. Percent change in O_3 for increases in $CFC\ell_3$ and $CF_2C\ell_2$ from 0.14 and 0.22 ppb to 0.7 and 1.8 ppb, respectively. The dash-dot line shows a calculation that did not include temperature feedback. The dashed line includes temperature feedback, but does not include hydrostatic adjustment, and the full line shows the results of a fully coupled calculation.

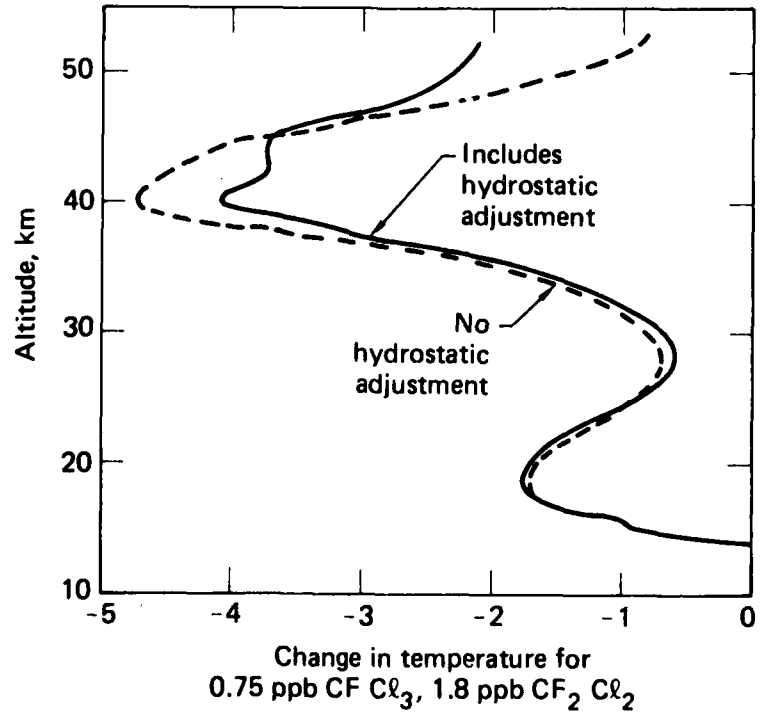

Figure 35b. Change in temperature for the same calculation as in Fig. 35a (see caption for 35a).

TABLE 13. Percent change in O_3 concentration at 2 mb.

Perturbation	Temperature feedback and hydrostatic adjustment (%)	Temperature feedback only (%)	No temperature feedback (%)
2 x N_2O	-12	-12	-13
0.75 ppb $CFC\ell_3$[a]	-23	-23	-27
1.8 ppb $CF_2C\ell_2$			
2 x CO_2 (ΔT_s = 2 K)	27	21	0.0
2 x H_2O	-7.1	-7.2	-8.8

[a] The calculated changes in ozone are with respect to an ambient atmosphere containing 0.22 ppb $CF_2C\ell_2$ and 0.14 ppb $CFC\ell_3$.

TABLE 14. Percent change in total ozone column.

Perturbation	Temperature feedback and hydrostatic adjustment (%)	Temperature feedback only (%)	No temperature feedback (%)
2 x N_2O	-2.3	-2.2	-1.9
0.75 ppb $CFC\ell_{3a}$	-12.4	-12.4	-12.3
1.8 ppb $CF_2C\ell_2$			
2 x CO_2 (ΔT_s = 0)	5.4	4.6	0.0
2 x CO_2 (ΔT_s = 2 K)	5.8		
2 x H_2O	-1.9	-1.8	-3.5

[a] The changes in total ozone are with respect to an ambient atmosphere containing 0.22 ppb $CF_2C\ell_2$ and 0.14 ppb $CFC\ell_3$ (approximately present day conditions). The computed change in total ozone at steady state with no temperature feedback is -14.2% compared to an ambient atmosphere without CFC's.

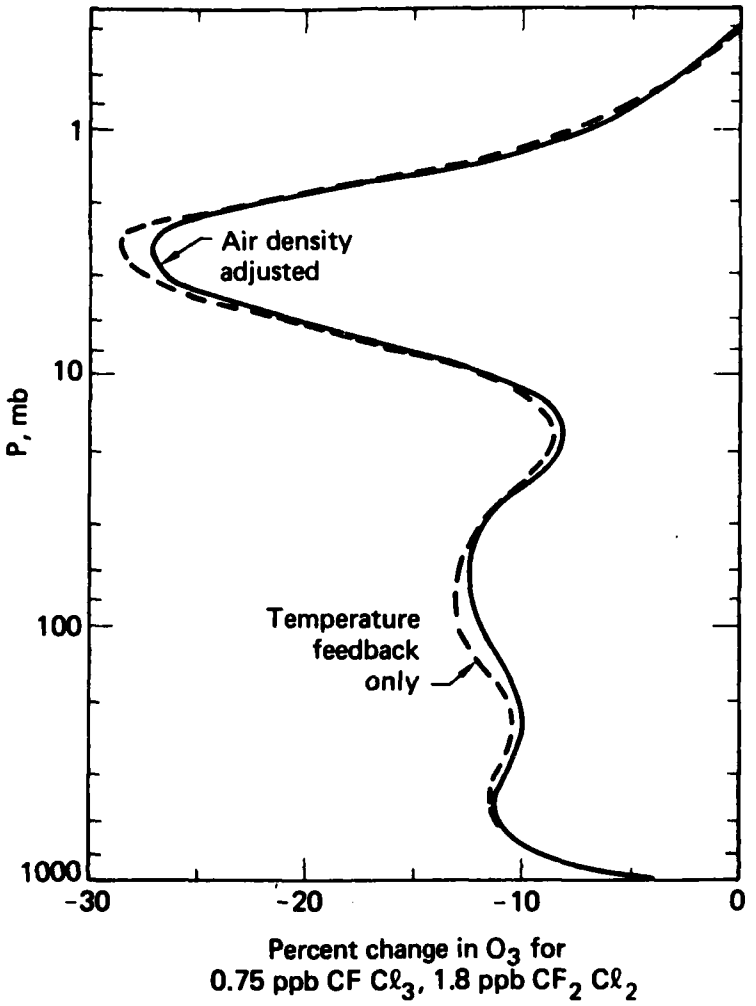

FIGURE 35c. Percent change in O_3 at constant pressure levels for the same calculation as Fig. 35a. The full line includes all feedbacks, while for the dashed line the background air density was held constant.

constant pressure coordinates. Because the calculated local ozone changes are largest on a percentage basis at high altitude (for each of the perturbations considered), monitoring high-altitude ozone changes may provide an early warning signal for perturbations to ozone caused by man's activities and a method for validating models (NASA 1049, 1979). It is important, therefore, to include the effects of temperature feedback and changes in the air density when computing local changes in ozone for comparison with observational data. Including hydrostatic adjustment in a constant altitude frame of reference or air density adjustment in a constant pressure frame of reference is particularly important for calculations of the local ozone depletion due to CFC's, CO_2 and H_2O perturbations because large changes in the temperature structure are predicted.

In the atmosphere there is a complex coupling between chemistry, temperature and dynamics. We have explored in more detail the coupling between chemistry and temperature, but the effect of changes in atmospheric composition and temperature on dynamics was not included. To explore the coupling with dynamics, all of these effects will have to be included in a three-dimensional general

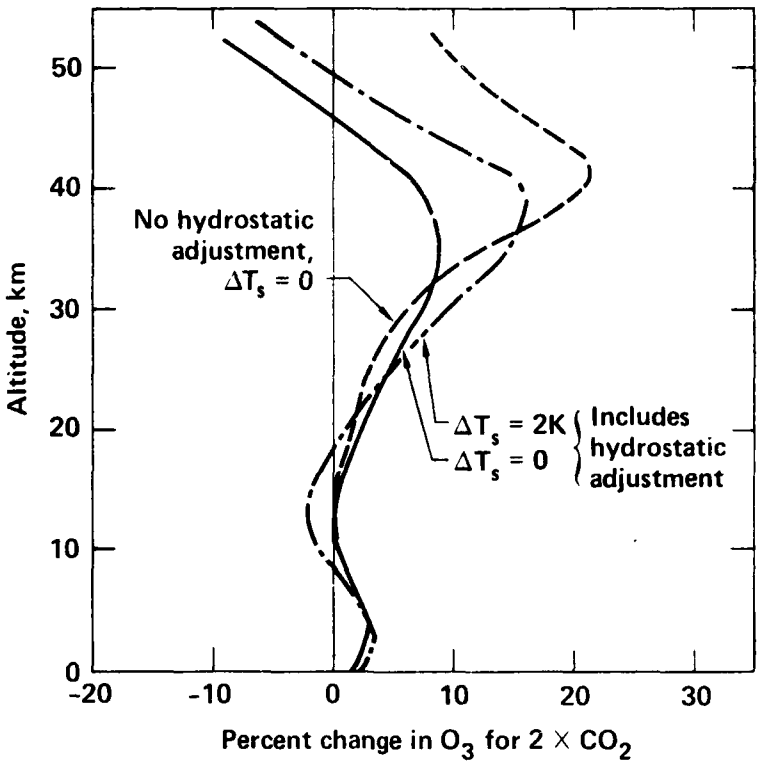

FIGURE 36a. Percent change in O_3 for a doubling of the atmospheric CO_2 concentration. The dashed line shows a calculation with temperature feedback but without hydrostatic adjustment. The full and dash-dot curves include hydrostatic adjustment and temperature feedback. For the curve marked $\Delta T_S = 0$, the ambient tropospheric temperature was used. For the curve marked $\Delta T_S = 2$ K, the ambient tropospheric temperature was increased by 2.0 K.

circulation model. Because of computational limitations, it is not possible to include all of these effects in a three-dimensional model at this time. The problem is compounded by the fact that the model simulations must cover 10s to 100s of years for these perturbations to reach steady state. In the meantime, considerable insight is gained by the use of one- and two-dimensional models.

2.6 Accuracy of the LLNL Mutiple Scattering Algorithm

Multiple scattering and ground reflection have been shown to have significant effects on atmospheric photodissociation rates. Several numerical schemes have been developed for treating these effects in transport-kinetics models (Sze, 1976; Yung, 1976; Isaksen et al., 1977; Anderson and Meier, 1979). The scheme for treating multiple scattering presented here differs in its assumptions compared to that of Isaksen et al. (1977), but it lends itself to a very fast solution technique similar to theirs.

The multiple scattering algorithm is derived based on conservation of energy. In the development of the two-stream model, first consider attenuation of the downward direct beam as it passes between grid levels k and k+1 (see Fig. 38). Considering fluxes in the spectral interval $\Delta\lambda$, let

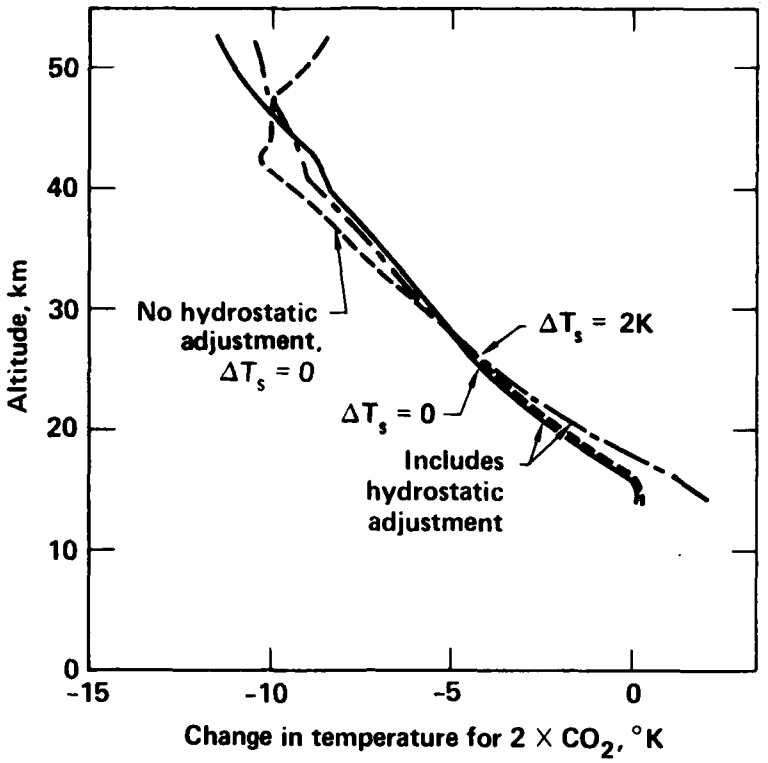

FIGURE 36b. Change in temperature for a doubling of the CO_2 concentration (see caption for Fig. 36a).

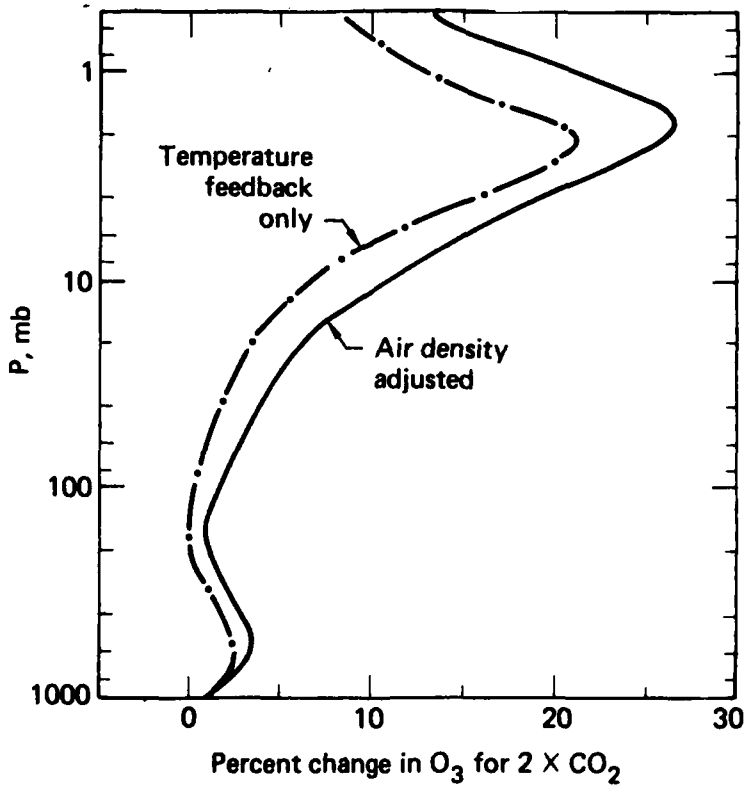

FIGURE 36c. Percent change in O_3 at constant pressure levels for the same calculation as Fig. 36a. The full line includes all feedbacks, while for the dashed line the background air density was held constant.

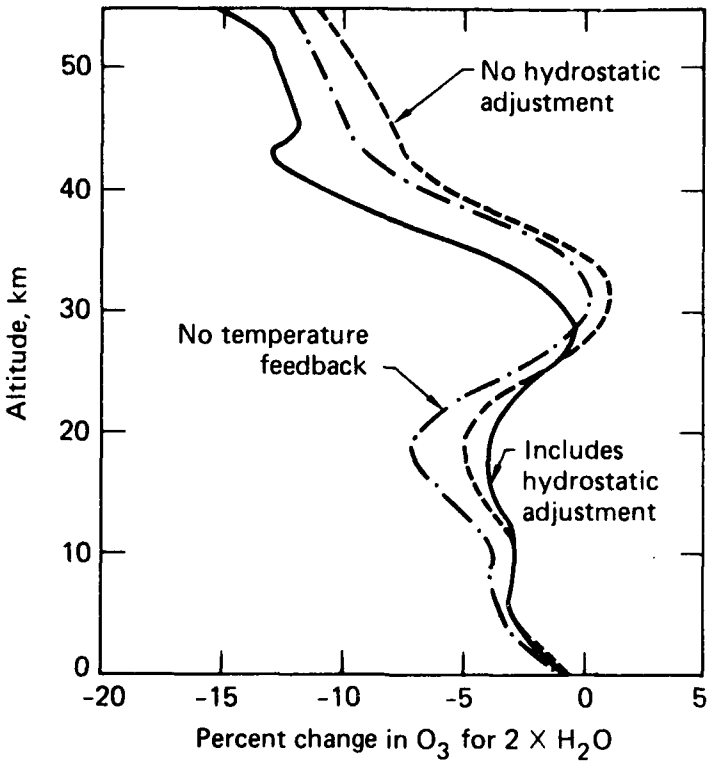

FIGURE 37a. Percent change in O_3 for a doubling of the stratospheric H_2O concentration. The dash-dot line shows a calculation that did not include temperature feedback. The dashed line included temperature feedback but did not include hydrostatic adjustment. The full line was calculated using the fully coupled model.

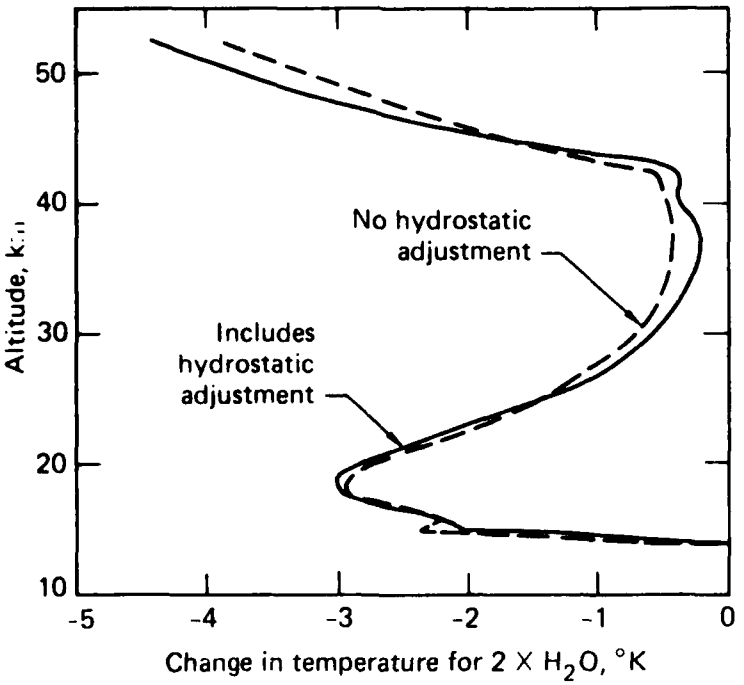

FIGURE 37b. Change in temperature for a doubling of the stratospheric H_2O concentration (see caption for Fig. 37a).

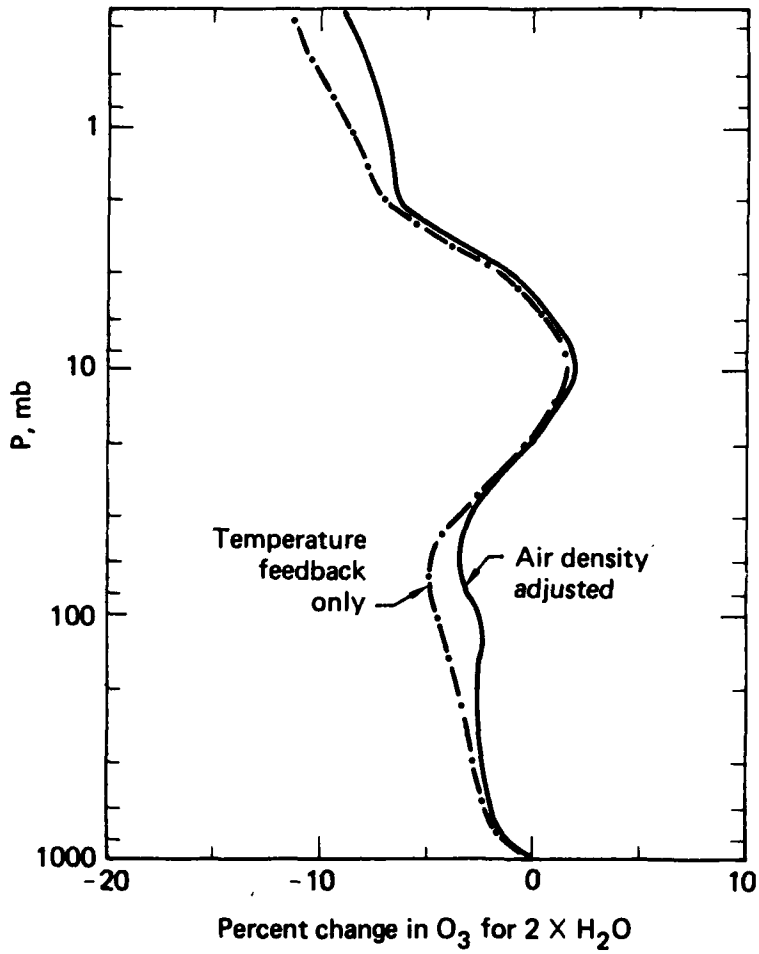

FIGURE 37c. Percent change in O_3 at constant pressure levels for the same calculation as Fig. 37a. The full line includes all feedbacks, while for the dashed line the air density was held constant.

F_S = direct solar flux in the direction of propagation.

$F_{e\downarrow}$ = downward diffuse flux of energy across a horizontal surface.

$F_{e\uparrow}$ = upward diffuse flux of energy across a horizontal surface.

For the k-th atmospheric layer (extending between levels k and k+1), let

$f_{so}(k)$ = fraction of incident direct solar flux that is scattered out of the layer.

$f_s(k)$ = fraction of incident diffuse flux that is scattered out of the layer.

$f_t(k)$ = fraction of incident diffuse flux that is transmitted through the layer.

$\Delta\tau(k)$ = vertical optical depth of the layer at wavelength λ including scattering and absorption.

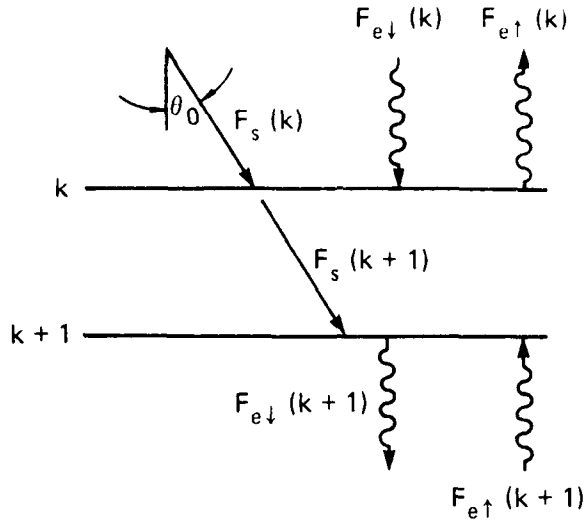

FIGURE 38. Schematic of direct and diffuse fluxes.

Using the above definitions, the direct solar flux is determined by

$$F_s(k+1) = F_s(k)\, e^{-\Delta\tau(k) \sec \theta_o} \quad . \tag{12}$$

The contribution to the diffuse fluxes at levels k and k+1 due to scattering out of the direct beam as it passes through the layer k is

$$\Delta F_{e\downarrow}(k) + \Delta F_{e\uparrow}(k+1) = f_{so}(k) \cos \theta_o \, [F_s(k) - F_s(k+1)] \quad . \tag{13}$$

The shape of the Rayleigh scattering phase function is such that regardless of the zenith angle of the incident radiation, half the scattered radiation goes up and half goes down (for single scattering). If the atmospheric layers are optically thin, then we can assume that half the energy scattered out of the layer goes into the upward diffuse flux and half into the downward diffuse flux, i.e., $\Delta F_{e\downarrow}(k) = \Delta F_{e\uparrow}(k+1)$. Scattering also occurs within a layer when the flux entering is diffuse. The flux scattered out of the layer is partitioned the same way as when the incident flux is direct.

For the upward and downward diffuse fluxes, we assume an average value for sec θ such that the transmissivity of the flux passing through a layer is $e^{-\Delta\tau(k)\,\overline{\sec\theta}}$. We use a value of 1.66 for $\overline{\sec\theta}$. The results are not very sensitive to the choice of $\overline{\sec\theta}$.

At the earth's surface, the upward scattered flux of energy is given by

$$F_{e\uparrow} = R\,(F_s \cos\theta_o + F_{e\downarrow}) \tag{14}$$

where R is the albedo of the surface.

The downard flux of energy due to diffuse radiation is given by

$$F_{e\downarrow} = \int_0^{2\pi} \int_0^{\pi/2} I(\theta,\phi) \cos\theta \sin\theta \, d\theta \, d\phi \tag{15}$$

where $I(\theta,\phi)$ is the intensity of the radiation, θ is zenith angle, and ϕ is azimuth angle. Of course, $F_{e\downarrow}$ and $I(\theta,\phi)$ are functions of altitude.

The contribution of downward diffuse radiation to flux density $F_{d\downarrow}$ is given by

$$F_{d\downarrow} = \int_0^{2\pi} \int_0^{\pi/2} I(\theta,\phi) \sin\theta \, d\theta \, d\phi \quad . \tag{16}$$

Assuming that the diffuse radiation is isotropic (i.e., I is a function of altitude only), then

$$F_{d\downarrow} = 2\pi I$$

and

$$F_{e\downarrow} = \pi I \quad ,$$

so

$$F_{d\downarrow} = 2F_{e\downarrow} \quad . \tag{17}$$

Similarly,

$$F_{d\uparrow} = 2F_{e\uparrow} \quad . \tag{18}$$

The total flux density F_d is given by

$$F_d = F_s + F_{d\downarrow} + F_{d\uparrow} \quad . \tag{19}$$

Since the method of Isaksen et al. (1977) is used in a number of transport-kinetics models, the differences between their method and the method presented here should be described. The differences are summarized in Table 15.

Note that the expressions involving scattering of the direct beam differ by a factor of 2 cos θ_o. Consequently, the Isaksen et al. (1977) model computes smaller flux densities for $\theta_o < 60°$ and larger flux densities for $\theta_o > 60°$.

The system of equations involving $F_{d\downarrow}$ and $F_{d\uparrow}$ described above may be solved using a successive scattering technique like that used by Isaksen et al. (1977), or they may be solved using a matrix inversion techhnique. The following system of equations is used with the matrix inversion technique:

$$F_{d\downarrow}(k+1) = f_t(k) \, F_{d\downarrow}(k) + f_s(k)[F_{d\downarrow}(k+1)]/2 + f_{so}(k) \, F_s(k) \cos\theta_o \tag{20}$$

$$F_{d\uparrow}(k) = f_t(k) \, F_{d\uparrow}(k+1) + f_s(k)[F_{d\downarrow}(k) + F_{d\uparrow}(k+1)]/2 + f_{so}(k) \, F_s(k) \cos\theta_o \quad . \tag{21}$$

Solving for the flux density at 44 atmospheric levels for 110 wavelength intervals requires 0.7 s of computer time (CDC 7600) using the matrix inversion technique and

TABLE 15. Differences between the LLNL multiple scattering algorithm and that of Isaksen et al. (1977).

Present method	Isaksen et al. (1977)
Isotropic scattering with $\overline{\sec\theta} = 1.66$	Scattered radiation is columnated with $\overline{\sec\theta} = \sec\theta_o$
Contribution to flux densities by scattering out of direct solar beam $\Delta F_{d\uparrow}(k) + \Delta F_{d\downarrow}(k+1) =$ $f_{so}(k)\,[F_s(k) - F_s(k+1)]\,2\cos\theta_o$	Contribution to flux densities by scattering out of direct solar beam $\Delta F_{d\uparrow}(k) + \Delta F_{d\downarrow}(k+1) =$ $f_{so}(k)\,[F_s(k) - F_s(k+1)]$
Contribution to flux density at the ground by scattering of the incident direct radiation $\Delta F_{d\uparrow}(K) = 2R\cos\theta_o F_s(K)$	Contribution to flux density at the ground by scattering of the incident direct radiation $\Delta F_{d\uparrow}(K) = R\,F_s(K)$

0.3 s using the successive scattering technique. Since the successive scattering algorithm uses less computer time and requires less computational storage space, we use this method in the LLNL transport-kinetics model. The computationally fast scheme enables multiple scattering to be included in diurnal transport-kinetics models.

In order to verify the accuracy of the model, flux densities and photodissociation rates were compared with a much more detailed calculation. The model used for comparison (see Luther and Gelinas, 1976) computes the intensity of the diffuse radiation as a function of zenith angle, then integrates over solid angle to determine flux density. The detailed model includes isotropic scattering at the earth's surface.

The flux densities computed using the simplified model are compared with the highly detailed flux density calculation in Figs. 39-43. The results shown are for a solar zenith angle of 30°. The simplified model overestimates flux densities in the wavelength interval 290-320 nm. This is the transition region between strong absorption (λ < 290 nm) and weak absorption (λ > 320 nm). At wavelengths greater than 320 nm, the results are accurate to within a few percent in the upper stratosphere, but the flux densities are underestimated in the troposphere and lower stratosphere.

The accuracy of photolysis rates computed using the simplified model (relative to the detailed calculation) is shown in Tables 16 and 17 for reactions where molecular scattering has a significant effect. The reactions are grouped by wavelength region. For the first group, photolysis cross sections are within the region 190-420 nm, and the rate coefficients vary by less than two orders of magnitude between the top and bottom of the atmosphere. For the second group, the primary contribution to photodissociation is at wavelengths less than 325 nm,

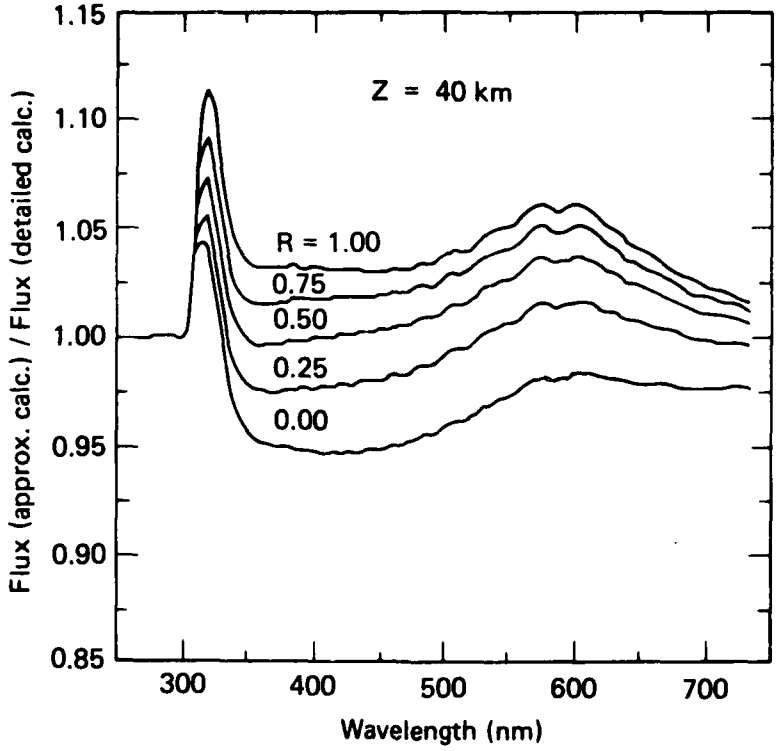

FIGURE 39. Ratio of photon fluxes at 40 km for a solar zenith angle of 30° computed using the LLNL algorithm (approx. calc.) and a detailed calculation. R is the surface albedo.

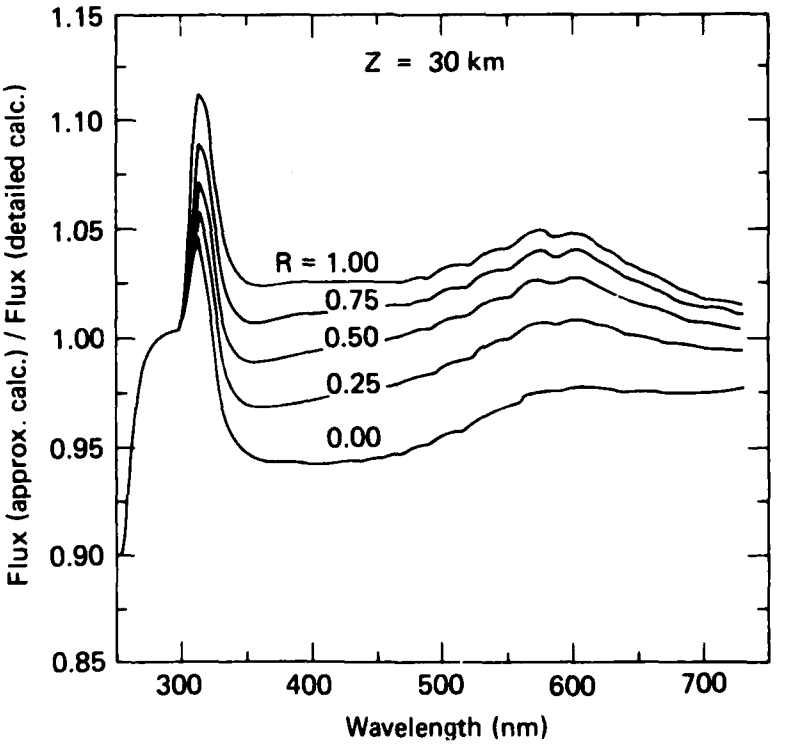

FIGURE 40. Ratio of photon fluxes at 30 km for a solar zenith angle of 30°.

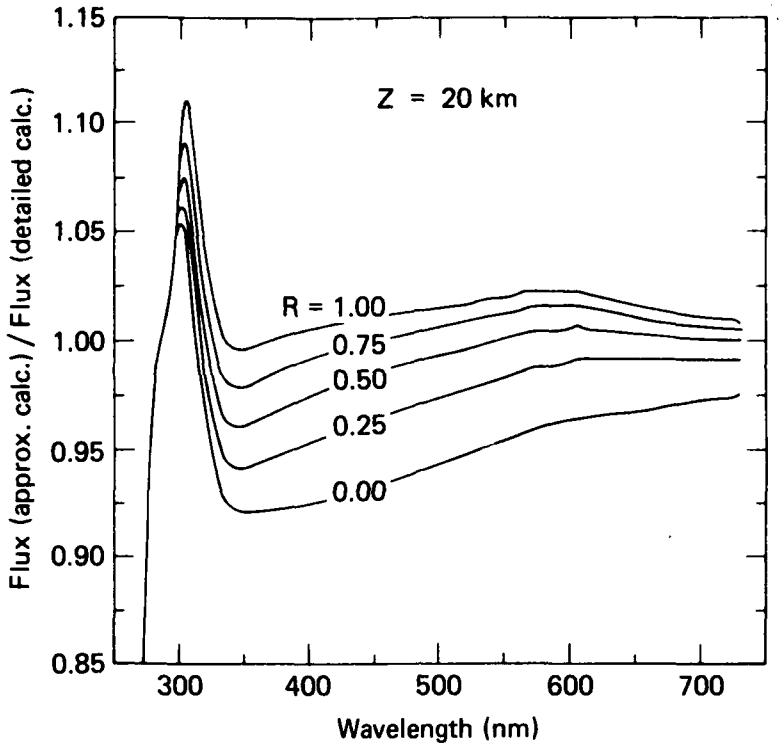

FIGURE 41. Ratio of photon fluxes at 20 km for a solar zenith angle of 30°.

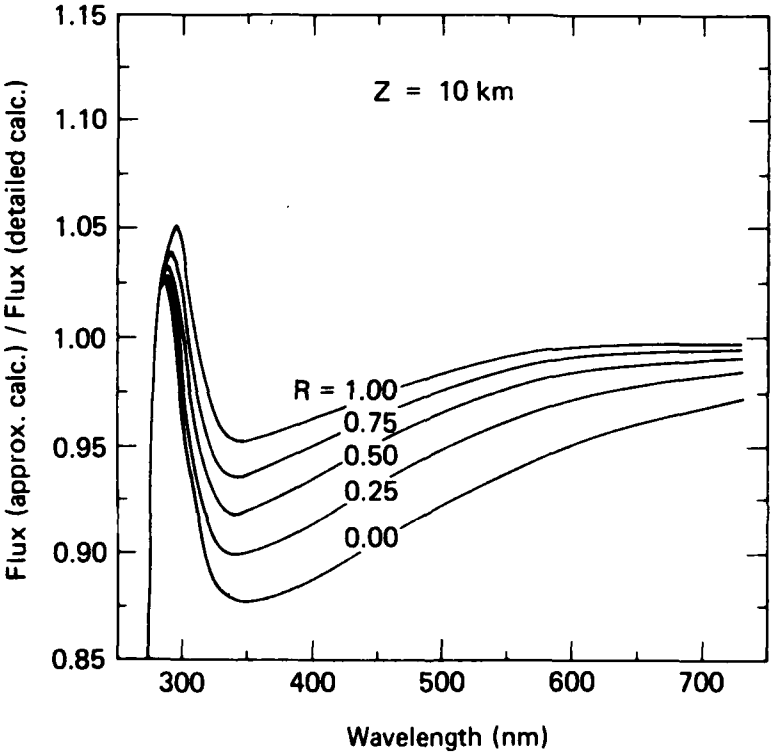

FIGURE 42. Ratio of photon fluxes at 10 km for a solar zenith angle of 30°.

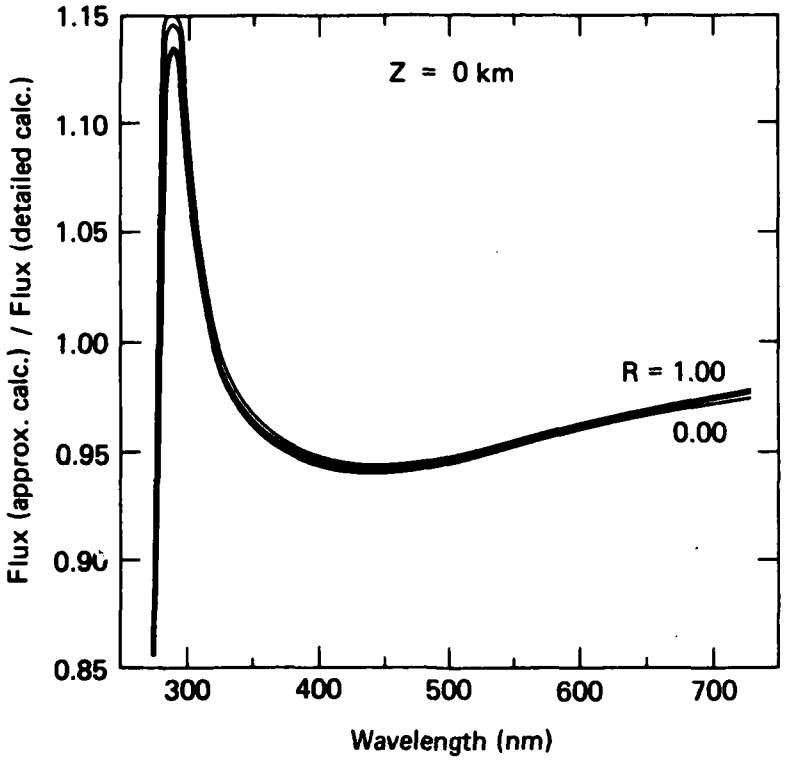

FIGURE 43. Ratio of photon fluxes at the ground for a solar zenith angle of 30°.

TABLE 16. Accuracy of computed photolysis rates for reactions where J(0 km)/ J(55 km) > 10^{-2}.

Reaction	Percent error			
	0-2 km	2-10 km	10-25 km	25-40 km
$O_3 + h\nu \rightarrow O + O_2$	-3 to -5	-5 to -6	-5 to 0	0 to +1
$H_2O_2 + h\nu \rightarrow 2OH$	-3 to -9	-9 to -11	- 11 to 0	0 to +1
$Cl ONO_2 + h\nu \rightarrow Cl + NO_3$	-3 to -9	-9 to -11	-11 to -1	-1 to +1
$Cl NO_2 + h\nu \rightarrow Cl + NO_2$	-3 to -9	-9 to -11	-11 to -2	-2 to +1
$HOCl + h\nu \rightarrow OH + Cl$	-3 to -9	-9 to -11	-11 to -2	-2 to +1
$CH_3OOH + h\nu \rightarrow CH_3O + OH$	-3 to -9	-9 to -11	-10 to 0	0 to +1
$HNO_4 + h\nu \rightarrow OH + NO_3$	-2 to -9	-9 to -11	-10 to 0	0 to +2
$NO_2 + h\nu \rightarrow NO + O$	-4 to -9	-9 to -10	-10 to -4	-4 to -2
$CH_2O + h\nu \rightarrow HCO + H$	-2 to -9	-9 to -11	-10 to +2	+1 to +2
$CH_2O + h\nu \rightarrow CO + H_2$	-3 to -9	-9 to -11	-11 to -2	-2 to +1
$HONO + h\nu \rightarrow OH + NO$	-4 to -9	-9 to -11	-10 to -4	-4 to -2

TABLE 17. Accuracy of computed photolysis rates for reactions where J(0 km)/J(55 km) is between 10^{-2} and 10^{-5}.

Reaction	Percent error			
	0-2 km	2-15 km	15-30 km	30-40 km
$O_3 + h\nu \rightarrow O(^1D) + O_2$	+1 to -6	-7 to 0	0 to +5	0 to +1
$C\ell O + h\nu \rightarrow C\ell + O$	+2 to -4	-6 to 0	0 to +5	0 to +1
$HNO_3 + h\nu \rightarrow OH + NO_2$	-1 to -7	-9 to -4	-4 to +2	0 to +1

where attenuation due to absorption and scattering is large. For both groups, the photodissociation rates are accurate to ±1% in the middle and upper stratosphere, but they are understimated in the troposphere by up to -11%. The accuracy varies with ground albedo and solar zenith angle. In general, the error in the radiative transfer model is less than the uncertainty in the photolysis cross sections.

2.7 Two-Dimensional Model Development

Based on our experience in the continuous development of the LLNL one-dimensional model and the aborted two-dimensional model of a few years ago, we are now coding up a fully modular two-dimensional model of stratospheric chemistry. Every physical process and mathematical algorithm is written as a separate subroutine. The main routine calls upon individual subroutines as needed to build and solve individual or family trace species conservation equations as illustrated in the flow diagram in Fig. 44. This flow diagram is essentially similar to our existing one-dimensional model except for the following subroutines. Subroutine SETKIN2D can set the chemical production and loss terms according to choices of families such as $O_X = O(^1D) + O + O_3$, not only the individual species $O(^1D)$, O and O_3. The choice of families can be specified at the beginning of each calculation. The associated partitioning within each family is determined in subroutine RADICAL. There is also the choice of fixing an individual family through the subroutine FIXY. This added feature allows more flexibility in using this model in interpreting specific field data when corroborative data are available. Subroutine RADICAL and the covergence test subroutine (CONVER) can be modified independent of any other subroutines. The model will have 19 latitudinal zones with equally spaced surface weighting and 25 equally spaced vertical grids for chemistry, extending from the surface to 50 km. The parameterized transport will be in pressure coordinates with the mean meridional velocities represented through stream functions so that along with the eddy diffusion transport we have a totally conservative transport diffusion equation to be solved. The chemical terms must be mapped to pressure coordinates at every time step using a second order interpolation algorithm.

We will use, at most, eight families or individual trace species (e.g., O_X, HO_X, $C\ell O_X$, NO_X, HNO_3, $C\ell ONO_2$, and $HC\ell$) plus an additional four to eight long-lived trace species (e.g., H_2O, CH_4, N_2O, $CF_2C\ell_2$, $CFC\ell_3$, etc.) depending on needs. The partition and choice of family grouping

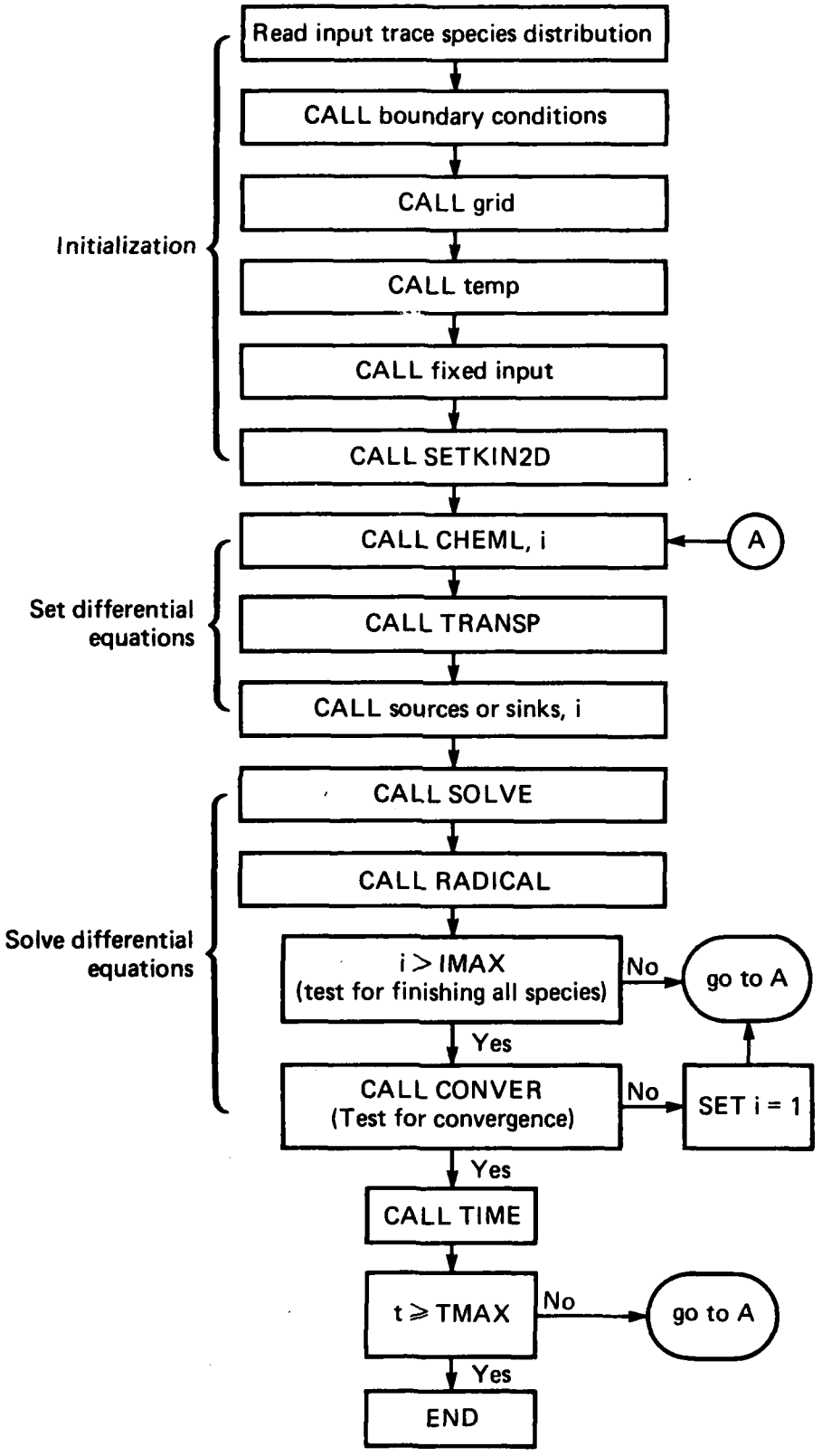

FIGURE 44. Flow diagram of the two-dimensional model.

will be determined through eigenstate analysis to preserve local physical relationships among trace species. For example, the interaction among NO, NO_2, and HNO_3 at 30 km can be represented by the vector equation

$$\frac{D}{Dt}\begin{pmatrix}[NO]\\[NO_2]\\[HNO_3]\end{pmatrix} = \begin{pmatrix}-\alpha_1 & \alpha_2 & 0\\ \alpha_1 & -\alpha_1-\gamma_2 & \gamma_3\\ 0 & \gamma_2 & -\gamma_3\end{pmatrix}\begin{pmatrix}[NO]\\[NO_2]\\[HNO_3]\end{pmatrix}$$

The characteristic solutions (eigenstate solutions) are

$$[NO] - .29[NO_2] + (4.8 \times 10^{-5})[HNO_3] = c_0\, e^{-(0.02)t}$$

$$[NO] + [NO_2] - .97[HNO_3] = c_1\, e^{-(6.74 \times 10^{-6})t}$$

$$[NO] + [NO_2] + [HNO_3] = c_2 \quad ,$$

from which we see that the sum of [NO] + $[NO_2]$ + $[HNO_3]$ remains constant. Hence, the total NO_x would be easy to solve. But in order to partition [NO] and $[NO_2]$ properly, we must consider the other two eigenstate solutions and consider the need to solve them simultaneously, since we can obtain c_0, c_1, and c_2 from the previous time step. We are currently setting up the algorithm for subroutines CHEML and RADICAL. The work on subroutine TRANSP is also in progress. We are hopeful of some preliminary test of the full code by mid-1981.

3. SATELLITE OZONE DATA PROCESSING, ARCHIVING, AND ANALYSIS

3.1 Overview

In March 1977 a multichannel filter radiometer (MFR) infrared sensor was first flown on a Defense Meteorological Satellite Program (DMSP) Block-5D-series satellite operated by the U.S. Air Force. The first four DMSP satellites (F1-F4) that were launched with MFR sensors measured infrared radiances in 16 channels, including the 9.6 μm band of ozone, from which it is possible to derive values of total column ozone. MFR sensor infrared measurements are taken day and night.

The combined data from these four sensors provided continuous global coverage for the time period from March 1977 to February 1980. The MFR data are the sole source of global ozone data for the period between mid-1977 and November 1978 (the end of the data record for Nimbus 4 and the beginning of Nimbus 7 measurements). The MFR data are also unique in that they are the only available global nighttime data and the only data in the polar night (high latitudes in winter).

All of the DMSP satellites are in polar, sun-synchronous orbits at altitudes of about 830 km. Their orbital parameters are essentially identical with the exception of F4, which is in a nighttime ascending orbit (i.e., F4 ascends from southeast to northwest on the night side), whereas the others are in daytime ascending orbits. The local overpass times for each satellite are shown in Table 18. Although F2 and F4 are only about an hour apart in their overpass times, their flight tracks are different, thereby better enabling F4 to fill data-void areas of F2 and F3.

Each MFR sensor measures infrared radiation emitted from the Earth's surface and constituents in the atmosphere at 16 narrow spectral intervals (channels). The spectral channels coincide with the atmospheric absorption (emission) bands of water vapor, carbon dioxide and ozone. One channel in the atmospheric window is used to sense thermal radiation from the Earth's surface. The spectral centers and other characteristics of the 16 channels are given in Table 19. Only channels 1, 3, 7 and 16 are currently used in the retrieval methodology.

The MFR scans side to side in discrete steps of 4° in look angle. The sensor takes infrared radiance measurements at 25 cross-track scanning locations every 32 seconds. Figure 45 shows the Earth-projected scan pattern for the 25 cross-track measurements. The instrument could take a theoretical maximum of 67,500 sets of measurements (of 16 radiances each) per day, but typically 35,000-45,000 measurements are taken per day due to instrument sun screens (F2, F3), scan position blockage (F3), and data receipt and recovery problems.

3.2 Ozone Retrieval Methodology

The ozone retrieval methodology is described schematically in Fig. 46. The ozone retrieval model is developed through regression analysis using sets of simulated MFR radiances derived from detailed radiative transfer calculations. Historical vertical profiles of temperature and ozone concentration are used as input to the calculations. Temperature-dependent molecular absorption coefficients for the 9.6-μm ozone band and the 15-μm carbon dioxide band are determined from high-resolution line-by-line calculations. These coefficients are used to compute transmittances at high spectral resolution for each of the temperature and ozone profiles. These high-resolution transmittances are input to the radiative transfer model that computes simulated MFR radiances. For each of the atmospheric profiles, simulated radiances are computed for different surface temperatures, cloud amounts, and instrument scan angles. Transmittances due to the water vapor continuum absorption in the atmospheric window are calculated with an "e-type" model. A regression model, based on data from line-by-line calculations, plus continuum effects, is used for the tropospheric water vapor transmittance calculations in the 15-μm spectral region. A Goody random band model is employed to calculate the transmittances due to the 14 μm ozone band.

3.2.1 Historical Ozonesonde Data

The historical ozonesonde data base consists of vertical soundings for which temperature and ozone partial pressure are available. The soundings have been collected by the Air Force Cambridge Research Laboratory Ozonesonde Network and the World Ozone Data Center (WODC) (operated by the Atmospheric Environment Service of Canada in cooperation with the World Meteorological Organization). This data base includes soundings from the early 1960's into 1980. Selected subsets of these data are used in the radiative transfer calculations.

3.2.2 Generation of Simulated Measurements

Sets of simulated radiance measurements are computed for each of the atmospheric soundings selected from the historical ozonesonde data base. For computational purposes, the globe is divided into 11 latitude bands. Twenty soundings are selected for each latitude band per month. The subsets of soundings are selected randomly and tested using principal components analysis and a student's

TABLE 18. The data periods covered by the MFR sensors on the DMSP satellites.

DMSP satellite	Data period	Local overpass time
F1	March 1977-July 1977	11-12 a.m. and p.m.
F2	July 1977-February 1980	9-10 a.m. and p.m.
F3	August 1978-January 1980	6-7 a.m. and p.m.
F4	June 1979-January 1980	10-22 a.m. and p.m.

TABLE 19. Nominal MFR channel characteristics.

Channel number	Center (μm)	Center (cm^{-1})	Half width (cm^{-1})	Species	NESR[b]
1[a]	15.0	668.5	3.5	CO_2	0.30
2	14.8	676.0	10.0	CO_2	0.09
3[a]	14.4	695.0	10.0	CO_2	0.10
4	14.1	708.0	10.0	CO_2	0.11
5	13.8	725.0	10.0	CO_2	0.11
6	13.4	747.0	10.0	CO_2	0.12
7[a]	12.0	835.0	8.0	Window	0.11
8[c]	18.7	535.0	16.0	H_2O	0.15
9	24.5	408.5	12.0	H_2O	0.14
10	22.7	441.5	18.0	H_2O	0.09
11	23.9	420.0	20.0	H_2O	0.12
12	26.7	374.0	12.0	H_2O	0.18
13	25.2	397.5	10.0	H_2O	0.16
14	28.2	355.4	15.0	H_2O	0.25
15	28.3	353.5	11.0	H_2O	0.33
16[a]	9.8	1022.0	12.5	O_3	0.05

[a]Used in the ozone retrieval model.

[b]NESR = Noise Equivalent Spectral Radiance in $mW/(m^2\ sr\ cm^{-1})$.

[c]Not on Flight Model 1.

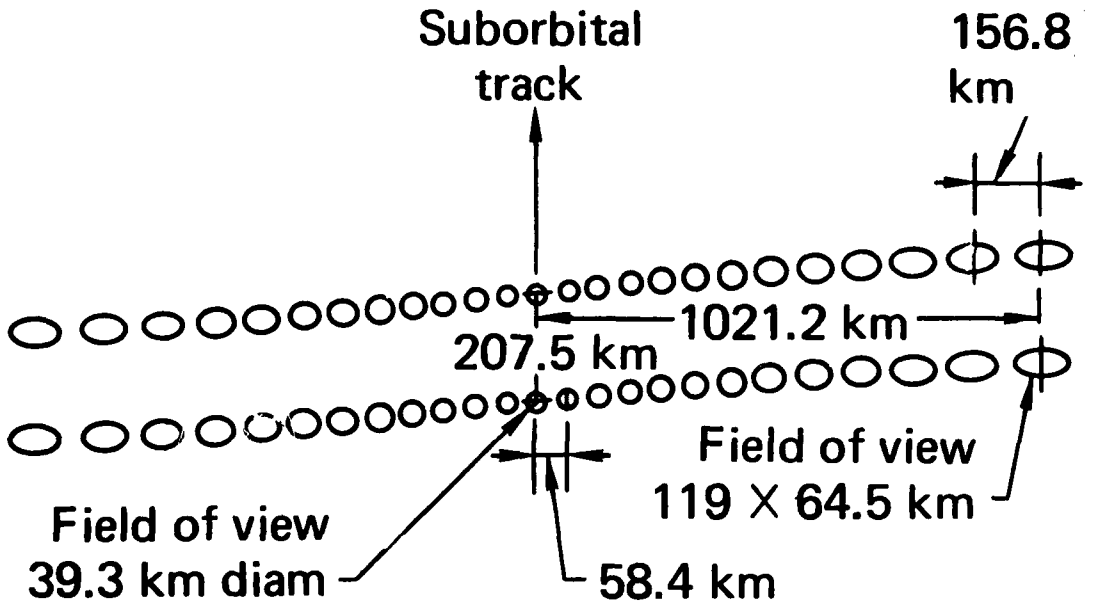

FIGURE 45. Earth-projected scan pattern for the MFR sensor (after Nichols, 1975).

t-test to make sure that the temperature and ozone profiles are representative of the full population. The "most representative" set of 20 is used among 500 random selections of 20 soundings.

High resolution transmittances for the 9.6-μm ozone band and 15-μm carbon dioxide band are computed between 21 atmospheric levels for each sounding. The accuracy of the model used to compute these high resolution transmittances has been tested by comparison with laboratory transmittance measurements.

The weighting function for Channel 1 extends from approximately 1-100 mb with a peak near 20 mb. The weighting function for Channel 3 extends from approximately 10-300 mb with a peak near 100 mb. The total transmittances for Channels 1 through 6 are the product of the carbon dioxide transmittances from the line-by-line derived regression calculations, the 14-μm ozone transmittances determined with the random band model and the tropospheric water vapor transmittances from the regression model. The transmittances for channel 16 are the product of line-by-line derived regression transmittances for the 9.6-μm ozone bands and e-type water vapor continuum transmittances in the lower troposphere. The transmittance profile for Channel 7 (the window channel) is from e-type model calculations only.

Simulated radiances for the various MFR channels are computed for several surface temperatures, cloud amounts and scan angles for each set of high-resolution transmittances. Cloud amounts are selected randomly for, at most, two cloud levels. The sets of cloud conditions are also chosen randomly, as are three surface temperatures (normally distributed with a defined mean and standard deviation) for each cloud condition. Cloud-free calculations are also computed for each surface temperature chosen. Calculations are made for four scan angles. Consequently, 72 sets of simulated radiance measurements are computed for each atmospheric sounding.

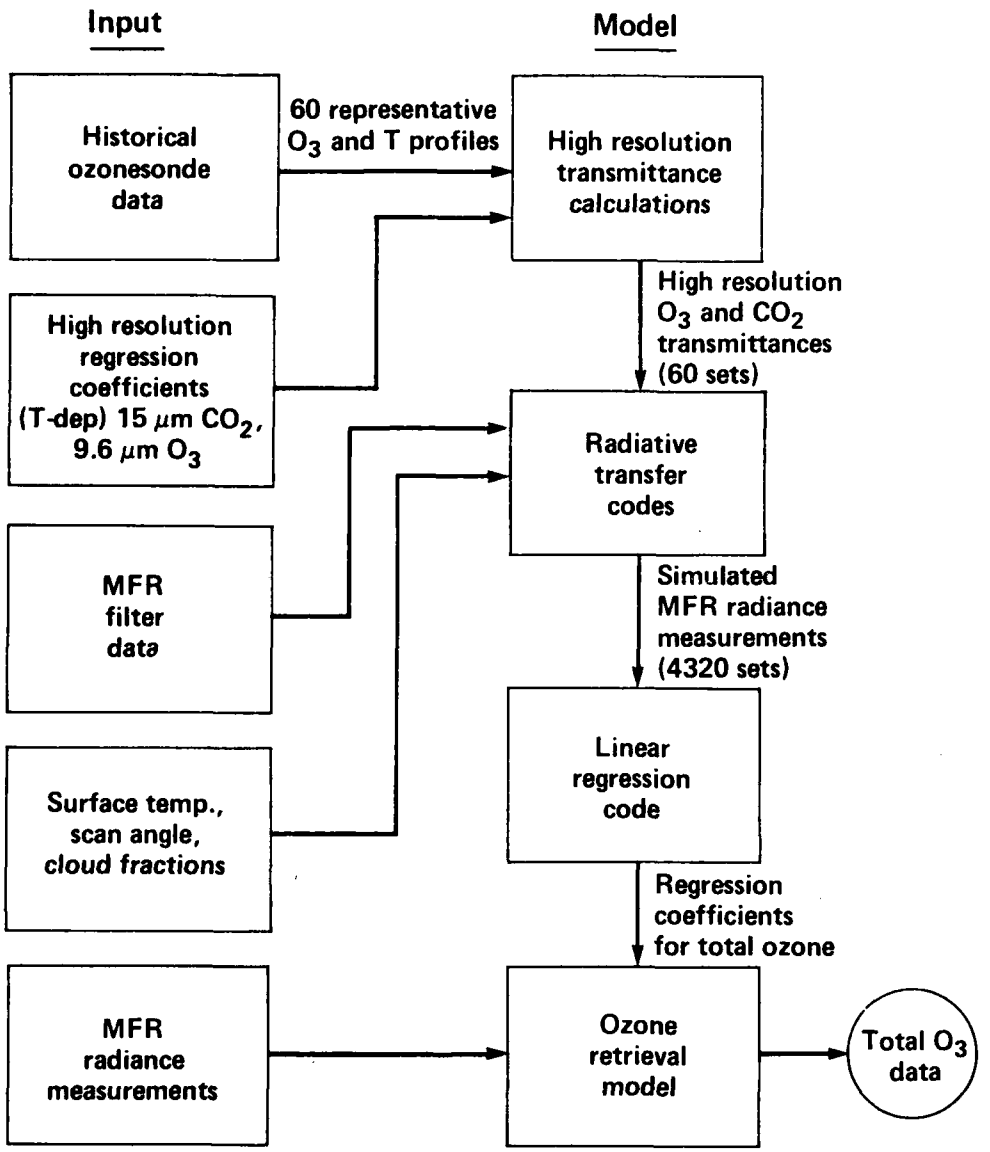

FIGURE 46. Development sequence for the ozone retrieval model.

3.2.3 Generation of Regression Coefficients

The simulated measurement sets generated for each latitude band and month are grouped into three-month sets. Each set of 60 soundings (4320 radiance sets) and the total column ozone corresponding to each sounding form the basis for the empirical retrieval scheme. Total ozone is modeled as a linear combination of two MFR channel radiances, nonlinear functions of the ozone and window channel radiance, and the secant of the zenith angle. The nonlinear functions are included primarily to account for the effects of clouds and background.

The total column ozone is determined using the linear model

$$O_3 = \beta_0 + \sum_{n=1}^{m} [\beta_n f_n(N,\theta)]$$

where O_3 is total ozone, β_0 and β_n are regression derived coefficients, and f_n are functions of the MFR radiances (N) and zenith angle (θ). The β coefficients are computed from the simulated radiances using linear regression analysis. Different sets of βs are generated for each of the 12 three-month data sets in each of the 11 latitude bands.

3.2.4 Retrieval Model Continuous in Space and Time

A retrieval model that is continuous in space and time is generated by blending across latitude band boundaries and by blending between "monthly" models. Latitudinal weighting is used across spatial boundaries and time weighting is used to blend between "monthly" models. The resulting model is a linear combination of submodels in discrete time and space domains.

3.3 Data Processing and Data Archiving

The MFR radiance data are transmitted from the DMSP satellites to the Air Force Global Weather Central (AFGWC). The data are shipped to LLNL on magnetic tape. Each tape contains approximately 24 h of data in an unprocessed (sensor bit stream) format as 36-bit packed integers. The data are converted to 60-bit words (word size of LLNLs CDC 7600 computers), then the data are calibrated and Earth-located. A check is made for erroneous data arising from either instrument failure, recording or transmission errors.

3.3.1 Data Processing

The calibrated, earth-located radiance data are input to the regression model that calculates corresponding total column ozone values. The processing code contains the regression models for each particular latitude band and month and applies the time-space averaging when the ozone retrieval is made.

In order to evaluate the quality of the retrieved ozone data, we routinely compare them with independent ground-based measurements of total ozone. The ground-based measurements used in this comparison consist of Dobson spectrophotometer total ozone observations that are taken close in time to the satellite MFR measurements in the vicinity of the Dobson observatory. In line with the data processing, MFR ozone data that are close to selected Dobson stations (within time and distance criteria) are paired with the Dobson data and saved in a separate file for later analysis.

3.3.2 Mapping of Total Ozone Data

The satellite ozone retrievals are averaged over 2.5° latitude-longitude grid intervals or bins. The bins remaining empty after 24 hours of data mapping require filling, which is accomplished by one of the following methods depending on the data available. The methods are listed in decreasing order of preference: (1) interpolate between the binned data of the day preceding and the day following, (2) use the binned data from the day preceding or the day following, (3) use the zonal average values that are computed from the binned data for that day, or (4) use zonal average values that are taken from known climatology.

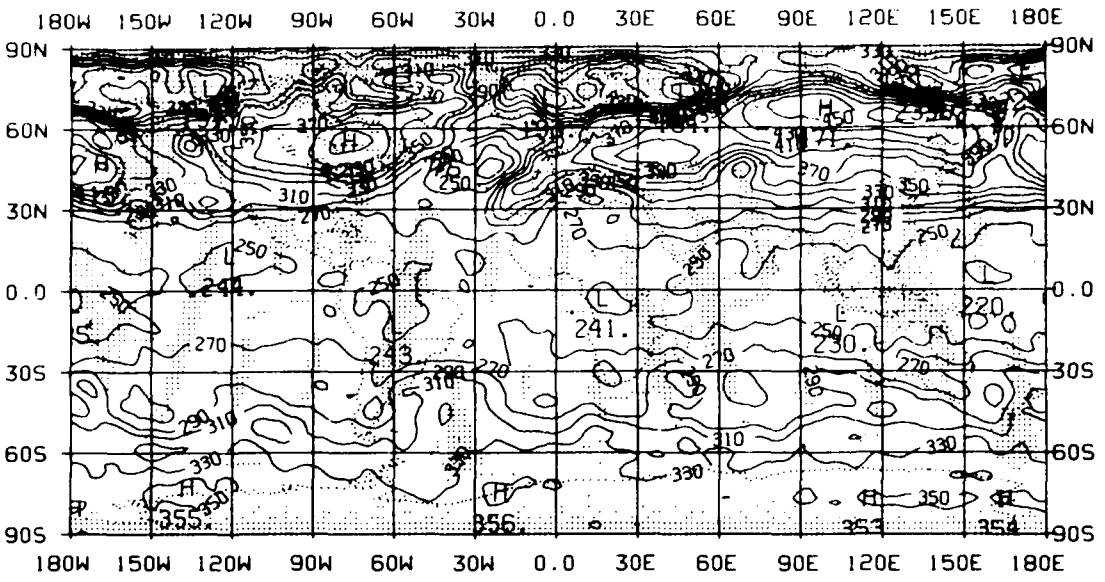

FIGURE 47. Contour map of total ozone for January 5, 1979. Shaded regions indicate data-void areas.

After data-void areas are filled, the resulting fill-field is smoothed. This process removes small-scale features (e.g., 5° horizontal wavelength and smaller) but retains large-scale features (e.g., a wavelength of 60° is retained at 96% of its original amplitude) in the data-void regions. Thus, only the large-scale features that change little from day to day are used as an "intelligent fill". The resulting global ozone grid is then filtered using a Lanczos filter (Duchon, 1979) with a wavelength cutoff at 10° or smaller, and plotted on an ozone contour map. A map of preliminary total ozone data for January 5, 1979, is shown in Fig. 47. Data-void regions are indicated by the shaded areas.

An ozone analysis that is to be displayed on a polar stereographic map projection is binned and data filled in the same manner as the above cylindrical equidistant projection, except the ozone data are gridded on the National Meteorological Center (NMC) grid rather than a 2.5° latitude-longitude grid. The NMC grid is a rectangular grid overlaying a polar stereographic map projection.

3.3.3 Data Basing

The computer capability at the Atmospheric Release Advisory Capability (ARAC) center at LLNL is used for data basing and data processing. Code development is done on the LLNL CDC 7600 computers, after which they are transferred to the DEC VAX 11/780 computer system in the ARAC center. Processing of preliminary ozone data for intercomparison with other satellite data has been done on the CDC 7600 computer while the data base management system was being implemented on the VAX 11/780 computer. The VAX system at LLNL is more cost efficient for large-scale data processing than is the CDC 7600.

A relational data base management system called FRAMIS (Jones and Ries, 1978) was chosen for use with the data base. FRAMIS was developed by LLNL's Computation Department for the CDC 7600, and was designed for large scientific data bases. It took about one year to convert all 400 subroutines from the CDC 7600 to the VAX, and the version on the VAX is currently being tested extensively on sample data sets. The ozone data base is designed in such a way that extraction of data subsets by time and/or geographical location is performed efficiently.

3.3.4 Data Archiving

High density magnetic tape (6250 bpi) has been selected as the long-term storage medium for the data base. One tape can store approximately one month of data (including the raw radiances, the retrieved ozone values, and related data).

3.4 Data Analysis

In early 1980, MFR data from January 1 to February 15, 1979, were processed for comparison with other satellite ozone measurements and with Dobson measurements of total ozone. The ozone data were preliminary in that they revealed some difficulties with the retrieval methodology. Various alternatives for improving the methodology were studied, and the retrieval methodology was finalized at the end of 1980. The data shown here are the preliminary data reported by Luther et al. (1980).

3.4.1 Latitudinal Distribution of Total Ozone

The daily average latitudinal distribution of ozone for January 1979 is shown in Fig. 48. The global mean total ozone is 291.3 DU,* and an average of 37,296 retrievals were made each day. The daily count was higher for the first 15 days in February 1979, averaging nearly 42,000 retrievals per day.

The latitudinal distribution of ozone varies qualitatively as expected with a minimum near the equator and maxima near the poles. However, the sharp drop in total ozone between 60°N and the pole appears to be anomalously large. The drop is even larger than shown during the early part of January when stratospheric temperatures were among the coldest recorded during the past 20 years. But later in the month as stratospheric temperatures warm, the decrease becomes progressively less with only a small decrease in total ozone between 60 and 90°N occurring for days near the end of January. The problem appears to be that the soundings of temperature and ozone partial pressure used in developing the regression model did not adequately include the temperature regime that existed in early January 1979.

3.4.2 Global and Hemispheric Total Ozone

The variation of global and hemispheric mean ozone values with time is shown in Fig. 49. The global mean ozone varies slowly with time, increasing only about 5 DU between mid-January and mid-February. The hemispheric mean values show

*Dobson Unit, or the thickness in millicentimeters of the column of ozone at standard temperature and pressure (1 atm); also referred to as m•atm•cm.

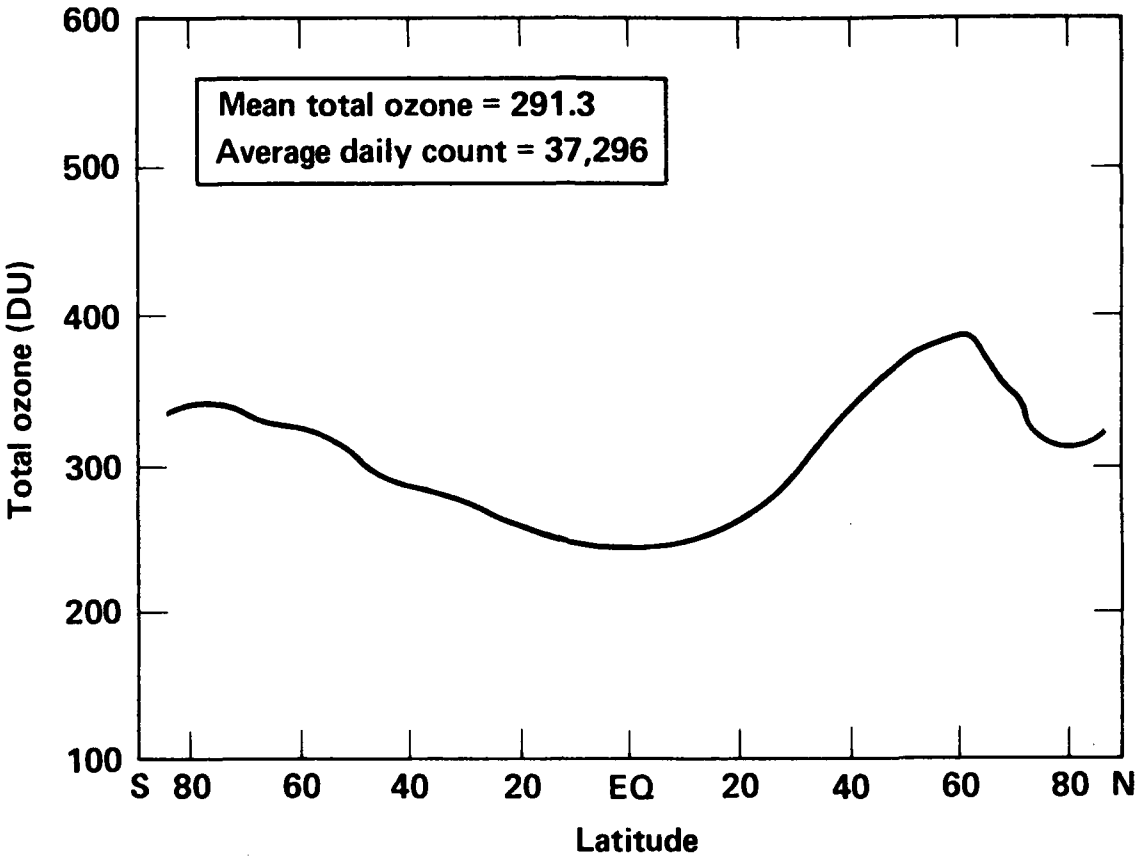

FIGURE 48. Average latitudinal distribution of total ozone for January 1979.

larger variations, with the Southern Hemisphere decreasing about 10 DU and the Northern Hemisphere increasing about 15 DU during the 46-day period. The variations in hemispheric ozone amounts are consistent with the variations reported by London et al. (1976).

The global mean of 291.3 DU for the MFR ozone data is somewhat higher than the average for January reported by London et al. (1976) of 285 DU. When hemispheric ozone amounts are compared, it is seen that most of the increase occurs in the Northern Hemisphere. The averages are 302 and 280 DU for the Northern and Southern Hemispheres, respectively, for the MFR ozone data compared to 293 and 277 DU from London et al. (1976). The difference is 9 DU for the Northern Hemisphere and 3 DU for the Southern Hemisphere.

3.4.3 Comparison with Preliminary Nimbus 7 SBUV Data

Global mean ozone amounts were compared with preliminary SBUV data from Nimbus 7 for January 1979 (Don Heath, private communication, 1980). The two sets of data have similar means and day-to-day variations as summarized in Table 20 for the 22 days that are common to both data sets.

3.4.4 Data in 10° Latitude Bands

Daily mean ozone values are shown in Figs. 50a, b and c for 10° latitude bands in the Northern Hemisphere. For comparison, the ozone data for 10°-latitude bands

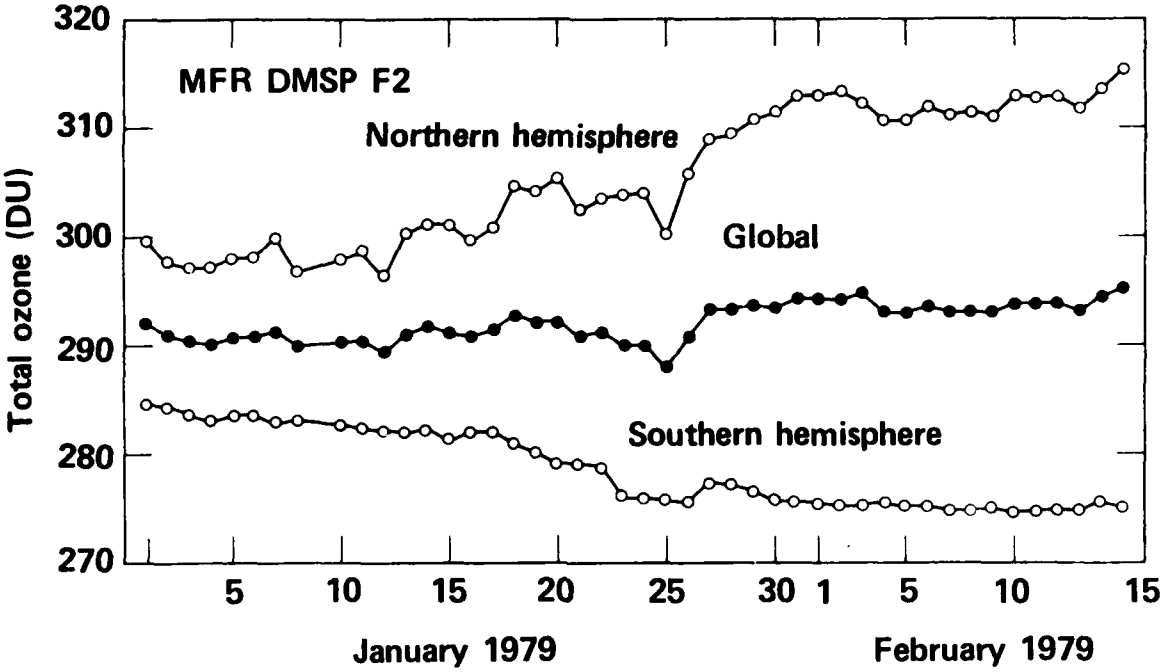

FIGURE 49. Daily global and hemispheric ozone amounts during January and February 1979.

from London et al. (1976) are given in Table 21. The data are a summary of January mean data taken between 1958-1967.

The January 1979 MFR data for 10° latitude bands are higher than the average of the January data between 1958 and 1967, but they are not as large as the maximum values observed during that period. The difference between ozone amounts for adjacent latitude bands obtained from the MFR data closely match the difference between the average values for the 1958-1967 period. Consequently, the latitude distribution of MFR ozone amounts is very similar to the observed distribution, however, the MFR data are larger by 10-15 DU.

There is a noticeable decrease in the amount of ozone on January 25 for the 40-50°N-latitude band (Fig. 50b). This change in ozone turns out not to be real, but is the result of a reduction in spatial coverage. The number of data points was only about 22,000 on Janury 25 compared to approximately 30,000 on the preceding days. The reduced spatial coverage would not generally be a significant source of error, but in this particular case some regions of high ozone content are missed at high northern latitudes. This feature also appears in the data for the 50-60°N band (Fig. 50c).

The 50-60°N-band data show a significant increase in ozone amount beginning about the third week of January. This coincides with the onset of a stratospheric warming event that lasted into late February.

3.4.5 Comparison with Dobson Data

The MFR total ozone data are compared with Dobson measurements in order to evaluate the ozone retrieval methodology. A total of 37 Dobson observatories have taken special ozone measurements near DMSP satellite overpass times. The locations of these Dobson observatories are shown in Fig. 51. MFR total ozone data

TABLE 20. Comparison of global mean total ozone.

	Mean (DU)	Standard deviation (DU)
MFR DMSP F2	291.0	1.1
SBUV Nimbus 7	291.5	1.3

TABLE 21. Comparison of MFR and London et al. (1976) total ozone data for January.

	Average total ozone			
	London et al. (1976)			MFR
Band	Min.	Avg.	Max.	1979
0-10°N	223	233	246	246
10-20°N	230	243	257	253
20-30°N	250	264	279	274
30-40°N	287	300	319	314
40-50°N	311	340	378	356
50-60°N	328	368	421	380

have been compared with Dobson measurements taken between January 1 and February 15, 1979, and the results are summarized in Table 22. Table 22 shows comparisons where the MFR and Dobson measurements are within 300 km and 300 min of each other. Percentages are computed with respect to the Dobson values. On the average, the MFR ozone values are 2.2% less than the Dobson values. For the 607 comparisons, the RMS difference was 7.2%, which is the result of the bias between the two data sets and the amount of noise and measurement error inherent in each observational system.

3.5 Major Accomplishments During the Reporting Period

During 1980, the ozone retrieval methodology was finalized, and we are preparing to begin processing of the MFR data. Many tasks needed to be accomplished in order to get to this point. Some tasks progressed continuously throughout the reporting period, whereas others were rather intense efforts for short periods of time.

The reporting period may be broken into three sections where there were significant differences in emphasis:

1. October 1979-February 1980. The major emphasis was on the initial processing of 46 days of MFR data (January 1-February 15, 1979) for intercomparison with other satellite ozone data.

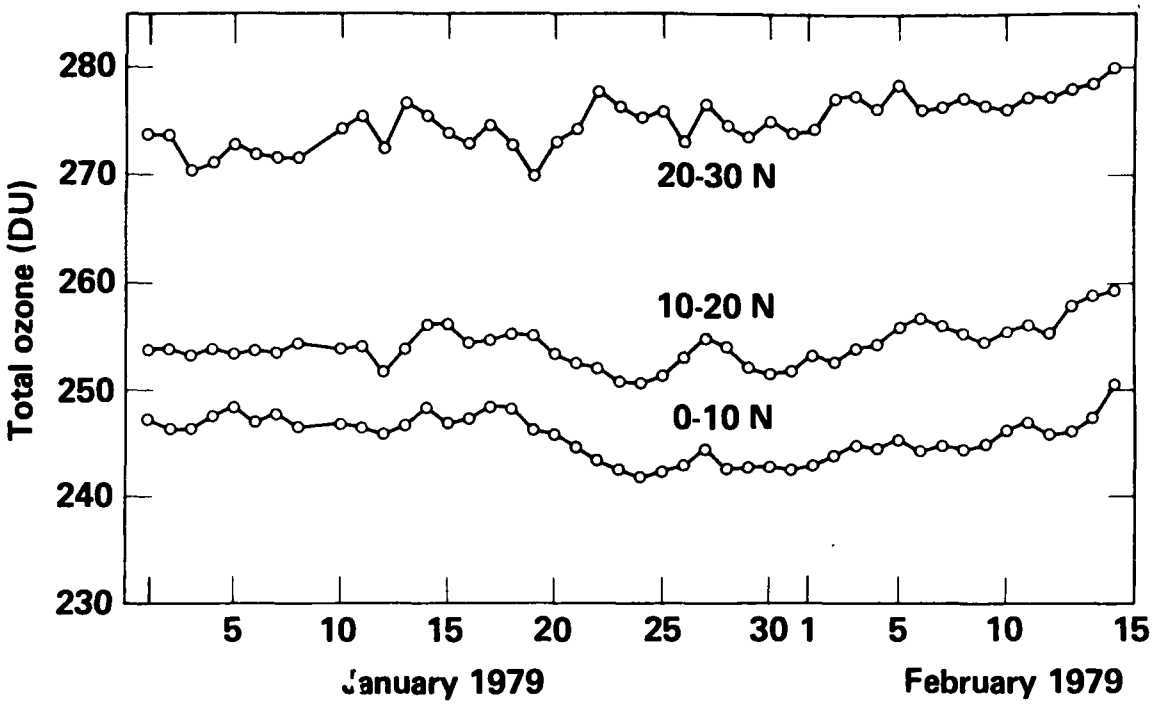

FIGURE 50a. Daily ozone amounts for latitude bands 0-10°N, 10-20°N, and 20-30°N.

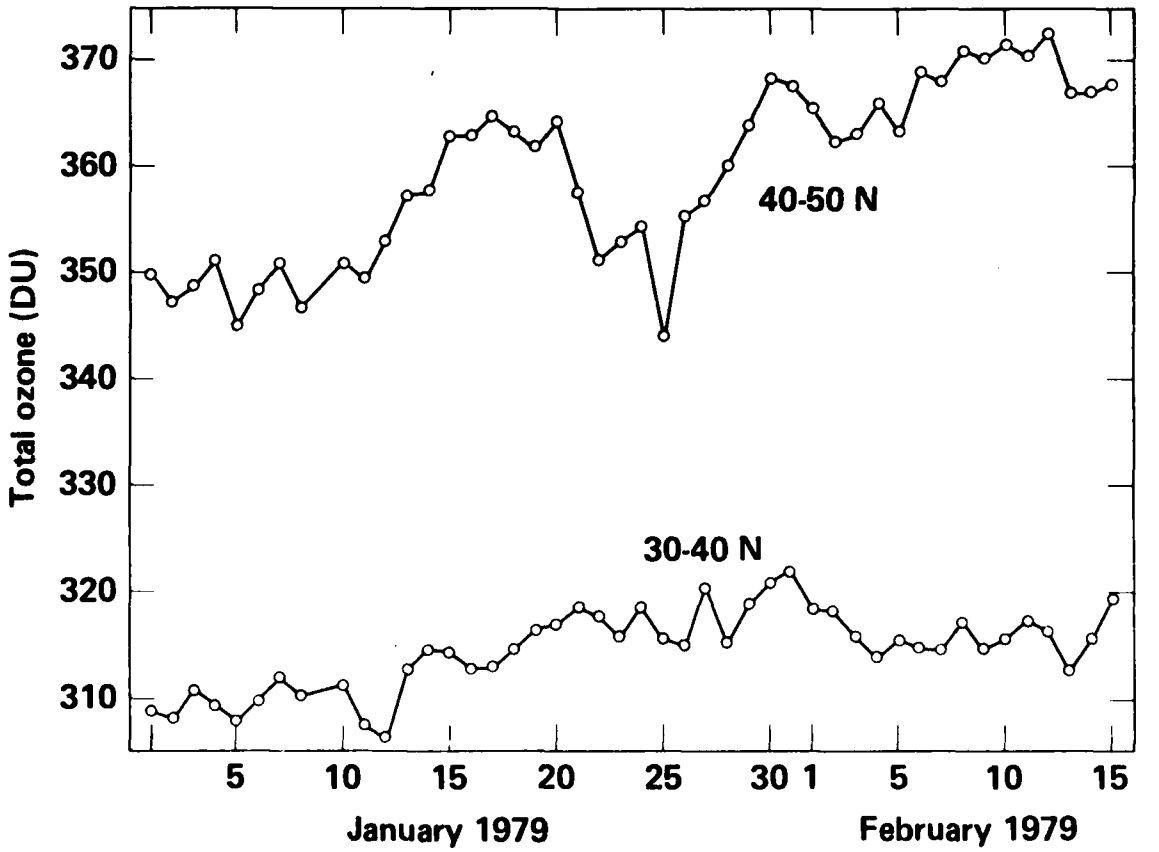

FIGURE 50b. Daily ozone amounts for latitude bands 30-40°N and 40-50°N.

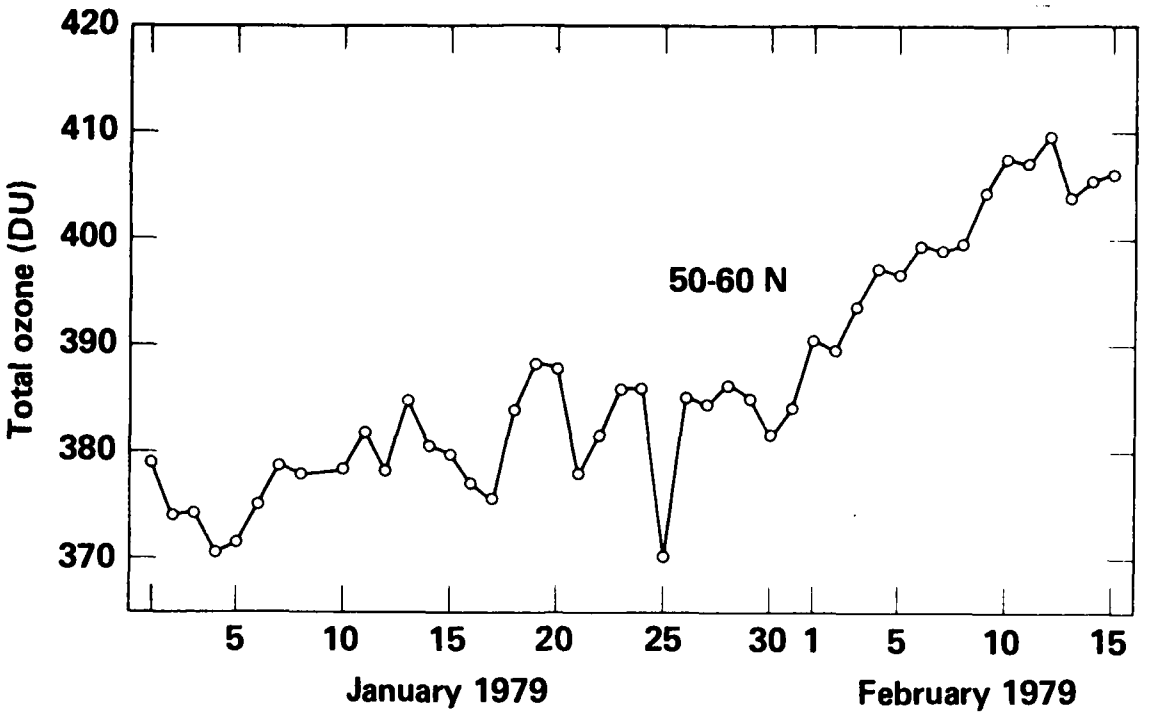

FIGURE 50c. Daily ozone amounts for the latitude band 50-60°N.

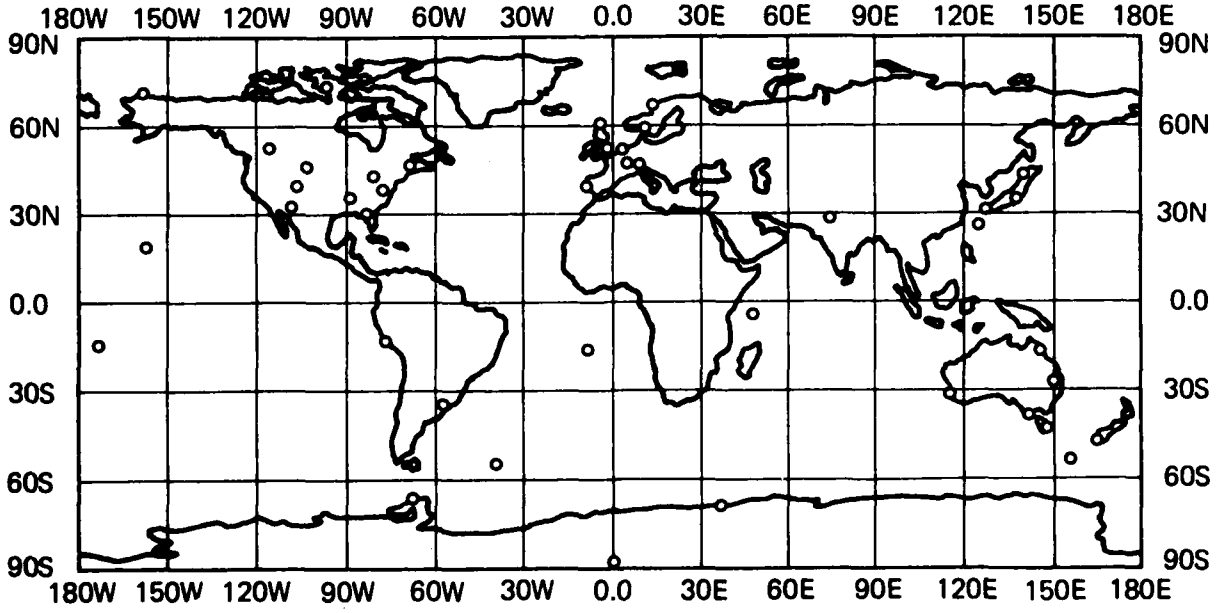

FIGURE 51. Locations of the Dobson spectrophotometer observatories where special measurements of total ozone have been taken for comparison with MFR-derived total ozone data.

TABLE 22. Comparison of preliminary MFR and Dobson data taken between January 1 and February 15, 1979.

Station	Lat.	Days	Δ Dist (km)	Δ Time (min)	O_3 (sat.) (DU)	O_3 (Dob) (DU)	Δ O_3 (DU)	Δ O_3 (%)	RMS diff (DU)	RMS diff (%)
Resolute	75N	8	42	149	355	389	-34.0	-8.7	46.3	11.9
Lerwick	60N	5	154	204	328	339	-11.0	-3.2	25.0	7.4
Oslo	60N	12	45	132	384	373	11.8	3.2	22.7	6.1
Edmonton	54N	25	82	262	392	412	-20.0	-4.8	39.3	9.5
Bracknell	51N	7	187	233	349	351	-2.5	-0.7	18.6	5.3
Hohenpeissenberg	48N	4	150	231	358	361	-3.1	-0.9	6.7	1.9
Caribou	47N	10	88	262	391	429	-37.2	-8.7	41.6	9.7
Arosa	47N	24	55	181	352	342	9.6	2.8	25.9	7.6
Bismark	47N	15	83	230	373	391	-17.8	-4.6	31.5	8.1
Toronto	44N	19	60	189	369	407	-38.5	-9.5	46.0	11.3
Sapporo	43N	18	86	213	385	416	-31.1	-7.5	43.5	10.5
Boulder	40N	16	108	211	332	347	-15.5	-4.5	27.7	8.0
Lisbon	39N	5	81	164	310	299	11.2	3.8	21.6	7.2
Wallops Island	38N	10	124	243	336	362	-25.5	-7.0	33.1	9.2
Nashville	36N	16	120	222	314	350	-36.0	-10.3	42.4	12.1
Tateno	36N	30	106	180	340	343	-3.1	-0.9	20.2	5.9
White Sands	32N	23	69	182	306	324	-17.8	-5.5	27.5	8.5
Kagoshima	32N	24	91	174	306	301	5.4	1.8	15.4	5.1
Tallahassee	30N	17	92	194	285	295	-9.6	-3.3	16.6	5.6
New Delhi	29N	11	68	80	307	318	-11.3	-3.6	16.5	5.2
Naha	26N	18	79	139	261	266	-4.5	-1.7	10.5	4.0
Mauna Loa	20N	11	106	184	266	266	0.4	0.1	9.8	3.7
Seychelles	5S	29	75	24	244	262	-17.4	-6.6	19.0	7.3
Huancayo	12S	23	65	179	249	258	-9.5	-3.7	13.1	5.1
Samoa	14S	5	49	97	244	255	-10.8	-4.2	12.8	5.0
St. Helena Island	16S	12	71	109	265	273	-8.0	-2.9	12.4	4.5
Cairns	17S	13	75	226	245	257	-12.1	-4.7	20.4	7.9
Brisbane	27S	9	92	233	267	268	-0.7	-0.3	11.6	4.3
Perth	32S	19	78	124	273	281	-7.8	-2.8	10.5	3.7
Aspendale	38S	30	88	142	276	287	-11.4	-4.0	14.8	5.1
Hobart	43S	27	106	170	279	262	16.9	6.4	20.8	7.9
Invercargill	46S	5	83	230	287	306	-18.7	-6.1	30.3	9.9
So Georgia Island	54S	37	63	34	309	305	3.7	1.2	21.4	7.0
Macquarie	54S	2	27	173	328	320	7.7	2.4	7.9	2.5
Argentine Island	65S	38	60	29	318	299	18.6	6.2	24.5	8.2
Syowa	69S	30	58	157	326	320	6.9	2.1	14.2	4.4
Station average:		607	81	156	312	319	-7.0	-2.2	23.0	7.2

2. March-August 1980. The major emphasis was on improving the ozone retrievals at high latitudes, particularly in the polar night.

3. August-December 1980. When the changes to the methodology were implemented and MFR data from January 1979 were reprocessed, we were not pleased with the results. Consequently, the major emphasis was on studies to determine why the changes did not improve our retrievals and to develop alternative methods that would give better results.

3.5.1 October 1979-February 1980

The modification, optimization, and documentation of the computer codes used for generating simulated radiances from which ozone retrieval models are developed was completed. Improvements were made in the way absorber amounts

were determined for layers of the various multilevel atmospheric models under the "plane parallel" assumption for paths through the atmospheres. The technique used for making 14 μm band model calculations was also changed. Also, major revisions were made to the codes in order to improve the I/O, decrease the computer run time, and to make the files simpler to manage. The result of these optimization efforts was a reduction of total computer time by a factor of 15, with additional savings to be realized for each satellite requiring calculations. These codes were implemented for the ozonesonde data applicable to the January-February 1979 intercomparison effort.

Additional ozonesonde data were obtained from the WODC in order to enlarge our ozonesonde data base and to incorporate the most recent available data. Our ozonesonde data base includes nearly 7000 sondes from which representative sets of data are selected for each month of the year. The sonde data were checked for accuracy, and sondes with obvious or suspected instrument problems were eliminated.

It was determined that measurements in Channel 2 (the carbon dioxide channel that has a peak response near the level of ozone maximum) were affected by a mirror stepping problem on flight models F2-F4. The design problem, causing a movement of the field of view during the radiance measurement for this channel, was confirmed by the Air Force and its contractor. Ozone retrieval models with and without Channel 2 were generated and tested using F2 data for the intercomparison period. Initial retrieval results using these models indicated that retrievals using models including Channel 2 were not as good as those using models without it.

A versatile code was developed to analyze the derived ozone data and satellite radiance data. Data for specific regions can be extracted and printed or displayed graphically. The code is used to analyze retrieval problems, such as are likely to occur in cloudy or cold background conditions. The goal was to improve the retrievals in these problem areas. In addition, the data calibration code was modified to handle the different data format of the F4 satellite.

We completed an evaluation of various data fill and data smoothing techniques. Data void areas were filled with data using the "intelligent fill" technique described in Section 3.3. Codes were also developed that generate analyses at 2.5° latitude-longitude grid intervals that match the NMC global temperature and pressure height grid.

Several multivariate analysis techniques were applied to the limited data set from June 1977. These methods provided a means for discerning relationships among atmospheric variables and for characterizing the variability of the data field. Several promising graphical display and data analysis codes were developed that should prove to be very useful when we begin regular data processing.

Several routine tasks continued throughout this period. We sent monthly DMSP satellite overpass prediction times to each of the Dobson stations taking special measurements. We forwarded the Dobson data that we received to NOAA and NASA on a monthly basis as well. Steady progress was made on the conversion of the FRAMIS data base management system to the VAX 11/780 computer system. About half of the utility routines had been rewritten to run on the VAX up to this time.

The simulated radiances were used to investigate several approaches to improving the ozone retrieval models. Problems stemming from the ozonesonde data and initial processing, especially the insertion of a climatological upper stratosphere, were detected. The formulations of two of the parameters used in the retrieval model were changed to allow for band-dependent terms, achieving improvement in model accuracy.

MFR data from January 1-February 5, 1979 were processed and data summaries prepared for intercomparison with other ozone data sets. A significant improvement in retrieval methodology was achieved relative to that used in the feasibility study in that no satellite radiance sets were eliminated due to extremely cloudy or cold backgrounds. As a result, daily data coverage was more than doubled in comparison to the earlier feasibility study model.

3.5.2 March-August 1980

A major effort during this period was directed toward improvement of the temperature climatology used to extrapolate the measured temperature profiles above the sonde cut-off altitude. A method was developed whereby the temperature at specified pressure levels above P_{min} (sonde cut-off pressure) was computed based on the measured temperatures at lower altitudes. To validate this procedure, a method was first developed to predict temperature fields that were computed using MFR data for several days in January 1979 for regions for which we have temperature analyses from the Free University of Berlin (FUB). Agreement between the two independent temperature fields was very good. The temperature contours defining features of local temperature maxima or minima agreed very well in the location of the features, although the magnitudes of the features were different in many instances. By averaging the MFR-derived results over several degrees in latitude and longitude, the satellite temperature field showed a smoothness typical of the FUB analyses. This smoothing process however, led to poorer agreement near areas of maximum and minimum temperatures.

We added the necessary coding to the ozonesonde processing code so that the new method of extrapolating the temperature upward could be applied to all soundings in the ozonesonde data base.

Improvements were made in the sonde selection process so that the soundings selected for input to the radiative transfer codes are representative of the complete sonde data base for that band and month. We now make 500 random selections of 20 soundings each for each latitude band and for each month. The "best" set of 20 soundings is chosen based on a principal components analysis of 9 variables (4 ozone densities, 4 temperatures, and total ozone for each of the soundings).

The FRAMIS data management system became operative on the VAX computer, although it was still working at a basic version level. There was a DEC system problem with their SORT routine and system debug codes. The LLNL Data Management Group fixed the problem by writing a machine independent FORTRAN SORT, both internal and disk-based. This provided the breakthrough needed to continue with testing.

Coding was completed on the statistics code that summarizes ozone data in 10° lat. x 20° long. boxes on a global scale. The code is used to compare the MFR ozone data with similar data calculated by NASA and NOAA.

The AVIV high-density (6250 bpi) tape-drive unit and associated software arrived and was installed in June. This hardware component completed the data archive system on the VAX computer. Work continued on conversion of the calibrate code to run on the VAX computer, and addressed several of the input file/word-size problems. Numerous areas of improvement in the major subroutines of this code package were identified and were undergoing tests.

During this period, the analysis effort was concerned with research directed towards a better understanding of the dynamics associated with the evolution of the polar vortex breakdown and the ensuing stratospheric warming. A stratospheric warming occurred during January and February 1979. We were studying (1) the ozone data provided by the satellite MFR and (2) the stratospheric temperature, height field and wind data provided by conventional, non-satellite data sources, that have been analyzed by the FUB. Our preliminary analyses indicated low amounts of total ozone in the polar regions prior to the initiation of the vortex breakdown. Approximately 2-3 days after the stratosphere began to noticeably warm at 10 mb, the total ozone column began to increase dramatically — an increase that lasted several days. As the three stratospheric temperature pulses proceeded during January and February, the total ozone column poleward of 60°N remained considerably above the pre-vortex breakdown amounts observed during the first three weeks of January.

In August we began to reprocess the MFR data from January and February 1979, at which time we discovered that the retrievals were not an improvement over our earlier processing.

3.5.3 August-December 1980

Many tasks were completed during this period leading to the finalization of the ozone retrieval methodology. Beginning in August, a series of tasks was initiated in order to evaluate why the changes that were made to the retrieval methodology did not result in improved retrievals. In addition to knowing why the changes did not lead to the desired result, we also needed to develop new modifications for improving the results.

3.5.3.1 Calculation of regression coefficients.

1. Issue: Which functions should be used? Models were developed and tested using various combinations of independent functions. The models were tested using satellite data in the vicinity of Dobson stations and the retrieved ozone values were compared with the Dobson measurements. Correlations and automatic correlation coefficients were computed for each function with total ozone and for each function with all other functions. A theoretical study was made of how correlations between functions and the magnitudes of their means and standard deviations affect the regression coefficient. We found that certain independent functions were highly correlated with each other, thus causing problems in the computed regression coefficients. We also tried normalizing the functions in order to account for differences in the means and standard deviations among the simulated and measured function values, but this did not lead to significant improvement. More could be done in this area of research, but not on the time scale for start-up of data processing. As a result of this study, we reduced the number of independent functions from 6 to 3 (although one latitude band uses 4) and obtained a higher percent variance explained in the retrievals.

2. Issue: Which stations in the ozonesonde data base should be used to derive the regression coefficients? Models were developed from sondes at a dozen stations and tested against models derived from the actual satellite data and Dobson measurements. Various combinations of independent functions were used in this analysis. By deriving models from satellite data, we were able to determine the best possible percent variance explained by the retrievals. These values were compared with those obtained using models derived from simulated radiances. Certain stations were found to have a low maximum possible percent variance explained, and a few stations proved to be unreliable when models were derived from sondes at these stations. Some improvement was possible by narrowing the time interval over which the sonde data were taken from 3 months to 2 months.

3. Issue: How many latitude bands? Statistics were developed on the latitude variation of each of the independent functions. Regions with large gradients were noted, and these regions may shift in latitude as the seasons change. Also, models that were developed on a particular sonde station were tested on other stations to determine the latitude extent of the model applicability. We found that the coefficients (other than the constant term) did not vary rapidly with latitude except near the tropics. The constant term reflects the effect of changes in the mean values of the independent functions with latitude. Consequently, the constant varied widely over the full pole-to-pole region. As a result of this study, we increased the number of latitude bands from 5 to 11. The bands are generally 10-20° wide. Even more bands could be added if there were sufficient sonde data in the Southern Hemisphere from which to derive regression coefficients.

4. Issue: Can the data be split by meteorological situations? What outside information could be used to determine the meteorological situation? Analysis of the sonde data revealed groupings of similar meteorological regimes, particularly at high northern latitudes. A model based on a particular meteorological regime performed much differently than one based on the combined population that included several regimes. Although the approach looks very promising, it has not progressed to the point of being operational at this time.

5. Issue: What affect does combining sondes from various stations have on the regression coefficients? For bands where there is a significant gradient of total ozone, the sets of sondes for various stations within that band can have significantly different means. A model based upon the combined set of sondes would then try to predict the difference in the mean values between stations. A model based upon data from one station, however, would predict the change in ozone about the mean value, but it would likely have a bias when applied to other locations within that band. We tested both approaches and found that the latter approach gave better predictability of ozone at Dobson stations within a band. The method does have a higher mean bias, but all statistics other than the bias were better when coefficients were based on station data. We now develop coefficients for each station separately and average them in developing a band model.

3.5.3.2 Sensitivity studies. The tasks above involved testing the model's sensitivity to various changes that might be made in the methodology. In addition to those studies, several other tests were made.

1. Independent data sets from one station. A test of the stability of a model is to work with two independent sets of data, in this case, two sets of sonde data from Hohenpeissenberg. Models were derived from each set separately and tested against the other set. The effect of deleting one or two sondes from the sets of 20 was also tested.

2. Variation of surface temperature and cloud fractions. Models were developed from the same set of sonde data, but different means and standard deviations were used for surface temperature and different cloud amounts were specified. The models were then tested on data near Dobson stations and were found to be not very sensitive to these parameters.

3. The specification of τ_{avg} in the O3CORR term. One of the independent functions, O3CORR, uses a specified mean transmittance for the stratosphere, τ_{avg}, in its formulation. The parameter τ_{avg} varies with latitude and season, but not greatly. We found, however, that variations in τ_{avg}, though slight, can cause a bias to show up in the retrievals if the value used in the retrieval is not exactly the same as that used in the simulation. Slight differences occurred in the past due to the manner in which data from different months were combined. The procedure has now been modified to eliminate any bias due to such differences in τ_{avg}.

3.5.3.3 Evaluation of accuracy of retrieval. Special coding was developed so that global retrieval models could be tested against the Dobson data for January 1979. Because repetitive processing of a month of satellite data to test retrieval schemes is a significant task, the magnitude and cost were reduced by working only with satellite data in the vicinity of the Dobson stations. The Dobson/satellite comparison statistics code was modified to include comparison of the mean of all satellite measurements taken within specified time/distance criteria from Dobson measurements. The model previously compared only the retrieval point nearest in distance and time to the Dobson measurement. Additional statistical tests were also included in the analysis along with data presentation plots.

Through special arrangements with scientists at Dobson observatories, measurements were obtained from five additional Dobson stations for January and February 1979. These stations were: Churchill, Goose Bay, Manila, El Qahira (Egypt), and Mexico City. These stations are in previously data-void areas and will be useful in model evaluation comparisons. We also obtained data from Amundsen-Scott (South Pole) for January and February 1979 that were not previously available.

Two approaches were followed in developing the first global models for testing. One approach used information available from the testing of various models against Dobson data, and the other approach excluded this information. The latter approach is the more desirable or since it is less manpower-intensive and does not require double processing of the satellite data. The former method can be used as a standard for comparison. When these two models were evaluated against the Dobson data, both performed nearly equally well except for the amount of bias. The latter method had a larger bias, but both were equal overall in their ability to predict the variations in ozone at the Dobson sites. Subsequent analysis into the source of the

bias revealed the problem with τ_{avg} that was described above, and the bias has been reduced. Our goal is not to reduce the bias, but rather to increase the predictability. Since our data are not calibrated to match the Dobson values, a bias is expected in the results. Globally, the DMSP MFR ozone values are lower than the Dobson values by a few percent was also true of the results obtained using the methodology developed during the feasibility study (Lovill et al., 1978, 1979).

3.5.3.4 Summary. Tremendous strides have been taken in our understanding of the sensitivity and limitations of the ozone retrieval methodology. Tasks which were originally scheduled for special studies later in the project were completed because of the necessity to improve the methodology. The present methodology gives better results than either of our two previous models for January 1979. Data processing is underway, and we are in the process of automating many routine production operations.

4. WORK IN PROGRESS

We are in the process of developing a two-dimensional transport-kinetics model that will be in the programming and validation stage during most of fiscal year 1981. This model will be used to study latitudinal and seasonal effects of various atmospheric perturbations.

A reassessment will be made of the potential effects of emissions from projected fleets of high-altitude aircraft. Coupled effects will be considered, along with studies relating to detectability of ozone trends.

Processing of the DMSP MFR data will begin in early 1981. Data from satellites with overlapping coverage over a three-year period will be processed. Daily maps of total ozone and monthly statistics and comparisons with Dobson data will be prepared for analysis and distribution to the scientific community. We will also be conducting studies of the spatial and temporal variability of ozone related to natural and man-made influences.

5. REFERENCES

Anderson, D. E., Jr. and R. R. Meier, "Effects of Anisotropic Multiple Scattering on Solar Radiation in the Troposphere and Stratosphere," Appl. Optics., 18, 1955-1960, 1979.

Anderson, J. G., H. J. Grassl, R. E. Shetter, and J. J. Margitan, "Stratospheric Free Chlorine Measured by Balloon-Borne In Situ Resonance Fluorescence," J. Geophys. Res., 85, 2869-2887, 1980.

Bass, A. M., L. C. Glasgow, C. Miller, J. P. Jesson, and D. L. Filkin, "Temperature Dependent Absorption Cross Sections for Formaldehyde (CH_2O): The Effect of Formaldehyde on Stratospheric Chlorine Chemistry," in Proceedings of the NATO Advanced Institute on Atmospheric Ozone, Portugal, 1980, available as U.S. Dept. of Transportation Report FAA-EE-80-20, 1980.

Blake, D. and R. S. Lindzen, "Effect of Photochemical Models on Calculated Equilibria and Cooling Rates in the Stratosphere," Mon. Wea. Rev., 101, 783-802, 1973.

Chandra, S., D. M. Butler and R. S. Stolarski, "Effect of Temperature Coupling on Ozone Depletion Prediction," Geophys. Res. Lett., 5, 199-202, 1978.

Chang, J. S., "Simulations, Perturbations, and Interpretations," in Proceedings of the 3rd CIAP Conference, U. S. Dept. of Transportation, Cambridge, MA, Report DOT-TSC-OST-74-15, 330-341, 1974.

Chang, J. S., Eddy diffusion profile described in First Annual Report of Lawrence Livermore Laboratory to the High Altitude Pollution Program, edited by F. M. Luther, Lawrence Livermore Laboratory, Livermore, CA, UCRL-50042-76, 1976.

Chang, J. S. and H. S. Johnston, "The Effect of NO_x Effluents on Ozone," in Proceedings of the 3rd CIAP Conference, Cambridge, MA, U.S. Dept. of Transportation Report DOT-TSC-OST-74-15, 323-329, 1974.

Chang, J. S., D. J. Wuebbles, and W. H. Duewer, "Sensitivity to Parameter Uncertainties for Ozone Reduction for Chlorofluoromethanes," Lawrence Livermore Laboratory, Livermore, CA, UCRL-77432, 1975.

Duchon, C. E., "Lanczos Filtering in One and Two Dimensions," J. Appl. Meteoro., 18, 1016-1022, 1979.

Duewer, W. H., D. J. Wuebbles, H. W. Ellsaesser, and J. S. Chang, "NO_x Catalytic Ozone Destruction: Sensitivity to Rate Coefficients," J. Geophys. Res., 82, 935-942, 1977.

Ehhalt, D. H., "In Situ Measurements of Stratospheric Trace Constituents," Rev. Geophys. Space Phys., 16, 217-224, 1978.

Ehhalt, D. H. and A. Tonnissen, "Hydrogen and Carbon Compounds in the Stratosphere," in Proceedings of NATO Advanced Study Institute on Atmospheric Ozone: Its Variations and Human Influences, FAA Report FAA-EE-80-20, 1980.

Evans, W. F. J., J. B. Kerr, D. I. Wardle, J. C. McConnell, B. A. Ridley, and H. I. Schiff, "Intercomparison of NO, NO_2, and HNO_3 Measurements with Photochemical Theory," Atmosphere, 14, 189, 1976.

Fabian, P., R. Borchers, K. H. Weiler, U. Schmidt, A. Volz, D. H. Ehhalt, W. Seiler, and H. Oeser, "Simultaneously Measured Vertical Profiles of H_2, CH_4, CO, N_2O, F-11, F-12, NO and O_3 in the Midlatitude Stratosphere and Troposphere," J. Geophys. Res., 84, 3149-3154, 1979.

Goldan, P. D., W. C. Kuster, D. L. Albritton, and A. L. Schmeltekopf, "Stratospheric $CFCl_3$, CF_2Cl_2 and N_2O Height-Profile Measurements at Several Latitudes," preprint, NOAA Aeronomy Laboratory, Boulder, CO, 1979.

Grobecker, A. J., S. C. Coroniti, and R. H. Cannon, Jr., "CIAP Report of Findings, The Effects of Stratospheric Pollution by Aircraft," Report DOE-TST-75-50, U. S. Dept. of Transportation, Washington, D.C., 1974.

Harries, J. E., "Ratio of HNO_3 to NO_2 Concentration in the Daytime Stratosphere," Nature, 274, 235, 1978.

Harries, J. E., D. G. Moss, N. R. W. Swann, and G. F. Neill, "Simultaneous Measurements of H_2O, NO_2, and HNO_3 in the Daytime Stratosphere from 15 to 35 km," Nature, 259, 300-302, 1976.

Heidt, L. E. and D. H. Ehhalt, "Correction of CH_4 Concentrations Measured Prior to 1974," Geophys. Res. Lett., 7, 1023, 1980.

Hill, W. J., P. N. Sheldon, and J. J. Tiede, "Analyzing World Wide Total Ozone for Trends," Geophys. Res. Lett., 4, 21-24, 1977.

Isaksen, I. S. A., K. M. Midtbo, J. Sunde, and P. J. Crutzen, "A Simplified Method to Include Molecular Scattering and Reflection in Calculations of Photon Fluxes and Photodissociation Rates," Geophysica Norvegia, 31, 11-26, 1977.

Jet Propulsion Laboratory, "Chemical Kinetic and Photochemical Data for Use in Stratospheric Modeling," NASA Panel for Data Evaluation, Publication 79-27, 1979.

Jet Propulsion Laboratory, "Chemical Kinetic and Photochemical Data for Use in Stratospheric Modelling," JPL Publication 81-3, 1981.

Johnston, H. S., "Reduction of Stratospheric Ozone by Nitrogen Oxide Catalysts from Supersonic Transport Exhaust," Science, 173, 517-522, 1971.

Jones, S. E. and D. R. Ries, "A Relational Data Base Management System for Scientific Data," Lawrence Livermore National Laboratory Report UCRL-80769, 1978.

Keyser, L. F., "Kinetics of the Reaction $OH + H_2O_2 \rightarrow HO_2 + H_2O$ from 245 to 435 K," J. Phys. Chem., 84, 1659-1663, 1980.

Littlejohn, D. and H. S. Johnston, "Rate Constant for the Reaction of Hydroxyl Radicals and Peroxynitric Acid," presented at the AGU Fall Meeting, San Francisco, CA, Dec. 8-12, 1980.

London, J., R. D. Bojkov, S. Oltmans, and J. I. Kelley, "Atlas of the Global Distribution of Total Ozone July 1957-June 1967," NCAR/TN/112+STR, National Center for Atmospheric Research, Boulder, CO, 1976.

Lovill, J. E., J. S. Ellis and P. P. Weidhaas, "The Global Observation of Atmospheric Ozone by Satellite," WMO Technical Conference on Regional and Global Observation of Atmospheric Pollution Relative to Climate, Boulder, CO, WMO Publication 549, 281-286, 1979.

Lovill, J. E., T. Sullivan, R. Weichel, J. S. Ellis, J. G. Huebel, J. A. Korver, P. P. Weidhaas, and F. A. Phelps, Total Ozone Retrieval from Satellite Multichannel Filter Radiometer Measurements, Lawrence Livermore Laboratory, CA, UCRL- 52473, 1978.

Luther, F. M. (principal investigator), Annual Report of Lawrence Livermore Laboratory to the High Altitude Pollution Program — 1976, Lawrence Livermore Laboratory, Livermore, CA, UCRL-50042-76, 1976.

Luther, F. M. (principal investigator), Annual Report of Lawrence Livermore Laboratory to the High Altitude Pollution Program -- 1977, Lawrence Livermore Laboratory, Livermore, CA, UCRL-50042-77, 1977.

Luther, F. M. (principal investigator), Annual Report of Lawrence Livermore Laboratory to the High Altitude Pollution Program — 1978, Lawrence Livermore Laboratory, Livermore, CA, UCRL-50042-78, 1978.

Luther, F. M. (principal investigator), Annual Report of Lawrence Livermore Laboratory to the FAA on the High Altitude Pollution Program — 1979, Lawrence Livermore Laboratory, Livermore, CA, UCRL-50042-79, 1979a.

Luther, F. M. and R. J. Gelinas, "Effect of Molecular Multiple Scattering and Surface Albedo on Atmospheric Photodissociation Rates," J. Geophys. Res., 81, 1125-1132, 1976.

Luther, F. M., J. S. Chang, W. H. Duewer, J. E. Penner, R. L. Tarp, and D. J. Wuebbles, "Potential Environmental Effects of Aircraft Emissions," Lawrence Livermore National Laboratory Report UCRL-52861, 1979.

MacCracken, M. C. (principal investigator), DOT-CIAP Program — Third Annual Report, Lawrence Livermore Laboratory, Livermore, CA, UCRL-51226-75, 1975.

Manabe, S. and R. T. Wetherald, "Thermal Equilibrium of the Atmosphere with a Given Distribution of Relative Humidity," J. Atmos. Sci., 24, 241-259, 1967.

Molina, L. T. and M. J. Molina, "Ultraviolet Absorption Cross Sections of HO_2NO_2 Vapor," presented at the 14th Informal Conference on Photochemistry, Newport Beach, CA, March 30-April 3, 1980; also U.S. Dept. of Transportation Report FAA-EE-80-7, 1980.

Murcray, D. G., private communication in Hudson and Reed, 1979.

Murcray, D. G., A. Goldman, F. H. Murcray, F. T. Murcray, and W. J. Williams, "Stratospheric Distribution of $ClONO_2$," Geophys. Res. Lett., 6, 857-859, 1979.

NASA Reference Publication 1010, "Chlorofluoromethanes and the Stratosphere," R. D. Hudson (ed.), 1977.

NASA Reference Publication 1049, "The Stratosphere: Present and Future," R. D. Hudson and E. I. Reed (eds.), 1979.

NBS Special Publication 513, "Reaction Rate and Photochemical Data for Atmospheric Chemistry — 1977," R. F. Hampson, Jr. and D. Garvin (eds.), National Bureau of Standards, Washinton, D. C., 1978.

NBS Technical Note 866, "Chemical Kinetics and Photochemical Data for Modeling Atmospheric Chemistry," R. F. Hampson, Jr. and D. Garvin (eds.), National Bureau of Standards, Washington, D. C., 1975.

National Research Council, Halocarbons: Environmental Effects of Chlorofluoromethane Release, National Academy of Sciences, Washington, D. C., 1976.

National Research Council, "Stratospheric Ozone Depletion by Halocarbons: Chemistry and Transport," National Academy of Sciences, Washington, D. C. 1979.

Nichols, D. A., "DMSP Block 5D Special Meteorological Sensor H, Optical Subsystem," Opt. Engr., 14, 284-288, 1975.

Oliver, R. C., E. Bauer, H. Hidalgo, K. A. Gardner, and W. Wasylkiwskyj, "Aircraft Emissions: Potential Effects on Ozone and Climate: A Review and Progress Report," FAA Report FAA-EQ-77-3, 1977.

Penner, J. E., "Increases in CO_2 and Chlorofluoromethanes: Coupled Effects on Stratospheric Ozone," in Proceedings of the Quadrennial International Ozone Symposium, Boulder, CO, Aug. 4-9, 1980; also UCRL-84058, 1980.

Penner, J. E., L. P. Golen, and R. W. Mensing, "A Time Series Analysis of Umkehr Data from Arosa," Lawrence Livermore National Laboratory UCRL-85420, 1981.

Schmidt, U., J. Rudolph, F. J. Johnen, D. H. Ehhalt, A. Volz, E. P. Roth, R. Borchers, and P. Fabian, "The Vertical Distribution of $CH_3C\ell$, $CFC\ell_3$, and $CF_2C\ell_2$, in the Mid-Latitude Stratosphere," submitted for Proceedings of International Ozone Symposium, Boulder, CO, Aug. 3-8, 1980.

Schneider, S. H., "On the Carbon Dioxide Climate Confusion," J. Atmos. Sci., 32, 2060, 1975.

Sze, N. D., "Variational Methods in Radiative Transfer Problems," J. Quant. Spectrosc. Radiat. Trans., 16, 763-780, 1976.

U. S. Standard Atmosphere, 1976, NOAA-S/T 76-1562, U. S. Government Printing Office, Washington, D. C., 1976.

Wang, W. C., Y. L. Yung, A. A. Lacis, T. Mo, and J. E. Hansen, "Greenhouse Effects Due to Man-Made Perturbations of Trace Gases," Science, 194, 685-689, 1976.

Wine, P. H., A. R. Ravishankara, N. M. Kreutter, R. C. Shah, J. M. Nicovich, R. L. Thompson, and D. J. Wuebbles, "Rate of Reaction of OH with HNO_3," J. Geophys. Res., 86, 1105-1112, 1981.

Wuebbles, D. J. and J. S. Chang, "A Study of the Effectiveness of the C&X Catalytic Ozone Loss Mechanisms," in Proceedings of the Quadrennial International Ozone Symposium, Boulder, CO, August 4-9, 1980; also UCRL-84071, 1980.

Wuebbles, D. J. and W. H. Duewer, "Effect of Recent Kinetics Measurements on our Understanding of Chemical Processes in the Troposphere and Stratosphere," presented at 14th Informal Conf. on Photochemistry, Newport Beach, CA March 30-April 3, 1980; also UCRL-83960, 1980.

Yung, Y. L., "A Numerical Method for Calculating the Mean Intensity in an Inhomogeneous Rayleigh Scattering Atmosphere," J. Quant. Spectrosc. Radiat. Trans., 16, 755-761, 1976.

APPENDIX A. CURRENT CHEMISTRY IN THE LLNL ONE-DIMENSIONAL TRANSPORT-KINETICS MODEL

TABLE A-1. Chemical reactions and rate coefficients where $k = Ae^{B/T}$ used in the 1980 model chemistry.

	Reaction	A	B	Note
1.	$O + O_2 + M \rightarrow O_3 + M$	see Table A-2		3
2.	$O + O_3 \rightarrow 2O_2$	1.5×10^{-11}	-2218	1
3.	$O_3 + NO \rightarrow NO_2 + O_2$	2.3×10^{-12}	-1450	1
4.	$O + NO_2 \rightarrow NO + O_2$	9.3×10^{-12}	0	1
5.	$N_2O + O(^1D) \rightarrow N_2 + O_2$	5.1×10^{-11}	0	1
6.	$N_2O + O(^1D) \rightarrow 2NO$	6.6×10^{-11}	0	1
7.	$N + O_2 \rightarrow NO + O$	4.4×10^{-12}	-3220	1
8.	$N + NO \rightarrow N_2 + O$	3.4×10^{-11}	0	1
9.	$O(^1D) + H_2O \rightarrow 2OH$	2.2×10^{-10}	0	1
10.	$O_3 + OH \rightarrow HO_2 + O_2$	1.6×10^{-12}	-940	1
11.	$O + OH \rightarrow O_2 + H$	2.3×10^{-11}	+110	1
12.	$O_3 + HO_2 \rightarrow OH + 2O_2$	1.1×10^{-14}	-580	1
13.	$O + HO_2 \rightarrow OH + O_2$	4.0×10^{-11}	0	1
14.	$H + O_2 + M \rightarrow HO_2 + M$	see Table A-2		3
15.	$O_3 + H \rightarrow OH + O_2$	1.4×10^{-10}	-470	1
16.	$HO_2 + HO_2 \rightarrow H_2O_2 + O_2$	see Table A-2		3
17.	$HO_2 + OH \rightarrow H_2O + O_2$	4.0×10^{-11}	0	1
18.	$OH + NO_2 + M \rightarrow HNO_3 + M$	see Table A-2		1
19	$OH + HNO_3 \rightarrow H_2O + NO_3$	1.52×10^{-13}	+649	1,10
20.	$H_2O_2 + OH \rightarrow H_2O + HO_2$	2.7×10^{-12}	-145	1
21.	$N_2 + O(^1D) + M \rightarrow N_2O + M$	see Table A-2		3
22.	$N + NO_2 \rightarrow N_2O + O$	2.1×10^{-11}	-800	1
23.	$NO + O + M \rightarrow NO_2 + M$	see Table A-2		3
24.	$NO + HO_2 \rightarrow NO_2 + OH$	3.5×10^{-12}	+250	1
25.	$H_2 + O(^1D) \rightarrow OH + H$	9.9×10^{-11}	0	1
26.	$OH + OH \rightarrow H_2O + O$	4.5×10^{-12}	-275	1
27.	$N + O_3 \rightarrow NO + O_2$	2.0×10^{-11}	-3000	4
28.	$NO_2 + O_3 \rightarrow NO_3 + O_2$	1.2×10^{-13}	-2450	1

TABLE A-1. Continued

	Reaction	A	B	Note
29.	$OH + OH + M \rightarrow H_2O_2 + M$	see Table A-2		3
30.	$H_2O_2 + O \rightarrow OH + HO_2$	2.8×10^{-12}	-2125	1
31.	$CO + OH + M \rightarrow H + CO_2 + M$	see Table A-2		3
32.	$O(^1D) + M \rightarrow O + M$	2.1×10^{-11}	99	5
33.	$Cl + O_3 \rightarrow ClO + O_2$	2.8×10^{-11}	-257	1
34.	$Cl + NO_2 + M \rightarrow ClNO_2 + M$	see Table A-2		3
35.	$ClO + O \rightarrow Cl + O_2$	7.7×10^{-11}	-130	1
36.	$NO + ClO \rightarrow NO_2 + Cl$	6.5×10^{-12}	280	1
37.	$ClO + NO_2 + M \rightarrow ClONO_2 + M$	see Table A-2		3
38.	$HCl + O(^1D) \rightarrow Cl + OH$	1.4×10^{-10}	0	1
39.	$OH + HCl \rightarrow H_2O + Cl$	2.8×10^{-12}	-425	1
40.	$O + HCl \rightarrow OH + Cl$	1.14×10^{-11}	-3370	1
41.	$Cl + HO_2 \rightarrow HCl + O_2$	4.8×10^{-11}	0	1
42.	$CFCl_3 + O(^1D) \rightarrow 3Cl$	2.2×10^{-10}	0	1,6
43.	$CF_2Cl_2 + O(^1D) \rightarrow 2Cl$	1.4×10^{-10}	0	1,6
44.	$Cl + H_2 \rightarrow HCl + H$	3.5×10^{-11}	-2290	1
45.	$Cl + H_2O_2 \rightarrow HCl + HO_2$	1.1×10^{-11}	-980	1
46.	$ClONO_2 + O \rightarrow ClO + NO_3$	3.0×10^{-12}	-808	1,10
47.	$CH_3Cl + OH \rightarrow Cl + H_2O + HO_2$	1.8×10^{-12}	-1112	1,6
48.	$NO + NO_3 \rightarrow 2NO_2$	2.0×10^{-11}	0	1
49.	$NO_2 + O + M \rightarrow NO_3 + M$	see Table A-2		3
50.	$NO_2 + NO_3 + M \rightarrow N_2O_5 + M$	see Table A-2		3
51.	$N_2O_5 + M \rightarrow NO_2 + NO_3 + M$	see Table A-2		3
52.	$N_2O_5 + H_2O \rightarrow 2HNO_3$	1.0×10^{-20}	0	7
53.	$O(^1D) + O_3 \rightarrow 2O_2$	1.2×10^{-10}	0	1
54.	$HO_2 + HO_2 + H_2O \rightarrow H_2O_2 + O_2 + H_2O$	see Table A-2		3
55.	$O + NO_3 \rightarrow O_2 + NO_2$	1.0×10^{-11}	0	1
56.	$HO_2 + NO_2 + M \rightarrow HNO_4 + M$	see Table A-2		3
57.	$HNO_4 + M \rightarrow HO_2 + NO_2 + M$	see Table A-2		3
58.	$OH + HNO_4 \rightarrow H_2O + NO_2 + O_2$	8.0×10^{-13}	0	1,10
59.	$Cl + HNO_4 \rightarrow HCl + NO_2 + O_2$	3.0×10^{-12}	-300	8
60.	$HO_2 + ClO \rightarrow O_2 + HOCl$	4.6×10^{-13}	710	1
61.	$Cl + HOCl \rightarrow HCl + ClO$	3.0×10^{-12}	-300	8

TABLE A-1. Continued

	Reaction	A	B	Note
62.	$OH + HOCl \rightarrow H_2O + ClO$	3.0×10^{-12}	-150	1
63.	$O + HOCl \rightarrow OH + ClO$	1.0×10^{-11}	-2200	1
64.	$OH + CH_4 \rightarrow CH_3 + H_2O$	2.4×10^{-12}	-1710	1
65.	$O + CH_4 \rightarrow CH_3 + OH$	3.5×10^{-11}	-4550	1
66.	$O(^1D) + CH_4 \rightarrow CH_2O + H_2$	1.4×10^{-11}	0	1
67.	$O(^1D) + CH_4 \rightarrow CH_3 + OH$	1.4×10^{-10}	0	1
68.	$CH_4 + Cl \rightarrow HCl + CH_3$	9.6×10^{-12}	-1350	1
69.	$Cl + CH_3Cl \rightarrow HO_2 + CO + 2HCl$	3.4×10^{-11}	-1256	1,6
70.	$CH_3O_2 + NO \rightarrow NO_2 + CH_3O$	7.4×10^{-12}	0	1
71.	$Cl + CH_2O \rightarrow HCl + HCO$	9.2×10^{-11}	-68	1
72.	$CH_3O_2 + HO_2 \rightarrow CH_3OOH + O_2$	7.7×10^{-14}	+1300	1
73.	$CH_3O + O_2 \rightarrow CH_2O + HO_2$	9.2×10^{-13}	-2200	1
74.	$OH + CH_2O \rightarrow H_2O + HCO$	1.0×10^{-11}	0	1
75.	$O + CH_2O \rightarrow HCO + OH$	3.2×10^{-11}	-1550	2,10
76.	$HCO + O_2 \rightarrow CO + HO_2$	5.0×10^{-12}	0	1
77.	$OH + CH_3OOH \rightarrow CH_3O_2 + H_2O$	2.1×10^{-12}	-145	1,10
78.	$CH_3 + O \rightarrow CH_2O + H$	1.0×10^{-10}	0	1
79.	$CH_3O_2 + O_3 \rightarrow CH_3O + 2O_2$	1.0×10^{-14}	-600	9
80.	$CH_3O_2 + O \rightarrow CH_3O + O_2$	3.0×10^{-11}	0	9
81.	$ClO + OH \rightarrow HO_2 + Cl$	9.1×10^{-12}	0	1,10
82.	$CH_3 + O_2 + M \rightarrow CH_3O_2 + M$	see Table A-2		3
83.	$ClO + OH \rightarrow HCl + O_2$	Not used ($\sim 10^{-22}$)		
84.	$H_2 + OH \rightarrow H_2O + H$	1.2×10^{-11}	-2200	1
85.	$H + HO_2 \rightarrow H_2 + O_2$	4.2×10^{-11}	-350	1
86.	$OH + CH_3OOH \rightarrow CH_2O + H_2O + OH$	5.0×10^{-12}	-750	1,10
87.	$O + HNO_4 \rightarrow OH + NO_2 + O_2$	7.4×10^{-12}	-2630	1,10
88.	$OH + ClONO_2 \rightarrow HOCl + NO_3$	1.2×10^{-12}	-333	1,10
89.	$Cl + ClONO_2 \rightarrow 2Cl + NO_3$	1.7×10^{-12}	-607	1,10
90.	$HONO + OH \rightarrow H_2O + NO_2$	6.6×10^{-12}	0	1
91.	$OH + NO + M \rightarrow HONO + M$	see Table A-2		3
92.	$O + OClO \rightarrow ClO + O_2$	2.5×10^{-11}	-1166	1
93.	$NO + OClO \rightarrow NO_2 + ClO$	2.5×10^{-12}	-600	1
94.	$OH + CH_3CCl_3 \rightarrow H_2O + 3Cl$	5.4×10^{-12}	-1820	1

NOTES TO TABLE A-1

1. Draft report of NASA Panel on Laboratory Measurements (1980).

2. NASA Reference Publication 1049 (Hudson and Reed, 1979).

3. The reaction is pressure dependent. See Table A-2 for discussion.

4. Estimate designed to be compatible with upper limit given in reference 1, and low enough to have no significant effect on model performance. Reaction is retained only to facilitate reintroduction if the evaluated upper limit should prove to be in error.

5. Weighted average of the rates of $O(^1D) + N_2$ and $O(^1D) + O_2$ from reference 1.

6. Product chemistry has been simplified.

7. Estimated reaction rate. This estimate is designed to include a possible heterogeneous contribution to the overall reaction. Important only in the lower troposphere.

8. Estimated reaction rate. This rate is estimated based on the assumption that HNO_4 and $HOC\ell$ resemble H_2O_2 (as treated in JPL, 1979) in reactions with $C\ell$ and OH.

9. Estimated reaction rate. Rate is estimated based on the assumption that CH_3O_2 closely resembles HO_2 in reaction with O or O_3.

10. Products are not given in references 1 or 2. The assumed products are based on products that seem the most chemically plausible.

TABLE A-2. Rate coefficients used for pressure-dependent reactions.

Expression 1:

$$k = \frac{A_o[M](300/T)^{n_o}}{1 + A_o[M](300/T)^{n_o}/A_i(300/T)^{n_i}} \; 0.6^{\left\{1 + \log_{10}\left(\frac{A_o[M](300/T)^{n_o}}{A_i(300/T)^{n_i}}\right)^2\right\}^{-1}}$$

Reaction	A_o	n_o	A_i	n_i	Note
$HO_2 + NO_2 + M \rightarrow HNO_4 + M$	2.1×10^{-31}	5.0	6.5×10^{-12}	2.0	1
$OH + NO_2 + M \rightarrow HNO_3 + M$	2.6×10^{-30}	2.9	2.4×10^{-11}	1.3	1
$Cl O + NO_2 + M \rightarrow Cl ONO_2 + M$	1.6×10^{-31}	3.4	1.5×10^{-11}	1.9	1,2
	3.5×10^{-32}	3.8	1.5×10^{-11}	1.9	1,2
$O + O_2 + M \rightarrow O_3 + M$	6.2×10^{-34}	2.1	—	—	1
$CH_3 + O_2 + M \rightarrow CH_3O_2 + M$	2.2×10^{-31}	2.2	2.0×10^{-12}	1.7	1
$O(^1D) + N_2 + M \rightarrow N_2O + M$	3.5×10^{-37}	0.45	—	—	1
$Cl + NO_2 + M \rightarrow Cl NO_2$	1.6×10^{-30}	1.9	3.0×10^{-11}	1.0	1
$H + O_2 + M \rightarrow HO_2 + M$	5.5×10^{-32}	1.4	—	—	1
$OH + NO + M \rightarrow HNO_2 + M$	6.7×10^{-31}	3.3	3.0×10^{-11}	1.0	1
$OH + OH + M \rightarrow H_2O_2 + M$	2.5×10^{-31}	0.8	3.0×10^{-11}	1.0	1
$NO_2 + NO_3 + M \rightarrow N_2O_5 + M$	1.4×10^{-30}	2.8	8.0×10^{-13}	0	1
$O + NO + M \rightarrow NO_2 + M$	1.2×10^{-31}	1.8	3.0×10^{-11}	-0.3	1
$O + NO_2 + M \rightarrow NO_3 + M$	9.0×10^{-32}	2.0	2.2×10^{-11}	0	1
$N_2O_5 + M \rightarrow NO_2 + NO_3 + M$	$1.18\times10^{-3}e^{-11180/T}$	2.8	$7.52\times10^{14}e^{-11180/T}$	-0.8	3

TABLE 2. (Continued.)

		Notes
$HNO_4 + M \rightarrow HO_2 + NO_2 + M$	$k = \frac{5.2\times10^{-6}\, e^{-10015/T}}{1+4.86\times10^{-12}M^{0.61}}$	5
$OH + CO + M \rightarrow H + CO_2 + M$	$k = 1.35\times10^{-13}(1 + \frac{M}{2.46\times10^{+19}}$	1
$HO_2 + HO_2 + H_2O \rightarrow H_2O_2 + H_2O + O_2$	$k = \frac{1.1\times10^{-34}\, e^{+3730/T}}{1+M\times3.5\times10^{-16}\, e^{-2060/T}}$	4
$HO_2 + HO_2 \rightarrow H_2O_2 + O_2$	$k = 2.3\times10^{-12}\, e^{+0.15z}$	$0 \leq z < 10$ km
	$k = 1.0\times10^{-11}$	$10 \leq z \leq 15$ km
	$k = 1.0\times10^{-11}\, e^{-0.088(z-15.)}$	$z > 15$ km

NOTES TO TABLE A-2

1. Draft report of NASA Panel on Laboratory Measurements (1980).
2. Both expressions are recommended with no clear preference. The upper one is used in most of the LLNL one-dimensional calculations.
3. Based on data in reference 1 and the equilibrium constant from NBS 513 (1978).
4. Based on Cox (1978).
5. Based on Graham et al. (1978).

TABLE A-3. Photolysis reactions. Alternative products of reaction are shown in parentheses, but they were not used in the 1980 chemistry.

	Reaction	Note
1.	$O_2 \rightarrow 2O$	1,2
2.	$O_3 \rightarrow O + O_2$	1,3
3.	$O_3 \rightarrow O(^1D) + O_2$	1,3
4.	$NO_2 \rightarrow NO + O$	1,4
5.	$N_2O \rightarrow N_2 + O(^1D)$	4
6.	$NO \rightarrow N + O$	5
7.	$HNO_3 \rightarrow OH + NO_2$	4
8.	$H_2O_2 \rightarrow 2OH$	4
9.	$HO_2 \rightarrow OH + O$	4
10.	$Cl ONO_2 \rightarrow Cl + NO_3$ ($Cl O + NO_2$)	4,6
11.	$HCl \rightarrow H + Cl$	4
12.	$Cl O \rightarrow Cl + O$	7
13.	$Cl O \rightarrow Cl + O(^1D)$	Not used
14.	$Cl NO_2 \rightarrow Cl + NO_2$	4
15.	$OCl O \rightarrow Cl O + O$	7
16.	$CF_2Cl_2 \rightarrow 2Cl$	4,8
17.	$CFCl_3 \rightarrow 3Cl$	4,8
18.	$CCl_4 \rightarrow 4Cl$	4,8
19.	$N_2O_5 \rightarrow NO_3 + NO_2$ ($2NO_2 + O$)	4,6
20.	$NO_3 \rightarrow NO + O_2$	4
21.	$NO_3 \rightarrow NO_2 + O$	4
22.	$H_2O \rightarrow H + OH$	9
23.	$HNO_4 \rightarrow HO + NO_3$ ($HO_2 + NO_2$)	10,6
24.	$HOCl \rightarrow OH + Cl$	4
25.	$CH_3OOH \rightarrow CH_3 + OH$	4
26.	$CH_2O \rightarrow HCO + H$	11
27.	$CH_2O \rightarrow CO + H_2$	11
28.	$CH_3Cl \rightarrow CH_3 + Cl$	4
29.	$HONO \rightarrow OH + NO$	4
30.	$CH_3CCl_3 \rightarrow 3Cl$	4,8

NOTES FOR TABLE A-3.

1. Contributes to the optical depth of the model atmosphere.

2. The Schumann-Runge bands are given a special treatment based on Hudson and Mahle (1972).

3. The quantum yields of reactions 2 and 3 are given a special treatment based on the temperature-dependent treatment of NASA Panel on Laboratory Measurements (1980).

4. Based on the data of NASA Panel on Laboratory Measurements (1980). Where data for several temperatures are given, we have used the data at $\sim$ 230 K.

5. Nitric oxide photolysis is based on the treatment of Frederick and Hudson (1979). We have averaged rates over the sunlit hemisphere for daytime photolysis.

6. The products used for XNO_3 (X = Cl, OH, NO_2) are all based on analogy with $ClONO_2$ data of Chang et al. (1979). This treatment is highly uncertain.

7. Based on data in Watson (1974).

8. Product chemistry has been simplified.

9. Treatment based on Thompson et al. (1963).

10. Treatment based on Molina and Molina (1980).

11. Treatment based on cross sections of Bass et al. (1980).

References

Bass, A. M., L. C. Glasgow, C. Miller, J. P. Jesson, and D. L. Filkin, "Temperature Dependent Absorption Cross Sections for Formaldehyde (CH_2O): The Effect of Formaldehyde on Stratospheric Chlorine Chemistry," in Proceedings of the NATO Advanced Institute on Atmospheric Ozone, Portugal, 1980, available as U.S. Dept. of Transportation Report FAA-EE-80-20, 1980.

Chang, J. S., J. R. Barker, J. E. Davenport, and D. M. Golden, "Chlorine Nitrate Photolysis by a New Technique: Very Low Pressure Photolysis," Chem. Phys. Lett., 60, 385-390, 1979

Cox, R. A, "Kinetics of HO_2 Radical Reactions of Atmospheric Interest," presented at the WMO Symposium on the Geophysical Aspects and Consequences of Change in the Composition of the Stratosphere, Toronto, June 26-30, 1978, WMO No. 511, 1978.

Frederick, J. E. and R. D. Hudson, "Predissociation of Nitric Oxide in the Mesosphere and Stratosphere," J. Atmos. Sci., 36, 737-745, 1979.

Graham, R. A., A. M. Winer and J. N. Pitts, Jr., "Pressure and Temperature Dependence of the Unimolecular Decomposition of NO_2NO_2," J. Chem. Phys., 68, 4505-4510, 1978.

Hudson, R. D. and S. H. Mahle, "Photodissociation Rates of Molecular Oxygen in the Mesosphere and Lower Thermosphere," J. Geophys. Res., 77, 2902-2914, 1972.

Hudson, R. D. and E. I. Reed, "The Stratosphere: Present and Future," NASA Reference Publication 1049, 1979.

Jet Propulsion Laboratory, "Chemical Kinetic and Photochemical Data for Use in Stratospheric Modeling," NASA Panel for Data Evaluation, Publication 79-27, 1979.

Molina, L. T. and M. J. Molina, "Ultraviolet Absorption Cross Sections of HO_2NO_2 Vapor," presented at the 14th Informal Conference on Photochemistry, Newport Beach, CA, March 30-April 3, 1980, also U.S. Dept. of Transportation Report FAA-EE-80-7, 1980.

NBS Special Publication 513, "Reaction Rate and Photochemical Data for Atmospheric Chemistry — 1977," R. F. Hampson, Jr. and D. Garvin (eds.), National Bureau of Standards, Washington, D. C. 1978.

Thompson, B. A., P. Harteck and R. R. Reeves, Jr., "Ultraviolet Absorption Coefficients of CO_2, CO, O_2, H_2O, N_2O, NH_3, NO, SO_2, and CH_4 Between 1850 and 4000 A," J. Geophys. Res., 68, 6431-6436, 1963.

Trevor, P. L., J. S. Chang, and J. R. Barker, "Kinetics of Some Bimolecular Reactions of Pernitric Acid (HO_2NO_2)," presented at the 14th Informal Conference on Photochemistry, Newport Beach, CA, March 30-April 3, 1980.

Watson, R. T., "Chemical Kinetics Data Survey VIII. Rate Constants [illegible] of Atmospheric Interest," NBSIR 74-516, National Bureau of Standards, Washington, D. C., 1974.

AD-A134 521 ANNUAL REPORT OF LAWRENCE LIVERMORE NATIONAL LABORATORY 2/2
TO THE FEDERAL AV.. (U) LAWRENCE LIVERMORE NATIONAL LAB
CA F M LUTHER DEC 80 UCRL-50042-80 FAA/EE-83-8
UNCLASSIFIED DOT-FA79WAI-034 F/G 4/1 NL

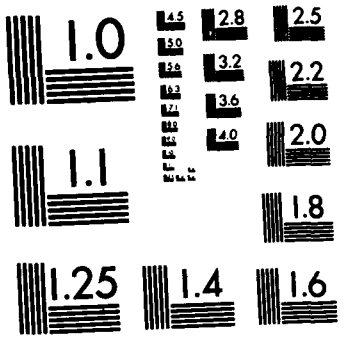

APPENDIX B. BIBLIOGRAPHY OF LLNL PUBLICATIONS AND TECHNICAL PRESENTATIONS ON THE HIGH ALTITUDE POLLUTION PROGRAM DURING THE PAST YEAR

Chang, J. S., "Stratospheric Chemistry: Theory and Models," The Institute of Atmospheric Physics, Chinese Academy of Science, Beijing, People's Republic of China, April-May 1980. A series of six lectures.

Chang, J. S. and D. J. Wuebbles, "One-Dimensional Coupled Transport and Chemical Kinetics Models of the Stratosphere," in Proceedings of the NATO Advanced Study Institute on Atmospheric Ozone: Its Variation and Human Influences, Aldeia das Acoteias, Algarue, Portugal, October 1-13, 1979; Lawrence Livermore National Laboratory Report UCRL-83790, 1980.

Duewer, W. H. and D. J. Wuebbles, "Tropospheric Methane: Response to Stratospheric Ozone Trends," presented at the International Meeting of the Union of Geodesy and Geophysics, Canberra, Australia, December 2-15, 1979.

Duewer, W. H. and D. J. Wuebbles, "Effects of Speculative Reactions and Mechanisms on Predicted Ozone Perturbations," presented at the 14th Informal Conference on Photochemistry, Newport Beach, CA, March 30-April 3, 1980; Lawrence Livermore National Laboratory Report UCRL-83950, 1980.

Luther, F. M. (principal investigator), "Annual Report of Lawrence Livermore Laboratory to the FAA on the High Altitude Pollution Program, — 1979," Lawrence Livermore National Laboratory Report UCRL-50042-80, 1980.

Luther, F. M., "Agents and Effects of Ozone Depletion," presented at the NATO Advanced Research Institute on the Effects of Solar Ultraviolet Radiation on Marine Ecosystems, Copenhagen, Denmark, July 28-31, 1980.

Luther, F. M., "Intercomparison of Preliminary MFR, SBUV, TOMS and TOVS Total Ozone Data," Lawrence Livermore National Laboratory Report UCID-18739, 1980.

Luther, F. M., "Ozone Depletion Models," presented at the NATO Advanced Research Institute on the Effects of Solar Ultraviolet Radiation on Marine Ecosystems, Copenhagen, Denmark, July 28-31, 1980.

Luther, F. M., "Photochemical Modeling: A Numerically Fast Scheme for Treating Multiple Scattering," in Volume of Extended Abstracts, International Radiation Symposium, Fort Collins, CO, August 11-16, 1980. Also, Lawrence Livermore National Laboratory Report UCRL-83031 Extended Abstract, 1980.

Luther, F. M., "UV-B Radiation Reaching the Ground Computed as a Function of Total Ozone, Solar Zenith and Surface Pressure," presented at the NATO Advanced Research Institute on the Effects of Solar Ultraviolet Radiation on Marine Ecosystems, Copenhagen, Denmark, July 28-31, 1980.

Luther, F. M., J. S. Ellis, J. E. Lovill, T. J. Sullivan and R. L. Weichel, "Global Distribution of Total Ozone During January and February 1979 as Determined from DMSP Multichannel Filter Radiometer Measurements," in Proceedings of the Quadrennial Ozone Symposium, Boulder, Colorado, August 4-9, 1980; Lawrence Livermore National Laboratory Report UCRL-84070, 1980.

Luther, F. M. and R. L. Weichel, "Determination of Total Ozone from DMSP Multichannel Filter Radiometer Measurements," in Proceedings of the Quadrennial Ozone Symposium, Boulder, CO, August 4-9, 1980; Lawrence Livermore National Laboratory Report UCRL-84069, 1980.

Penner, J. E., "Effect of Increased CO_2 in Stratospheric Ozone," presented at the Fall Annual Meeting of the American Geophysical Union, San Francisco, CA, December 8-12, 1980.

Penner, J. E., "Increases in CO_2 and Chlorofluoromethanes: Coupled Effects on Stratospheric Ozone," in Proceedings of the Quadrennial International Ozone Symposium, Boulder, CO, August 4-9, 1980; Lawrence Livermore National Laboratory Report UCRL-84058, 1980.

Penner, J. R., L. P. Golen, and R. W. Mensing, "A Time Series Analysis of Umkehr Data from Arosa," Lawrence Livermore National Laboratory Report UCRL-85420, 1981.

Penner, J. E. and F. M. Luther, "Effects of Temperature Feedback and Hydrostatic Adjustment in a Stratospheric Model," presented at the Fall Annual Meeting of the American Geophysical Union, San Francisco, CA, December 3-7, 1979; Lawrence Livermore National Laboratory Report UCRL-83250, accepted for publication in J. Atmos. Sci.

Rasmussen, R. A., M. A. K. Khalil, and J. S. Chang, "Atmospheric Trace Gases Over China," October 1980 (preprint).

Wine, P. H., A. R. Ravishankara, N. M. Kreutter, R. C. Shah, J. M. Nicovich, R. L. Thompson and D. J. Wuebbles, "Rate of Reaction of OH with HNO_3," J. Geophys. Res., 86, 1105-1112, 1981.

Wuebbles, D. J., "Impact of New OH + HNO_3 Rate Measurement on Models of Atmospheric Chemistry," Lawrence Livermore National Laboratory Report UCID-18727, 1980.

Wuebbles, D. J., "The Treatment of Dynamical Processes in Two-Dimensional Models of the Troposphere and Stratosphere," Lawrence Livermore National Laboratory Report UCID-18771, 1980.

Wuebbles, D. J. and J. S. Chang, "A Study of the Effectiveness of the CℓX Catalytic Ozone Loss Mechanisms," presented at, and published in the Proceedings of the Quadrennial International Ozone Symposium, Boulder, CO, August 4-9, 1980; Lawrence Livermore National Laboratory Report UCRL-84071, 1980; also to be published in J. Geophys. Res.

Wuebbles, D. J. and W. H. Duewer, "Effect of Recent Kinetics Measurements on Our Understanding of Chemical Processes in the Troposphere and Stratosphere," presented at 14th Informal Conference on Photochemistry, Newport Beach, CA, March 30-April 3, 1980; Lawrence Livermore National Laboratory Report UCRL-83960, 1980.

Wuebbles, D. J. and R. L. Tarp, "Sensitivity of Quantum Yield for $O(^1D)$ Production from Ozone Photolysis," Lawrence Livermore National Laboratory Report UCID-18734, 1980.

Wuebbles, D. J. and R. L. Tarp, "Potential Changes to Stratospheric Ozone from Possible Chlorofluorocarbon Production Scenarios," Lawrence Livermore National Laboratory Report UCID-18583, 1980 (sponsored by EPA).

END

FILMED

11-83

DTIC